Biological diversity of photosynthetic reaction centers and the solid-state photo-CIDNP effect

Roy, E.

Biological diversity of photosynthetic reaction centers and the solid-state photo-CIDNP effect

Esha Roy

ISBN: 978-90-9022219-6

Biological diversity of photosynthetic reaction centers and the solid-state photo-CIDNP effect

PROEFSCHRIFT

ter verkrijging van
de graad van Doctor aan de Universiteit Leiden,
op gezag van de Rector Magnificus Prof. mr. P. F. van der Heijden,
volgens besluit van het College voor Promoties
te verdedigen op donderdag 11 October 2007
klokke 13.45 uur

door

Esha Roy
geboren te Udaipur, India, in 1977

Promotiecommissie:

Promotor:
Prof. dr. H. J. M. de Groot

Copromotor:
Dr. J. Matysik

Referent:
Prof. dr. K. J. Hellingwerf, University of Amsterdam

Overige leden:
Dr. H. J. van Gorkom
Prof. dr. T. J. Aartsma
Prof. dr. S. Völker
Prof. dr. J. Brouwer

In loving memory of Dida

To my Parents

CONTENTS

List of Abbreviations

A	Primary electron acceptor
ADF	Amsterdam density functional
ALA	δ-Aminolevulenic acid
BChl	Bacteriochlorophyll
BPhe	Bacteriopheophytin
Chl	Chlorophyll
C.	*Chlorobium*
CD	Circular dichroism
CSA	Chemical shift anisotropy
DD	Differential decay
DFT	Density functional theory
DR	Differential relaxation
DZ	Double-zeta basis set
EDTA	Ethylene diamino tetra acetate
ENDOR	Electron nuclear double resonance
EPR	Electron paramagnetic resonance
ESEEM	Electron spin echo envelope modulation
FMO	Fenna Mathew Olson
FTIR	Fourier transfer infrared
Hba.	*Heliobacillus*
IUPAC	International union of pure and applied chemistry
LH I	Light harvesting complex I
LH II	Light harvesting complex II
MAS	Magic angle spinning
NMR	Nuclear magnetic resonance
P	Electron donor
PDB	Protein data bank
Phe	Pheophytin

Photo-CIDNP	Photo-chemically induced dynamic nuclear polarisation
ppm	parts per million
PSI	Photosystem I
PSII	Photosystem II
Rb.	*Rhodobacter*
RC	Reaction center
RNA	Ribonucleic acid
rRNA	Ribosomal ribonucleic acid
SOMO	Singly occupied molecular orbital
SDS-PAGE	Sodium dodecyl sulphate polyacrylamide gel electrophoresis
TPPM	Two pulse-phase modulation
TRIPLE	Electron nuclear nuclear triple resonance
TSM	Three spin mixing
TZP	Triple zeta polarisation
WT	Wild type
ZORA	Zero order regular approximation

1 Introduction

Photosynthesis is a light driven process that converts light energy to chemical energy providing almost all the free energy available to living organisms. The origin of photosynthesis on earth can be traced back to at least 3.5 billion years ago (1). The origin of photosynthesis appears to be complex. The photosynthetic apparatus has several components like the reaction center, antenna complexes, electron transfer complexes and carbon fixation machinery, each having its own unique evolutionary history (2). The presence of these components in various combinations in photosynthetic organisms is proposed to have occurred either by selective loss of parts or by genetic fusion (2). The process of photosynthesis takes place in pigment protein complexes that are located in membranes. First, light is captured by an antenna system. The collected light energy is then transferred to the reaction center complex. This RC complex contains a special pigment molecule called the primary electron donor and a chain of cofactors that form the electron transfer chain and serve as electron carriers. The RC complex is composed of different polypeptide chains that lace through the membrane, providing a supporting framework for metal ions and the other cofactors.

Photosynthetic electron transport involves a series of individual electron transfer steps. Upon photon absorption, the primary electron donor undergoes charge separation by releasing an electron to the next electron carrier, called the primary electron acceptor, which is then passed to a final electron acceptor. The initial charge separation is a highly optimized step having a quantum yield close to unity (3, 4). The translocation of the electron results in a difference in the electric potential across the membrane and produces reduced compounds that store chemical energy. Various (bacterio)chlorophylls and (bacterio)pheophytins are found in photosynthetic organisms like BChl *a*, *b*, *c*, *d*, *e*, *g*, Chl *a*, *b*, *c*, *d*, BPhe, Phe as well as carotenoids, iron sulphur clusters and quinones.

The RCs from different groups of photosynthetic organisms are generally divided into two categories, type I and type II (Fig. 1.1), based on the terminal electron acceptor (5):

(i) Type-I RCs contain iron sulphur clusters as the terminal electron acceptors. Photosystem I, heliobacteria and green sulphur bacteria are placed in this category.

(ii) Type-II RCs have quinones as the terminal electron acceptor. Photosystem II, RCs from purple bacteria and green filamentous bacteria (*Chloroflexaceae*) belong to this category. The pigment protein complexes that comprise the antenna system in these diverse organisms can be very different, while the functional structure of the RC core is remarkably conserved over

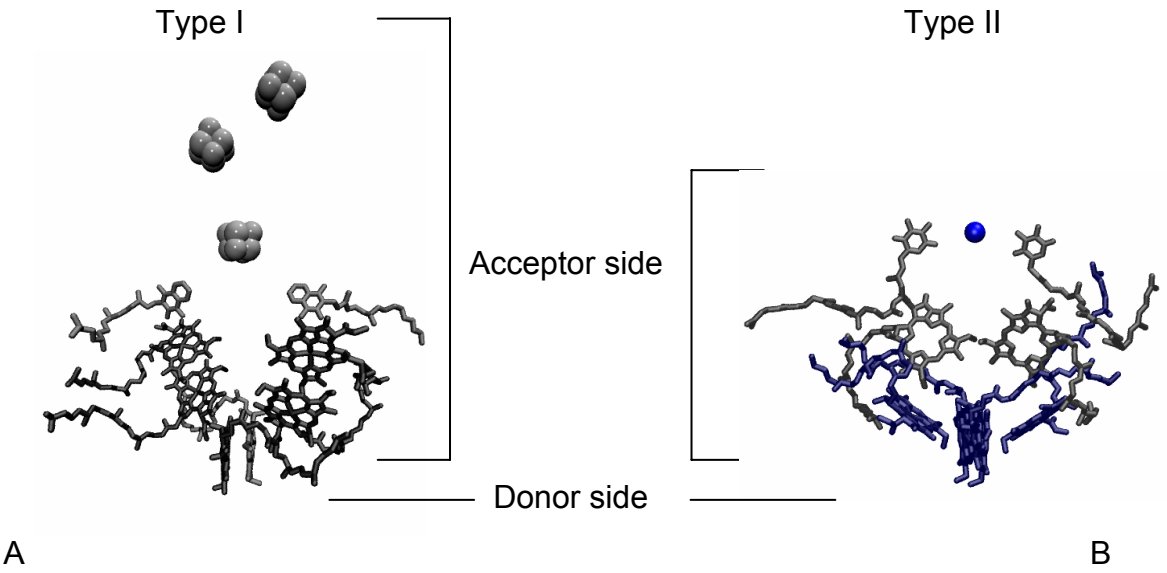

Figure 1.1. The general arrangement of cofactors in the electron transfer chain of type I (A) PSI RC from cyanobacterium *Synechococcus elongatus* (PDB file 1JBO) and type II (B) PSII from cyanobacterium *Thermosynechococcus elongatus* (PDB file 1S5L). The figures were made using the VMD molecular graphic programme (http://www.ks.uiuc.edu/Research/vmd/).

billions of years of evolution, and across many organisms.

This thesis aims to investigate the RC complexes from various organisms by applying solid-state photochemically induced dynamic nuclear polarization techniques in an attempt to explore the variability of the mechanisms of the photo-CIDNP effect in various type I and type II RCs. In addition, by studying diverse RC complexes, further insight may be gained in the functional principles that govern the efficient electron transfer in RCs. The next section gives a brief description of the photo-CIDNP technique in solid-state NMR and its application in the study of photosynthetic RCs. This is followed by a section describing the RCs from various photosynthetic organisms that were investigated.

1.1 Photo-CIDNP MAS NMR

Solid-state NMR spectroscopy is a widely used tool for a variety of applications, ranging from chemical analysis in organic and inorganic chemistry, to structure determination of large molecules like proteins (6-9). In solid-state NMR, magic angle spinning can be applied in order to average the chemical shift anisotropy and dipolar couplings, which improves the spectral resolution. In recent years MAS NMR has developed into a technique for the study of large biological systems like membrane proteins, prions, amyloids and nucleic acids. In addition, with solid-state NMR it is possible to perform a detailed analysis of the dynamics and functional mechanisms of membrane bound protein systems (9, 10).

Chemically induced dynamic nuclear polarization is a non-Boltzmann nuclear spin state

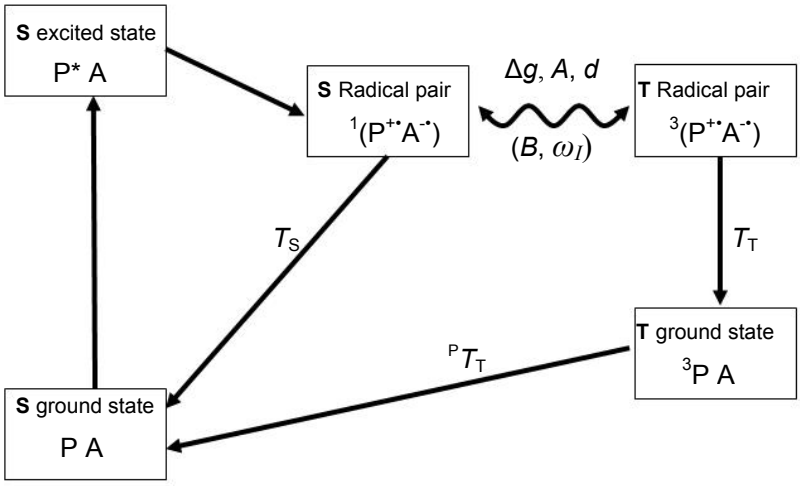

Figure 1.2. General reaction cycle scheme in quinone-blocked RCs. After light-induced electron transfer from P to A, initially the correlated radical pair is formed in a pure singlet state which evolves into a triplet radical pair due to Δg, d and hyperfine interactions. In the TSM contribution, the initial coherence in the electron pair is transformed into nuclear polarization by matching with the nuclear Zeeman frequency, ω_I. In the DD mechanism the build up of nuclear polarisation is due to the difference in lifetime (T_S and T_T) of the two radical pair states leading to a difference in contributions from the interconversion process between the radical pair states. The DR mechanism produces net nuclear spin polarization at the triplet branch, due to the long lifetime $^P T_T$ of the donor triplet ^{3}P (23). The oscillating arrow represents coherent evolution, while the solid arrows indicate (incoherent) decay processes towards the electronic ground state.

distribution which is produced in thermal or photochemical reactions. This nuclear spin state can be detected by NMR spectroscopy as enhanced positive or negative signals. Photo-CIDNP was observed for the first time by solution NMR in 1967 (11, 12). In the solid-state, photo-CIDNP is a powerful technique to study the function of light-induced electron transfer in photosynthetic membrane proteins at the atomic level. It was observed in quinone-blocked frozen bacterial RCs of *Rhodobacter sphaeroides* R-26 and subsequently in RCs of *Rb. sphaeroides* wild type (13-18). This resulted in studies of other RCs, like PSII from plants (19, 20, 21). The use of isotope labels is advantageous in strongly enhancing the NMR response. The combination of photo-CIDNP and isotope labelling enables the enhancement of both the intensity and the selectivity of the photo-CIDNP NMR signals (18, 22). The chemical shift provides information about the electronic structure of the ground state after the photo-reaction and recombination, while the intensities relate to the electron spin density distribution in the radical pair (23).

1.1.1 *Photo-CIDNP effect in solids*

After photochemical excitation of the electron donor P (Fig. 1.2), an electron is emitted to the primary acceptor A and a singlet radical pair $^1(P^{+\bullet}A^{-\bullet})$ is formed. Further electron transfer in RCs can be blocked by reducing or depleting the secondary electron acceptor. Under these conditions, the singlet radical pair can either decay to the electronic ground-state (P A) or it

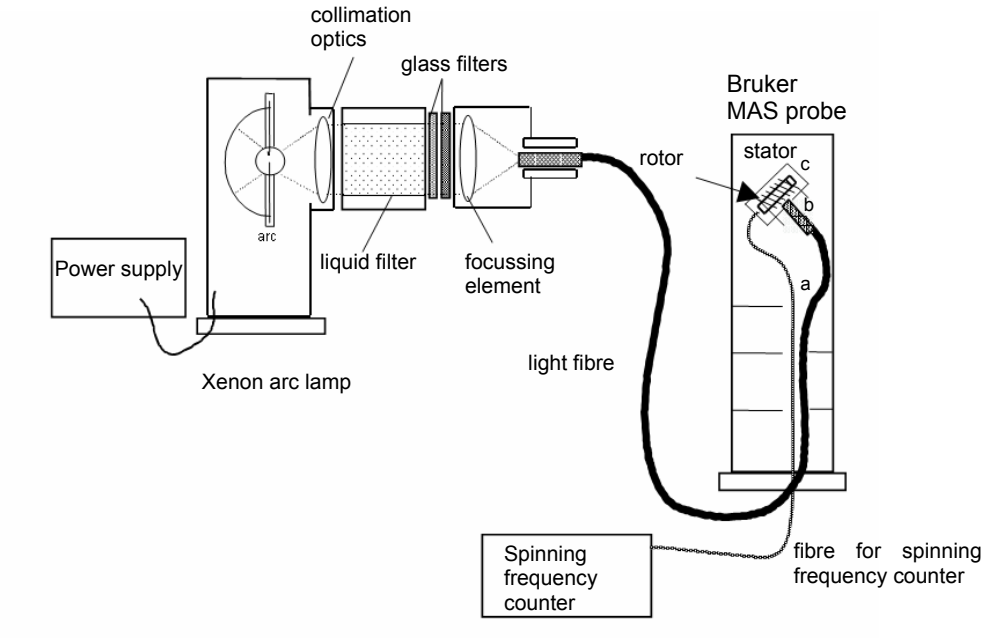

Figure 1.3. Schematic representation of the continuous illumination setup used for photo-CIDNP MAS NMR experiments. The points where modifications were made in the probe are (a) a bore drilled into upper partition plate separating electronics and stator chamber, (b) a small opening in the stator and (c) a thin silver wire coil allowing penetration of light.

can evolve into the triplet radical pair state $^3(P^{+\bullet}A^{-\bullet})$. The lifetime T_T of this triplet radical pair is short due to fast formation of a donor triplet state (^{3}P A). This donor triplet also relaxes to the singlet ground state (P A). During this photo-cycling process, three mechanisms are thought to occur that break the symmetry between the two branches and lead to an imbalance of the population of nuclear spin state distribution which is detected as net nuclear polarization (22, 23).

The spin-correlated radical pair is initially in a singlet state. Due to differences in *g*-value between the two electrons (Δg) and due to hyperfine interactions, the radical pair oscillates between singlet and triplet states (23). In the three spin mixing mechanism the magnitude of the photo-CIDNP effect is at its maximum when matching of the nuclear Zeeman frequency (ω_I) to coupling between the two electrons (d) and hyperfine interaction occurs (25, 26). In the differential decay mechanism, a net photo-CIDNP effect is caused due to the different lifetimes (T_S, T_T) of the two forms of the spin-correlated radical pair (27). This mechanism requires a single matching, of the nuclear Zeeman frequency to the hyperfine interaction. If the lifetime of the donor triplet state ^{3}P is long, the differential relaxation mechanism occurs (28). During this long lifetime, the triplet opens up relaxation channels that can contribute to establish net nuclear polarization.

In bacterial RCs of *Rb. sphaeroides* WT, contributions from both TSM and DD are observed. Emissive (negative) signals in this case arise due to the predominance of TSM over

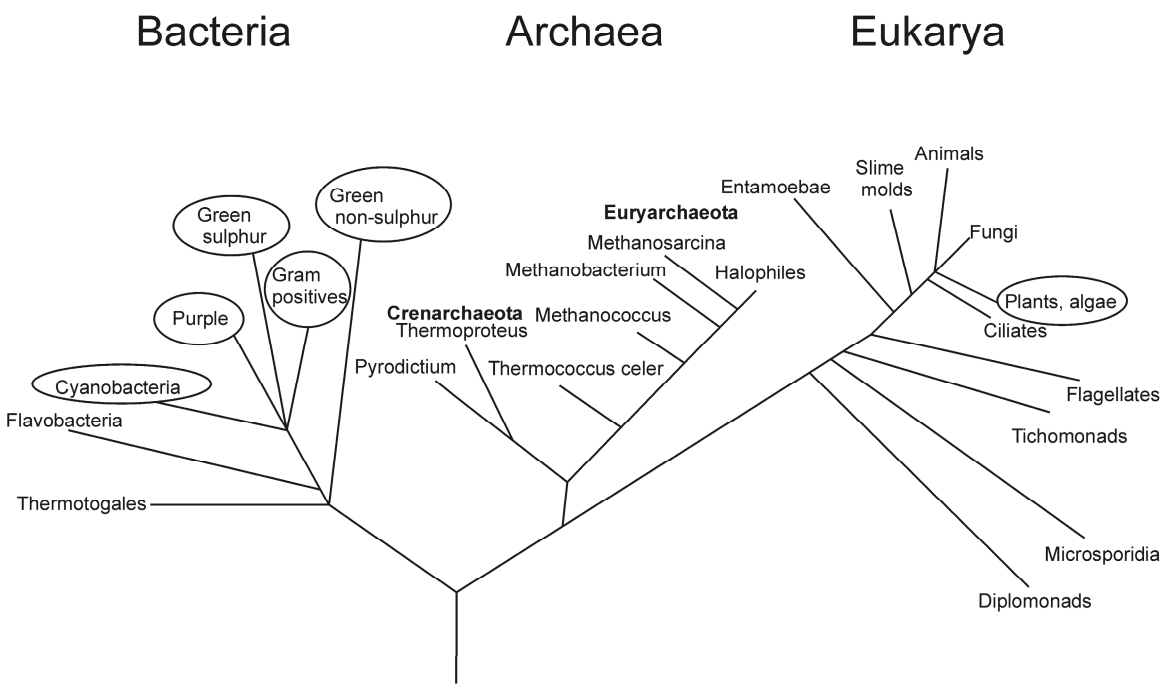

Figure 1.4. Phylogenetic tree based on the small subunit RNA method. Groups containing (B)Chl-based photosynthetic organisms are encircled (ref. 1). Heliobacteria belong to the Gram positive organisms.

DD (29). In RCs of *Rb. sphaeroides* R-26, both absorptive and emissive signals are observed. This difference in the sign change in the photo-CIDNP patterns between R-26 and WT RCs of *Rb. sphaeroides* can be explained by the contribution of the DR mechanism (30).

1.1.2 *Experimental setup*

The setup used for the photo-CIDNP experiments under continuous illumination is designed for a standard Bruker wide bore MAS NMR probe as shown in Fig. 1.3. The points that were modified in the probe are shown in the figure. The setup consists of a 1000-Watt xenon arc lamp containing collimation optics, a liquid filter and glass filters, a focusing element and a light fibre. The light is transported from the xenon arc lamp to the stator inside the probe with a light fibre bundle (16).

1.2 Photosynthetic organisms

Various methods are used for the classification of living organisms, one of which is based on the evolutionary relationships. This approach can be based on the small subunit rRNA method developed by Carl Woese (31). With the availability of more data on photosynthetic organisms, the phylogenetic trees continue to be improved. However, the data interpretation remains controversial. Organisms are placed into three domains, bacteria, archaea (also known as archaebacteria) and eukarya. Photosynthetic organisms that use tetrapyrrole based

photosynthesis are present in two of these domains (Fig. 1.4). Plants, algae and cyanobacteria perform oxygenic photosynthesis which results in the production of oxygen. Anoxygenic photosynthesis is carried out by bacteria that have only one type of photosystem, either type I or type II.

The origin and evolution of photosynthesis has been analysed and discussed over a long time. Phylogenetic and molecular studies on RC core proteins indicate that the two types of RC complexes may have evolved from a common ancestor but the nature of the earliest photosynthetic organisms has not yet been resolved (32-38). The bacteria capable of photosynthesis are purple sulphur bacteria, purple non-sulphur bacteria, green sulphur bacteria, green non-sulphur bacteria, obligate aerobic photosynthetic bacteria, heliobacteria and cyanobacteria. Purple bacteria contain type II RCs while cyanobacteria are the only group of bacteria that is oxygenic and contains both types of RCs. The first X-ray structure of an intrinsic membrane protein complex was determined from purple bacterial RCs (39). The most studied RC from green non-sulphur bacteria or green filamentous bacteria is from *Chloroflexus aurantiacus*. The photosynthetic apparatus in these bacteria is unique as it combines the properties of both the green sulphur bacteria and the purple bacteria (40). The light harvesting system is similar to that of green sulphur bacteria, while they are similar to purple non-sulphur bacteria (*Rhodospirillaceae*) regarding the optical properties of the RC (41).

The proposed hypotheses on the evolution of the RCs can be generalised into two models (2, 42). The selective loss model postulates that a common ancestor of type I and type II RCs was similar to oxygenic cyanobacteria which contained both types of RCs. The various anoxygenic forms of bacteria arose by the loss of one or the other photosystem. The most recent revision of this model suggest that a group termed 'procyanobacteria' containing type I RCs was the ancestral prototype from which an evolutionary precursor of type II RCs (37). The fusion model proposes that type I and type II RCs evolved independently. In this scheme the common ancestor gave rise to two separate lines one containing RCI and the other RCII. RC I evolved to form the RCs from heliobacteria and green sulphur bacteria, while RCII led to the formation of RCs from purple bacteria and green filamentous bacteria. The RCs of cyanobacteria were the result of a genetic fusion between an organism containing RCI and an organism containing RCII (2). A more recent version of this hypothesis places purple bacterial RCs as the ancestor which evolved along three different pathways. The first pathway led to the evolution of type II RCs found in green filamentous bacteria. The second led to the development of type II RCs found in cyanobacteria while the third pathway gave rise to type I RCs found in heliobacteria. The heliobacterial RC then further divided into two different pathways, one leading to the type I RC of green sulphur bacteria and the second to the type I RC found in cyanobacteria (2, 43, 44). Recent studies on phylogenetic analysis of the chlorophyll biosynthetic pathway indicate that anoxygenic photosynthetic organisms were the

first to evolve prior to oxygenic photosynthetic organisms (43). These studies also suggest that purple bacterial descendants may be most ancient with respect to the chlorophyll biosynthetic pathway (43) and that heliobacteria are the closest common ancestors of all oxygenic photosynthetic lineages despite their biochemical analysis, which reveals that they contain the most primitive photosynthetic machinery (45, 46).

1.2.1 *Plants and Cyanobacteria*

Plants are considered to be the most complex photosynthetic organisms. Plants, algae and cyanobacteria have a similar basic structure of their photosynthetic membrane. The photosynthetic machinery is embedded into folds of the cell membrane, the thylakoids and contains two photosystems, PSI and PSII. The photosynthetic process in these organisms is oxygenic and PSII oxidizes water to produce oxygen.

The X-ray structures of both cyanobacterial and plant PSI are available and provide information regarding the arrangement of the cofactors in the electron transport chain (47-49). They represent the only available crystal structures of RCs from type I. The cyanobacterial PSI structure is built from twelve protein subunits and 127 cofactors comprising 96 chlorophylls, 2 phylloquinones, three [Fe_4S_4] clusters, 22 carotenoids, four lipids, a putative Ca^{2+} ion and 201 water molecules (47). For higher plants the structure reveals an additional four different light-harvesting membrane proteins assembled in a half-moon shape on one side of the core (48, 49). The positions of chlorophylls in the core complex are found to be conserved between cyanobacterial and plant PSI. The plant RC moiety retains the location and orientation of the electron transfer components and most of the cyanobacterial transmembrane helices. In addition to these retained features, four RC proteins subunits, G, H, N, and O are present exclusively in plants and green algae (50, 51) while two subunits, X and M, are exclusively found in cyanobacteria. The central part of the RC is formed by a heterodimer, comprising the major subunits PsaA and PsaB. The organization of the antenna system in PSI contains a core antenna system surrounding the electron transfer chain. A peripheral antenna system is present on both sides.

The electron transfer chain in PSI comprises of six chlorophylls, two phylloquinones and three iron sulphur [Fe_4S_4] clusters. They are arranged in two branches. The first Chl pair termed as P700 is a heterodimer consisting of one Chl *a* and its epimer, a Chl *a'* molecule (52). The second pair is also Chl *a* and the third pair of Chl *a* molecules in both branches probably represents the primary electron acceptor assigned as A_0. One or both of the phylloquinones could be the secondary electron acceptor A_1. The arrangement of the three Fe_4S_4 clusters in the crystal structure is in agreement with spectroscopic studies and is in the order of F_X, F_A and F_B as shown in Fig. 1.1A on the acceptor side.

PSII is the only RC that has the capability of oxidising water to oxygen. The crystal structure of PSII from cyanobacteria is available with a resolution between 3.8 and 3.2 Å

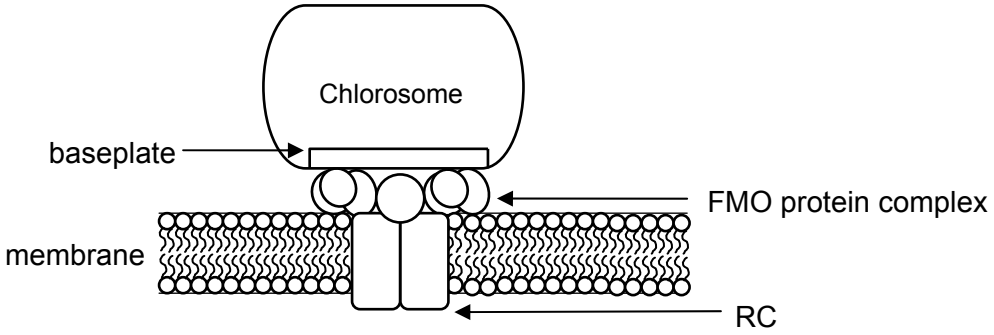

Figure 1.5. Schematic representation of antenna system and RC in green sulphur bacteria associated with the membrane (adapted from ref. 64).

(53-55). The core of the RC complex is a heterodimer, containing the D1 and D2 subunits. The cofactors in the electron transfer chain form two branches, comprising four Chl *a* molecules including a pair of Chl *a* molecules termed P_{D1} and P_{D2}, two Chl *a* molecules, two Phe molecules, $Pheo_{D1}$ and $Pheo_{D2}$ and two plastoquinone molecules. The inner antenna subunits are CP43 and CP47 which are found on adjacent sides to D1and D2, respectively.

Photo-CIDNP observed on PSI is presented in **chapter 2** of this thesis. The magnetic field dependence of photo-CIDNP MAS NMR signals observed in plant PSI and PSII is described in **chapter 3** of this thesis.

1.2.2 *Green sulphur bacteria*

Green sulphur bacteria are exclusively photoautotrophic. They are found in habitats which are anaerobic and abundant in reduced sulphur compounds, like the bottom of stratified lakes where there is low light intensity. They are also found growing below other photosynthetic organisms like algae, cyanobacteria and purple bacteria (56). Due to their habitat, which is characterised by low light intensity, they have large, highly specialised light harvesting complexes called chlorosomes. Recently a stable population of green sulfur bacteria has been isolated from the Black sea chemocline which represents the most extreme low light adapted and slowest growing type of phototroph known to date (57). A previously unknown green sulfur bacterial species has been isolated from a deep-sea hydrothermal vent, where the only source of light is geothermal radiation that includes wavelengths absorbed by photosynthetic pigments of this organism (58).

They belong to the family *Chlorobiaceae*, which is divided into two species, green and brown. The green species contains BChl *c* or *d*, and the carotenoid chlorobactene as a light harvesting pigment (59). The brown species contain BChl *e*, and carotenoids isorenieratene and β isorenieratene as light harvesting pigments (60). The photosynthetic pigment system consists of chlorosomes which are found attached to the inner side of the cytoplasmic membrane, Fenna-Matthews-Olson protein complexes and RC core complexes. The chlorosome is connected with the cytoplasmic membrane via the baseplate (61). The FMO

protein complex is located between the chlorosome and the RC complex. It contains only BChl *a* and is tightly bound to the RC complex. A schematic representation is shown in Fig. 1.5. In **chapter 4** the RCs isolated from the green sulphur bacterium *Chlorobium tepidum* are investigated.

On the basis of functional, structural and genetic data, the RC of green sulphur bacteria is believed to be similar to the RC of PSI (62). The RC core complex of green sulphur bacteria is formed by a homodimeric protein (62). The primary electron donor (P840) is a dimer of BChl *a* (64). The primary electron acceptor absorbs at 670 nm and has been shown to be a Chl *a* which is similar to plant and cyanobacterial Chl *a* except that it is esterified with Δ2,6-phytadienol rather than a phytol (65).

The putative quinone binding site appears to be conserved in PSI, green sulphur bacteria and heliobacteria (34), indicating that the secondary electron acceptor in green sulphur bacteria could be a quinone. On the other hand, experimental evidence shows that electron transport in the RC of green sulphur bacteria and heliobacteria can still function when the quinone is removed (66, 67).

1.2.3 *Heliobacteria*

In **chapter 5** of this thesis, the photosynthetic membrane fragments of the heliobacterium *Heliobacillus mobilis* have been investigated. The organisms belonging to this group are placed in a distinct family, termed *Heliobacteriaceae* (68). They are found in diverse habitats primarily in garden soil, soil from rice fields and in hot springs. Unlike purple and green bacteria, they require high light intensities. Based on 16S ribosomal RNA sequence analysis, they are classified together with Gram positive bacteria (69). All species belonging to this family are characterized by the presence of a unique BChl called BChl *g* (70).

Although the architecture of the photosynthetic system of the heliobacteria resembles the organisation in plant PSI and green sulphur bacteria, it is simpler, having a smaller antenna system associated with the RC. The antenna pigments and RC are bound to a single pigment protein complex (71, 72). This is a homodimer of two 65 kDa proteins (73). The RCs contain around 37 BChl along with six chlorins that constitute the two branches of electron transfer (74). The primary electron donor is called P798 (75) and is probably a dimer of BChl *g* (76, 77) or 13^2-epimer of BChl *g*, BChl *g*′ (78). On the basis of experimental data, the primary electron acceptor is proposed to be 8^1- hydroxy Chl *a* esterified with farnesol, absorbing at 670 nm (79). The electron transport pigment appears to be similar to that found in PSI (46, 80). Membranes of heliobacteria contain menaquinone in the RCs (81). EPR and optical spectroscopic data indicate the presence of iron sulphur centers F_X, F_A and F_B (82, 83).

References

1. Blankenship, R.E. In *Molecular mechanisms of photosynthesis*; Blackwell Science: Oxford, 2002.
2. Olson, J.M.; Blankenship, R.E., *Photosynth. Res.* **2004**, 80, 373-386.
3. Hoff, A.J.; Deisenhofer, J., *Phys. Rep.* **1997**, 287, 2-247.
4. Nelson, N.; Ben-Shem, A., *Nat. Rev. Mol. Cell Bio.* **2004**, 5, 971-982.
5. Golbeck, J.H., *Proc. Natl. Acad. Sci. U. S. A.* **1993**, 90, 1642-1646.
6. Laws, D.D.; Bitter, H.M.L.; Jerschow, A., *Angew.Chem. Int. Ed.* **2002**, 41, 3096-3129.
7. Castellani, F.; Van Rossum, B.J.; Diehl, A.; Rehbein, K.; Oschkinat, H., *Biochemistry* **2003**, 42, 11476-11483.
8. Lange, A.; Becker, S.; Seidel, K.; Giller, K.; Pongs, O.; Baldus, M., *Angew.Chem. Int. Ed.* **2005**, 44, 2089-2092.
9. Zech, S.G.; Wand, A.J.; McDermott, A.E., *J Am Chem Soc* **2005**, 127, 8618-8626.
10. de Groot, H.J.M., *Curr. Opin. Struc. Biol.* **2000**, 10, 593-600.
11. Bargon, J.; Fischer, H.; Johnsen, U., *Z. Naturforsch. C.* **1967**, A 22, 1556-1562.
12. Ward, H.R.; Lawler, R.G., *J. Am. Chem. Soc.* **1967**, 89, 5518-5519.
13. Zysmilich, M.G.; McDermott, A., *J. Am. Chem. Soc.* **1994**, 116, 8362-8363.
14. Zysmilich, M.G.; McDermott, A., *J. Am. Chem. Soc.* **1996**, 118, 5867-5873.
15. Zysmilich, M.G.; McDermott, A., *Proc. Natl. Acad. Sci. U. S. A.* **1996**, 93, 6857-6860.
16. Matysik, J.; Alia; Hollander, J.G.; Egorova-Zachernyuk, T.; Gast, P.; de Groot, H.J.M., *Indian J. Biochem. Biophys.* **2000**, 37, 418-423.
17. Matysik, J.; Alia; Gast, P.; Lugtenburg, J.; Hoff, A.J.; de Groot H.J.M. In *Perspectives on Solid State NMR in Biology*; Kiihne, S., de Groot H.J.M., Eds.; Kluwer: Dordrecht, 2001; p 215-225.
18. Schulten, E.A.M.; Matysik, J.; Alia; Kiihne, S.; Raap, J.; Lugtenburg, J.; Gast, P.; Hoff, A.J.; de Groot, H.J.M., *Biochemistry* **2002**, 41, 8708-8717.
19. Matysik, J.; Alia; Gast, P.; van Gorkom, H.J.; Hoff, A.J.; de Groot, H.J.M., *Proc. Natl. Acad. Sci. U. S. A.* **2000**, 97, 9865-9870.
20. Diller, A.; Alia; Roy, E.; Gast, P.; van Gorkom, H.J.; Zaanen, J.; de Groot, H.J.M.; Glaubitz, C.; Matysik, J., *Photosynth. Res.* **2005**, 84, 303-308.
21. Diller, A.; Roy, E.; Gast, P.; van Gorkom, H.J.; de Groot, H.J.M.; Glaubitz, C.; Jeschke, G.; Matysik, J. ; Alia, A. *Proc. Natl. Acad. Sci. U. S. A.* **2007**, 104, 12767-12771.
22. Matysik, J.; Schulten, E.; Alia; Gast, P.; Raap, J.; Lugtenburg, J.; Hoff, A.J.; de Groot, H.J.M., *Biol. Chem.* **2001**, 382, 1271-1276.
23. Daviso, E.; Jeschke, G.; Matysik, J. In *Biophysical techniques in photosynthesis*; Aartsma, T.J., Matysik, J., Eds.; Springer: Dordrecht, 2007, p 385-399.
24. Jeschke, G.; Matysik, J., *Chem. Phys.* **2003**, 294, 239-255.
25. Jeschke, G., *J. Chem. Phys.* **1997**, 106, 10072-10086.
26. Jeschke, G., *J. Am. Chem. Soc.* **1998**, 120, 4425-4429.
27. Polenova, T.; McDermott, A.E., *J. Phys. Chem. B* **1999**, 103, 535-548.
28. McDermott, A.; Zysmilich, M.G.; Polenova, T., *Solid State Nucl. Magn. Reson.* **1998**, 11, 21-47.

29. Prakash, S.; Alia; Gast, P.; de Groot, H.J.M.; Jeschke, G.; Matysik, J., *J Am Chem Soc* **2005**, 127, 14290-14298.
30. Prakash, S.; Alia; Gast, P.; de Groot, H.J.M.; Matysik, J.; Jeschke, G., *J. Am. Chem. Soc.* **2006**, 128, 12794-12799.
31. Woese, C.R.; Kandler, O.; Wheelis, M.L., *Proc. Natl. Acad. Sci. U. S. A.* **1990**, 87, 4576-4579.
32. Mulkidjanian, A.Y.; Junge, W., *Photosynth. Res.* **1997**, 51, 27-42.
33. Blankenship, R.E.; Hartman, H., *Trends Biochem. Sci.* **1998**, 23, 94-97.
34. Schubert, W.D.; Klukas, O.; Saenger, W.; Witt, H.T.; Fromme, P.; Krauss, N., *J. Mol. Biol.* **1998**, 280, 297-314.
35. Rivera, M.C.; Lake, J.A., *Nature* **2004**, 431, 152-.
36. Nelson, N.; Ben-Shem, A., *BioEssays* **2005**, 27, 914-922.
37. Mulkidjanian, A.Y.; Koonin, E.V.; Makarova, K.S.; Mekhedov, S.L.; Sorokin, A.; Wolf, Y.I.; Dufresne, A.; Partensky, F.; Burd, H.; Kaznadzey, D.; Haselkorn, R.; Galperin, M.Y., *Proc. Natl. Acad. Sci. U. S. A.* **2006**, 103, 13126-13131.
38. Allen, J.F.; Martin, W., *Nature* **2007**, 445, 610-612.
39. Deisenhofer, J.; Epp, O.; Miki, K.; Huber, R.; Michel, H., *Nature* **1985**, 318, 618-624.
40. Pierson, B.K.; Thornber, J.P., *Proc. Natl. Acad. Sci. U. S. A.* **1983**, 80, 80-84.
41. Reiner, F.; Shiozawa, J.A.; Ertlmaier, A. In *Anoxygenic photosynthetic bacteria*; Blankenship, R.E., Madigan, M.T., Bauer, C.E., Eds.; Kluwer: Dordrecht, 1995; p 699-708.
42. Xiong, J. *Genome Biol.* **2006**, 7, 245-249.
43. Xiong, J.; Bauer, C.E., *An. Rev. Plant Biol.* **2002**, 53, 503-521.
44. Xiong, J.; Bauer, C.E., *J. Mol. Biol.* **2002**, 322, 1025-1037.
45. Xiong, J.; Fischer, W.M.; Inoue, K.; Nakahara, M.; Bauer, C.E., *Science* **2000**, 289, 1724-1730.
46. Blankenship, R.E., *Trends Plant Sci.* **2001**, 6, 4-6.
47. Jordan, P.; Fromme, P.; Witt, H.T.; Klukas, O.; Saenger, W.; Krauss, N., *Nature* **2001**, 411, 909-917.
48. Ben-Shem, A.; Frolow, F.; Nelson, N., *Nature* **2003**, 426, 630-635.
49. Amunts, A.; Drory, O.; Nelson, N., *Nature* **2007**, 447, 58-63.
50. Scheller, H.V.; Jensen, P.E.; Haldrup, A.; Lunde, C.; Knoetzel, J., *Biochim. Biophys. Acta* **2001**, 1507, 41-60.
51. Knoetzel, H.; Mant, A.; Haldrup, A.; Jensen, P.E.; Scheller, H.V., *FEBS Lett.* **2002**, 510, 145-148.
52. Watanabe, T.; Kobayashi, M.; Hongu, A.; Nakazato, M.; Hiyama, T.; Murata, N., *FEBS Lett*. **1985,** 191, 252-256.
53. Zouni, A.; Witt, H.T.; Kern, J.; Fromme, P.; Krauss, N.; Saenger, W.; Orth, P., *Nature* **2001**, 409, 739-743.
54. Ferreira, K.N.; Iverson, T.M.; Maghlaoui, K.; Barber, J.; Iwata, S., *Science* **2004**, 303, 1831-1838.
55. Biesiadka, J.; Loll, B.; Kern, J.; Irrgang, K.D.; Zouni, A., *Phys. Chem. Chem. Phys.* **2004**, 6, 4733-4736.
56. Vila, X.; Abella, C.A., *Photosynth. Res.* **1994**, 41, 53-65.
57. Manske, A.K.; Glaeser, J.; Kuypers, M.A.M.; Overmann, J., *Appl. Environ. Microbiol.* **2005**, 71, 8049-8060.

58. Beatty, J.T.; Overmann, J.; Lince, M.T.; Manske, A.K.; Lang, A.S.; Blankenship, R.E.; Van Dover, C.L.; Martinson, T.A.; Plumley, F.G., *Proc. Natl. Acad. Sci. U. S. A* **2005**, 102, 9306-9310.
59. Gloe, A.; Pfennig, N.; Brockmann, H.; Trowitzsch, W., *Arch. Microbiol.* **1975**, 102, 103-109.
60. Imhoff, J.F. In *Anoxygenic photosynthetic bacteria*; Blankenship, R.E., Madigan, M.T., Bauer, C.E., Eds.; Kluwer: Dordrecht, 1995; p 665-685.
61. Staehelin, L.A.; Golecki, J.R.; Drews, G., *Biochim. Biophy. Acta* **1980**, 589, 30-45.
62. Feiler, U.; Hauska, G. In *Anoxygenic photosynthetic bacteria*; Blankenship, R.E., Madigan, M.T., Bauer, C.E., Eds.; Kluwer: Dordrecht, 1995; p 665-685.
63. Buttner, M.; Xie, D.L.; Nelson, H.; Pinther, W.; Hauska, G.; Nelson, N., *Proc. Natl. Acad. Sci. U. S. A.* **1992**, 89, 8135-8139.
64. Hauska, G.; Schoedl, T.; Remigy, H.; Tsiotis, G., *Biochim. Biophys. Acta.* **2001**, 1507, 260-277.
65. Kobayashi, M.; Oh-Oka, H.; Akutsu, S.; Akiyama, M.; Tominaga, K.; Kise, H.; Nishida, F.; Watanabe, T.; Amesz, J.; Koizumi, M.; Ishida, N.; Kano, H., *Photosynth. Res.* **2000**, 63, 269-280.
66. Kleinherenbrink, F.A.M.; Ikegami, I.; Hiraishi, A.; Otte, S.C.M.; Amesz, J., *Biochim. Biophys. Acta* **1993**, 1142, 69-73.
67. Frankenberg, N.; Hager-Braun, C.; Feiler, U.; Fuhrmann, M.; Rogl, H.; Schneebauer, N.; Nelson, N.; Hauska, G., *Photochem. Photobiol.* **1996**, 64, 14-19.
68. Beer-Romero, P.; Gest, H., *FEMS Microbiol. Lett.* **1987**, 41, 109-114.
69. Woese, C.R., *Microbiol. Rev.* **1987**, 51, 221-271.
70. Brockmann, H.; Lipinski, A., *Arch. Microbiol.* **1983**, 136, 17-19.
71. Trost, J.T.; Blankenship, R.E., *Biochemistry* **1989**, 28, 9898-9904.
72. van de Meent, E.J.; Kleinherenbrink, F.A.M.; Amesz, J., *Biochim. Biophys. Acta* **1990**, 1015, 223-230.
73. Liebl, U.; Mockensturm-Wilson, M.; Trost, J.T.; Brune, D.C.; Blankenship, R.E.; Vermaas, W., *Proc. Natl. Acad. Sci. U. S. A.* **1993**, 90, 7124-7128.
74. Neerken, S.; Amesz, J., *Biochim. Biophys. Acta.* **2001**, 1507, 278-290.
75. Fuller, R.C.; Sprague, S.G.; Gest, H.; Blankenship, R.E., *FEBS Lett.* **1985**, 182, 345-349.
76. Prince, R.C.; Gest, H.; Blankenship, R.E., *Biochim. Biophys. Acta* **1985**, 810, 377-384.
77. Brok, M.; Vasmel, H.; Horikx, J.T.G.; Hoff, A.J., *FEBS Lett.* **1986,** 194, 322-326.
78. Kobayashi, M.; van de Meent, E.J.; Erkelens, C.; Amesz, J.; Ikegami, I.; Watanabe, T., *Biochim Biophys Acta* **1991**, 1057, 89-96.
79. van de Meent, E.J.; Kobayashi, M.; Erkelens, C.; van Veelen, P.A.; Amesz, J.; Watanabe, T., *Biochim. Biophys. Acta* **1991**, 1058, 356-362.
80. Golbeck, J.H.; Bryant, D.A., *Curr. Top. Bioenerg.* **1991**, 16, 83-177.
81. Muhiuddin, I.P.; Rigby, S.E.J.; Evans, M.C.W.; Amesz, J.; Heathcote, P., *Biochemistry* **1999**, 38, 7159-7167.
82. Neerken, S.; Amesz, J., *Biochim. Biophys. Acta* **2001**, 1507, 278-290.
83. Heinnickel, M.; Golbeck, J.H., *Photosynth. Res.* **2007**, 92, 35-53.

2 Photo-CIDNP observed in photosystem I from plants

Photo-CIDNP has been observed in photosystem I of spinach by ^{13}C magic angle spinning solid-state NMR under continuous illumination with white light. All the light-induced ^{13}C NMR signals appear to be emissive. An almost complete set of chemical shifts of the aromatic ring carbons of a single Chl *a* molecule has been obtained.

2.1 Introduction

Photosynthesis in plants is driven by light-induced electron transfer in the two RCs, PSI and PSII. The oxidised primary electron donor of PSII, is a very powerful oxidising agent (1), even enabling the oxidation of water, while the electronically excited primary electron donor of PSI, is a strong reducing agent (2). The X-ray structure at a resolution of 2.5Å of PSI from the thermophilic cyanobacterium *Synechococcus elongatus* shows the arrangement of cofactors. They are in two branches called A and B corresponding to the protein subunits that comprise the core (Fig. 2.1) (3). The three dimensional structure shows that P700 is a heterodimer formed by one Chl *a* molecule and one Chl *a*′ molecule, which is the $C13^2$-epimer of Chl *a*. Due to their 5-coordination, both Chl macrocycles are domed. The interplanar distance between both macrocycles is 3.6 ± 0.3 Å. Chl *a*′ forms hydrogen bonds to its environment (Fig. 2.2) (3). There are no hydrogen bonds found on the Chl *a* side. In comparison to the special pair of purple bacterial RCs (4), P700 is a heterodimer, having a shorter distance between the chlorophylls. In addition there is partial overlap of rings I and II while in purple bacterial RCs the rings I have a more perfect overlap (5). The electronic structure of P700 remains under discussion (2). The available spectroscopic data are mainly from vibrational and electron paramagnetic resonance methods. The observation of a broad mid-IR transition (6, 7) in the oxidised and paramagnetic $P700^{+\bullet}$ is generally interpreted as proof for charge repartition over two Chl cofactors, called P1 and P2. As concluded from the C=O stretching vibrations, P1 is hydrogen-bonded on both keto-functions and can be assigned to the Chl *a*′. It carries all the triplet character of $^3P700$, while the carbonyl groups of P2 are free from hydrogen bonding interaction (8). Mutant studies provide evidence for electronic coupling between the two halves of the dimer (9). Data from different electron paramagnetic resonance spectroscopies, such as EPR (10-12), ENDOR (12-19) and ESEEM (20-24), have been interpreted quite differently. Originally, a symmetric dimer (10, 15) and a Chl monomer

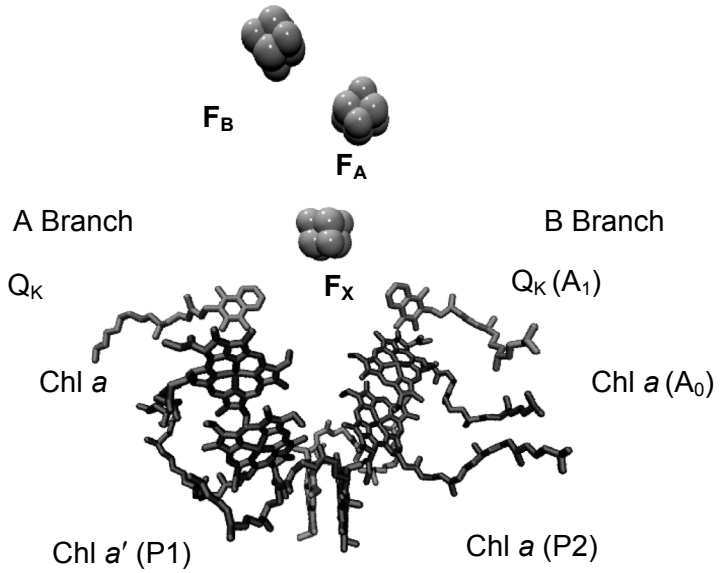

Figure 2.1. The arrangement of cofactors in the electron transfer chain in RC of PSI. The figure was made using VMD molecular graphic programme (http://www.ks.uiuc.edu/Research/vmd/).

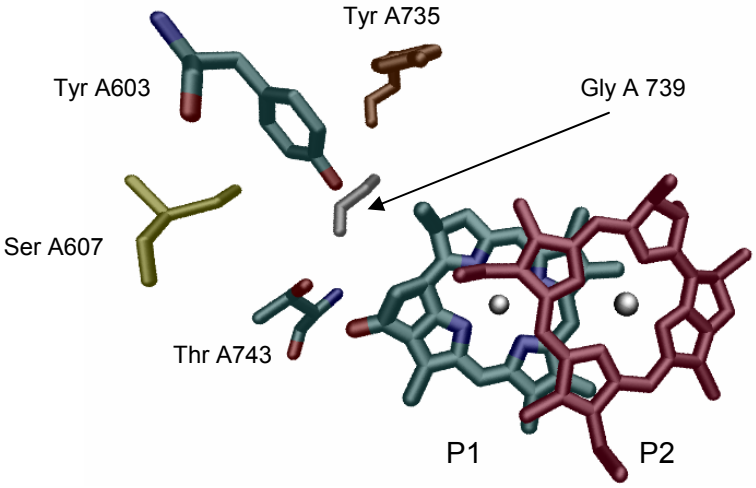

Figure 2.2. Structure of P700 showing residues in the environment involved in formation of hydrogen bond on the Chl *a*′ side. The figure was made using VMD molecular graphic programme.

(14) were proposed. More recently, an asymmetric dimer has been proposed (14, 18), in which the second Chl (P1) carries about ≤15% of the spin density (19). A very recent molecular orbital study based on the 2.5Å structure indeed described P700 as dimer with an asymmetric electron spin density distribution in favour of the monomeric Chl *a* (P2) half by a spin density ratio of almost 5:1 (25).

NMR chemical shift information allows for the exploration of spatial, protonic and electronic structures with atomic selectivity in the electronic ground state. Such an analysis can provide detailed insight into the functional mechanisms of proteins. For several

photosynthetic RCs of bacteria and plants it has been shown that photo-CIDNP can overcome the intrinsic insensitivity and non-selectivity of NMR spectroscopy by photochemical induction of a non-Boltzmann population of nuclear spin states. Photo-CIDNP has been observed in quinone-blocked bacterial RCs from *Rb. sphaeroides* R-26 (26-29) and WT (30) and PSII complexes from plants (31). The strong enhancement by the combination of selective ^{13}C-isotope labelling at several cofactor positions allows obtaining two-dimensional photo-CIDNP MAS NMR spectra (32). This has demonstrated that the electron density of the two BChl molecules of the special pair is already different in the electronic ground state of the bacterial RC. In addition, NMR signals were detected in entire membrane-bound bacterial photosynthetic units (>1.5 MDa) (33). In the D1D2 complex of PS II of plants, the observation of the pronounced electron spin density on rings III and V by photo-CIDNP MAS NMR was taken as an indication for a local electric field, leading to a hypothesis about the origin of the remarkable strength of the redox potential of the primary electron donor (31).

In PSI, light-induced electron spin polarisation has been observed for the first time in 1975 (37, 38). Photo-CIDNP solid-state NMR intensities are linked to the local electron spin densities occurring in the radical-pair state (34- 36). Photo-CIDNP intensities are proportional to the nuclear polarisation, and thus depend strongly on the anisotropy of the hyperfine coupling. The exact link between the local electron-spin densities and the photo-CIDNP intensities, however, remains a topic for further studies. The photo-CIDNP effect in solid-state is explained by three mechanisms, TSM, DD and DR (35, 36). This chapter investigates the photo-CIDNP data of PSI observed by ^{13}C MAS NMR.

2.2 Materials and Methods

2.2.1 *PSI particle preparation*

The PSI complex containing ~110 Chl/P700, termed the PSI-110 particles, was prepared from spinach according to Mullet *et al.* (39). The chloroplasts were isolated by grinding excised leaves in 0.4 M Sorbitol and 50 mM Tricine buffer (pH 7.8) as previously described (40). The isolated chloroplasts were then washed with 10 mM Tricine buffer (pH 7.8) containing 50 mM Sorbitol and 5 mM EDTA, and re-suspended in buffer containing 10 mM Tricine (pH 7.8) to obtain a final concentration of 0.8 mg Chl/mL. The membranes were solubilised with Triton X-100 to a final concentration of 0.8% w/v for 30 minutes at room temperature in the dark with continuous slow stirring. These solubilised membranes were centrifuged at 39,000 *g* for 20 min at a temperature of 4 ºC and the supernatant fraction was loaded onto a linear sucrose gradient (0.1 - 1.0 M sucrose, 10 mM Tricine, 0.02% Triton X-100, pH 7.8) which was prepared on a 2 M sucrose cushion followed by ultracentrifugation at 150,000 *g* for 18 h at 4 ºC. PSI-110 particles appeared as a dark green non fluorescent band just above the 2 M sucrose cushion. After collecting this band, the PSI-110 particles were

dialysed overnight against 10 mM Tricine and concentrated by ultracentrifugation at 150,000 *g* for 16 h. PSI-110 particles were finally suspended in 5 mM Tricine buffer (pH 7.8) containing 50 mM Sorbitol. The chlorophyll content of PSI-110 was determined by the method of Arnon *et al*. (41). PSI-110 particles equivalent to ~2 mg Chl/mL were used for NMR measurements.

CPI particles (PSI particles containing ~40 Chl/P700 and lacking the ferredoxin acceptors F_X, F_B, F_A) were prepared using a modification of the method of Rutherford and Mullet.(42) In brief, the PSI-110 particles (1 mg Chl/mL) were incubated with 2% lithium dodecyl sulphate for one hour at 4 °C. Subsequently, the particles were loaded on a linear sucrose gradient (0.1-1 M sucrose, 10 mM Tricine, 0.1% sodium cholate, pH 8) and centrifuged at 150,000 *g* for 16 h. The CPI particles appeared as a dark green band approximately 2 cm from the bottom of the centrifuge tube. This band containing CPI particles was dialysed overnight against 10 mM Tricine and concentrated by centrifugation at 150,000 *g* for 16 h. The purity of the PSI-110 particles and CPI particles was analysed by SDS-PAGE. PSI-110 was resolved into 12 clearly distinguishable bands (68, 66, 24.5, 24, 22, 22.5, 21, 17, 16.5, 11.5, 11 and 10.5 kDa). This pattern is similar to the SDS-PAGE data published earlier by Mullet *et al.* (39). CPI particles showed two bands at 66kDa and 68kDa corresponding to PsaA and PsaB polypeptides (43).

2.2.2 *MAS-NMR Measurements and DFT computations*

The NMR experiments have been performed using a DMX-400 NMR spectrometer (Bruker GmbH, Karlsruhe, Germany) equipped with a triple-resonance MAS light probe working at 396.5 MHz for protons and 99.7 MHz for ^{13}C specially designed for using the illumination set up (29). The samples were loaded into optically transparent 4 and 7 mm sapphire rotors. Reduction of ferredoxin acceptors F_B and F_A in PSI-110 particles was performed by addition of an aqueous solution of 10 mM sodium dithionite solution and 40 mM glycine buffer (pH 9.5) in an oxygen free atmosphere. Immediately following the reduction, slow freezing of the sample was performed directly in the NMR MAS probe inside the magnet with liquid nitrogen-cooled gas under continuous illumination with white light (29). In order to ensure a homogeneous sample distribution against the rotor wall a low spinning frequency ~600 Hz of the sample was used during this slow freezing. Photo-CIDNP ^{13}C MAS NMR spectra were obtained at a temperature of 223 K with continuous illumination. To distinguish the centrebands from the spinning sidebands, photo-CIDNP MAS NMR spectra were recorded at different spinning frequencies, 3.6, 4.0, 5.0, 6.4, 8.0 and 9.0 kHz. The light and dark spectra have been collected by a straightforward Bloch decay followed by a Hahn echo and TPPM proton decoupling (44). A recycle delay of 12 seconds was used and a total number of 14,000 scans per spectrum were collected over a period of 48 h.

Density functional computations were performed using ADF 2002.01 (45). Three different Chl structures were tested, i) a structure obtained from X-ray data (46) which was used without further optimisation, ii) a structure based on standard bond angles and bond lengths (47) and iii) an optimized starting structure of a BChl *a* which was edited in Titan 1.0 (Wavefunction Inc., Irvine, California, USA) to give the structure of Chl *a* in PSI shown in Fig. 2.6, with residue R substituted by a methyl group to save computation time. Further optimisation of this structure was done within ADF. A structure of an analogous Phe *a* was then obtained by deleting the Mg^{2+} ion and adding two hydrogens in Titan 1.0 allowing for a simple comparison of the principal axis frames of *g* tensors, which were computed for the optimized structure of the Chl *a* anion radical and the analogous pheophytin anion radical within the spin-restricted zeroth order relativistic approximation formalism with all-electron basis sets DZP for all atoms (48, 49). A non-relativistic spin-unrestricted computation with an all electron TZ2P basis set on all atoms was used to calculate the hyperfine tensors of Chl *a* cation and anion radicals.

2.3 Results

Fig. 2.3 shows ^{13}C MAS NMR spectra of natural abundance PSI-110 particles in the dark (A) and under continuous illumination with white light (B). Spectrum 2.3A shows the characteristic aliphatic features of a ^{13}C-MAS NMR spectrum of a protein, which is a broad signal between 0 and 50 ppm. The sharp signals at 175.7 and 41.9 ppm arise from glycine. The relatively broad signal at 179 ppm contains intensity of the protein carbonyl groups. In spectrum 2.3B, several strong emissive (negative) signals appear upon illumination. It is indeed remarkable to observe NMR signals of such intensity from the active site of a large membrane protein complex containing 110 Chls. Photo-CIDNP has been observed only in pre-reduced PSI-110 and PSI-CPI particles. The difference spectrum 2.3C shows that all the light-induced signals appear exclusively in the aromatic region.

In the spectra of the PSI-110 preparation, a total of twelve, centrebands have been identified (Fig. 2.4A-C). Using the chemical shifts reported for monomeric or aggregated Chl *a* these centrebands can be tentatively assigned to 17 carbon atoms of a single Chl *a* cofactor (Table 2.1). There is no evidence for signal doubling in the spectrum. In the carbonyl region, the carbon C-13^1 is detected as a relatively broad signal at 190.6 ppm.

The strongest signals are observed in the aromatic region between 120 and 170 ppm. The signal at 154.8 ppm shows a shoulder and can be assigned to both C-1 and C-6. The strong signal at 147.2 ppm is assigned to C-9 and C-11, which is in line with previous MAS NMR experiments on precipitated Chl *a* molecules, where these two signals are also not separated. Also the three carbons C-2, C-4 and C-8 can be detected. The broad signal at ≈132 ppm can be assigned to the carbons C-7, C-12 and C-13. The response at ≈105.4 ppm, can be assigned

Chl *a*		Carbon	PSII	PSI
σ_{liq} [a]	σ_{ss} [b]	no.	σ [c]	σ [d]
189.3	190.6	13[1]		~190.6 E
172.7	175.3	17[3]		
171.0	171.2	13[3]		
167.4	170.0	19	166.9 A	167.1 E
161.4	162.0	14	162.3 A	160.4 E
154.0	155.9	1	156.0 A	154.8 E
155.8	154.4	6		
151.4	154.0	16	151.7 A	152.6 E
148.0	150.7	4		149.9 E
147.7	147.2	11	147.7 A	147.2 E
146.1	147.2	9		
144.1	146.2	8		144.2 E
139.0	137.0	3	137.5 A	138.6 E
135.5	136.1	2		~136 E
134.2	134.0	12		
134.0	133.4	7	133.9 A	~132 E
131.5	126.2	13		
131.5	126.2	3[1]		
118.9	113.4	3[2]		
107.1	108.2	10	104.6 E	105.4 E
106.2	102.8	15		
100.0	98.1	5		
92.8	93.3	20		

Table 2.1. ^{13}C chemical shifts of the photo-CIDNP signals obtained at 9.4 Tesla when matched to published chemical shift data for Chl *a* lead to a first assignment of NMR signals. Abbreviations: σ = chemical shift, A = absorptive signal, E = emissive signal. (a) Ref. (58), the liquid NMR data have been obtained in tetrahydrofuran. (b) Ref. (59), the solid-state NMR data have been obtained from aggregates. (c) Ref. (31). (d) this work.

to both the C-10 and C-15 methine carbons.

No light induced signal is observed in the region of the aliphatic carbons. In bacterial RCs, emissive signals at about 118.5 and 134 ppm have been assigned to an axial histidine ligand of the special pair (50, 51). This is in contrast with the data for PSI, since all twelve centrebands can be conveniently assigned to a single Chl *a* cofactor.

The intensity of the photo-CIDNP signals of PSI-110 is very strong relative to the dark background. The strongest photo-CIDNP signals have about three times the intensity of the maximum of the aliphatic signals at 30 ppm. This is similar to the ratio observed from the best preparations of RCs of bacteria and of PSII in D1D2. The molecular mass of the PSI-110 preparation (≈300 kDa) is approximately a factor three larger. This means that PSI-110 shows the most intense photo-CIDNP signals ever observed in an unlabelled RC. This effect can be partially, but not exclusively attributed to the relatively narrow linewidth of 60-65 Hz, which is less than the linewidths of 80 to 100 Hz that are observed for PSII.

The spectrum obtained from the PSI-CPI preparation shows the same centrebands with a similar intensity pattern as found in PSI-110 at the same spinning frequency (Fig. 2.5). The signal at 154.8 ppm, which is assigned to both C-1 and C-6, however, is clearly reduced.

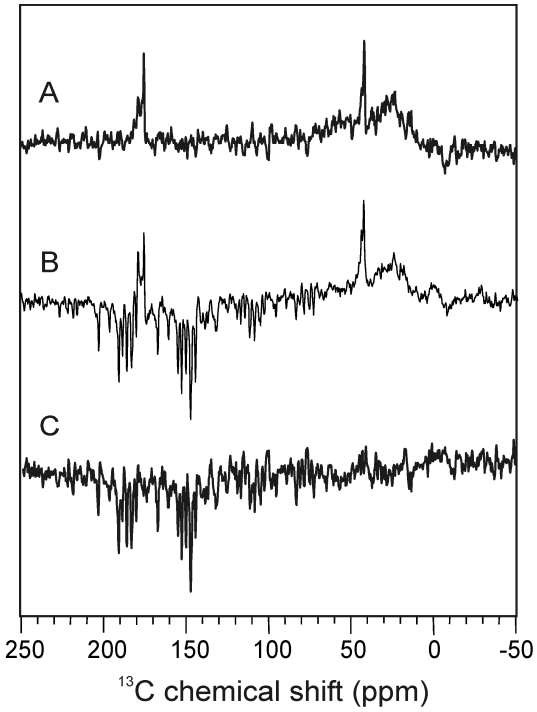

Figure 2.3. ^{13}C MAS NMR spectra of PSI-110 particles measured at 223K with a MAS frequency of 3.6 kHz. Spectra are obtained (A) in the dark, (B) under continuous illumination with white light, (C) by subtraction B – A.

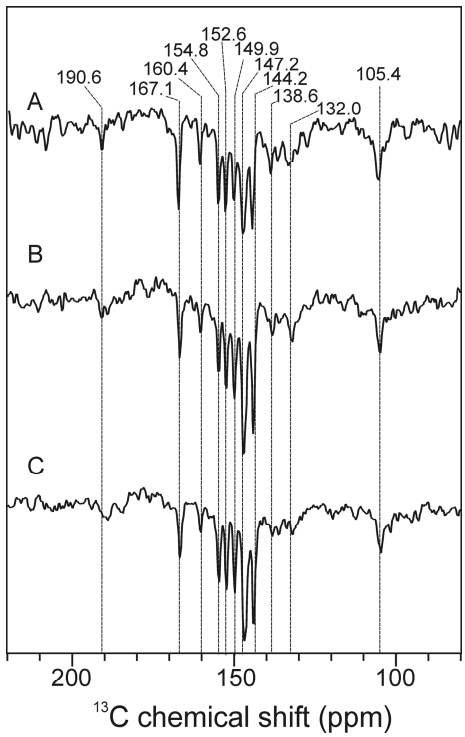

Figure 2.4. ^{13}C MAS NMR spectra of PSI-110 particles obtained under continuous illumination with white light using a MAS frequency of (A) 6.4 kHz, (B) 8.0 kHz and (C) 9.0 kHz. The assigned centerbands are shown by the dashed lines.

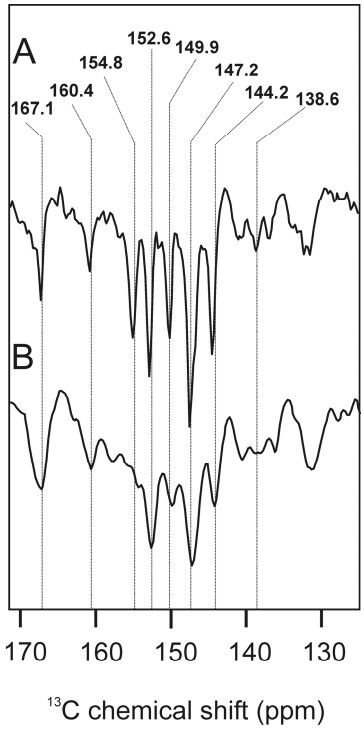

Figure 2.5. ^{13}C MAS NMR spectra of (A) PSI-110 and (B) PSI-CPI particles obtained with continuous illumination with white light at a temperature of 223K and using a MAS frequency of 3.6 kHz. In both spectra, a line-broadening of 50 Hz has been applied. The assigned centerbands are visualised by the dashed lines.

In addition, the linewidth of all signals is significantly increased. These effects indicate increased heterogeneity of the sample compared to the PSI-110 preparation. Probably the removal of the surrounding antenna apparently destabilises the RC in the PSI-CPI preparation.

2.4 Discussion

2.4.1 *The radical pair and the sign*

In the illumination experiments, photo-CIDNP enhancement can be observed. In reduced PSI-110 and PSI-CPI particles a $P_{700}^{+\bullet}$ $A_1^{-\bullet}$ radical pair is formed. The ferredoxins are removed in CPI-particles, which suggests that the quinone needs to be reduced in order to obtain photo-CIDNP. The radical pair $P_{700}^{+\bullet}$ $A_1^{-\bullet}$, produced upon illumination in the samples without pre-reduction by sodium dithionite does not produce photo-CIDNP, presumably because the electron-electron coupling is too weak. Under strong permanent illumination, the Chl *a* of the second pair of Chl *a* molecules next to P700 can also become photo-reduced (52). Since this radical pair is tightly coupled and does not produce electronic triplets, no photo-CIDNP can be expected from such an electronic structure. Therefore, it is reasonable to assume that the observed photo-CIDNP enhancement originates from the radical pair $P_{700}^{+\bullet}$ $A_0^{-\bullet}$.

The difference between a Chl *a* radical anion in PSI and a Phe *a* radical anion in PSII may

also be responsible for change of the sign of the photo-CIDNP enhancement, the most obvious difference between both RCs.

Recent EPR data on PSI suggest that the isotropic *g* value of the Chl *a* acceptor anion radical (53, 54) is closer to the isotropic *g* value of the P700 donor cation radical (55-57) rather than for the corresponding donor and acceptor in PSII and in bacterial RCs. A smaller Δg causes a smaller contribution of the DD mechanism to the nuclear polarisation and simultaneously a larger contribution of the TSM mechanism. Hence, it is possible that the TSM contribution dominates for PSI, which would explain why all signals have the same sign. For the DD contribution, the sign depends on the sign of several parameters and may even depend on orientation, while for the TSM contribution the sign depends only on the sign of the coupling between the two electron spins (35).

Earlier work demonstrated that DFT computations of the *g* tensor of the BPhe acceptor anion radicals within the ZORA formalism were in good agreement with experimental values (60). Such computations can also help to estimate differences between the *g* tensors of Chl *a* and Phe *a* anion radicals (Table 2.2). Since DFT predicts rather minor differences both in the principal values and in the principal axes directions, a sign change of the *g* tensor of the acceptor radical anion appears unlikely.

Alternatively, a change of the sign of the photo-CIDNP enhancement might be explained on the basis of the anisotropy of photo-CIDNP (35). In entire bacterial photosynthetic units containing selectively isotope labelled cofactors also a sign change occurred which has been tentatively explained by self-orientation of the membrane bound proteins induced by sample spinning around the magic angle before freezing (33). Due to the strong anisotropy of photo-CIDNP, oriented RCs are expected to show an enhancement pattern that is different from randomly oriented samples. However, the observation of a similar enhancement pattern in the smaller PSI-CPI sample makes this explanation unlikely.

	g_{11}	g_{22}	g_{33}	g_{iso}
Chl $a^{-\bullet}$	2.00461	2.00317	2.00206	2.00328
$Phe^{-\bullet}$	2.00415	2.00308	2.00211	2.00311
$\Delta\theta$	4.2°	2.6°	3.3°	-

Table 2.2. Deviations between the g tensors of a Chl *a* anion radical Chl $a^{-\bullet}$ and a pheophytin anion radical $Phe^{-\bullet}$ with analogous geometric structure from DFT computations with ADF ZORA. The directions of the principal axes deviate by $\Delta\theta$.

Photo-CIDNP sign rules (35) suggest that the difference between PSI and PSII could then be related either to a substantial difference in the electron-electron coupling, which would also shift the balance between the DD and TSM mechanisms, or to a difference in the hyperfine tensors of those nuclei for which non-equilibrium polarisation is observed.
Due to the broad similarity in the geometry of the RCs, the dipole-dipole coupling only differs slightly between the electron spins. DFT computations suggest that the SOMOs of the acceptor radical anions are rather similar, but given the lower symmetry of the donor in PSII, the SOMOs of P700 and P680 are likely to be different. If the P700 SOMO would have a strong overlap with its acceptor SOMO, this would result in a large exchange coupling and thus in a large TSM contribution. As discussed above, a larger TSM contribution would explain the uniform sign of the photo-CIDNP enhancements in PSI. As the spatial and electronic structure of the radical pair state of the whole RCs cannot be modelled precisely enough with current quantum-chemical approaches, these considerations however remain somewhat speculative. Finally, differences in the hyperfine couplings can give rise to photo-CIDNP sign and intensity changes. This point will be further elaborated after discussing the assignment of the NMR lines.

2.4.2 *Linewidth and chemical shifts*

The narrow linewidth of ≈60 Hz provides evidence for a rather rigid ordered as well as structurally and electrostatically stable donor site. Previous MAS NMR studies revealed similar properties of the donor site in bacterial RCs (61). It appears to be a general property of RCs to have a rigid donor side, keeping reorganisation energies of electron transfer low.

The photo-CIDNP signals of PSI appear considerably stronger than for unlabelled RCs of bacteria and PSII. In addition to the narrower lines, the photo-CIDNP signals may appear to be stronger due to a modified proportion of the two mechanisms producing nuclear enhancement. The predominant effect of the TSM over the DD mechanism in the stronger photo-CIDNP of PSI, as proposed here, would imply that both mechanisms cause opposite effects under current conditions, which is well in line with the model computations in ref (35).

The observed twelve photo-CIDNP signals appear in between 200 and 90 ppm. In this region, a comprehensive set of initial assignments can be obtained. The data are in agreement with previously measured photo-CIDNP spectra of unlabelled RCs of bacteria and of PSII, where no aliphatic carbons have been observed. The moderately high spinning frequency achieved here allows for the first time for an unequivocal detection of a carbonyl response of the aromatic macrocycle in a photo-CIDNP MAS NMR spectrum. The absence of aliphatic carbons is attributed to a weak pseudosecular coupling to the electron pair. There are no signals that can be attributed to amino acids of the surroundings.

The photo-CIDNP data can be assigned to a single Chl *a* cofactor. Since in PSI both the donor and the primary acceptor are Chl *a* cofactors, the possibility that the spectrum contains

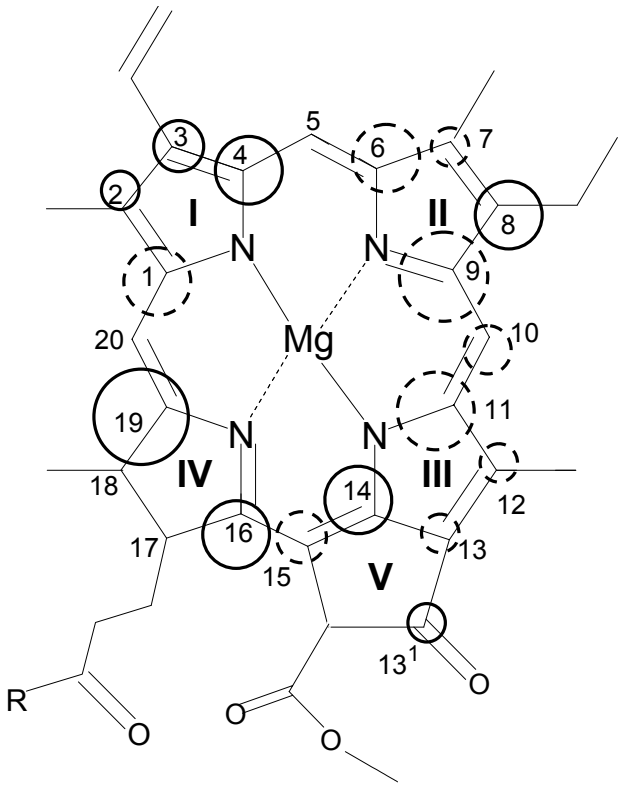

Figure 2.6. ^{13}C Photo-CIDNP patterns of Chl *a* molecule observed in PSI. The size of the circles is semi-quantitatively related to the signal intensity. All observed photo-CIDNP enhanced NMR signals are negative (emissive). The solid circles indicate a clear assignment; the dashed circles rely on signals assigned to two or three carbons (Table 2.1). The numbering of the carbons is according to IUPAC.

contributions from both the donor and the acceptor cofactors on the basis of only the chemical shifts cannot be completely excluded. However, the calculations suggest the appearance of stronger ^{13}C photo-CIDNP NMR signals from the donor than the acceptor as discussed in the following paragraph. This spectral predominance has also been observed in selectively isotope labelled bacterial RCs, for which an unambiguous assignment was possible (32).

2.4.3 *Assignment of the cofactors*

The assignment of observed carbon resonances allows for a semi-quantitative reconstruction of the electron-spin density pattern of π radical ions from the photo-CIDNP intensities of the observed Chl *a* (Fig. 2.6), as these intensities scale with the anisotropy of the hyperfine coupling (34). Since both the strong signals at 154.8 (C-1 and C-6) and 147.2 ppm (C-9 and C-11) are assigned to two carbons each, some uncertainty remains in the pattern. The pattern appears slightly asymmetric mainly due to the absence of photo-CIDNP intensities on the methine carbons 5 and 20. Comparison of the photo-CIDNP patterns in PSI and PSII (31) shows enhancement for mainly the same atoms. Especially the strong signals of C-4 and C-8 in PSI represent significant differences with PSII. Such an electron-spin density pattern correlates the electronic structure in the radical pair state of the RC to the chemical shift information that pertains to the ground state (35). As the electronic structures of the donor and

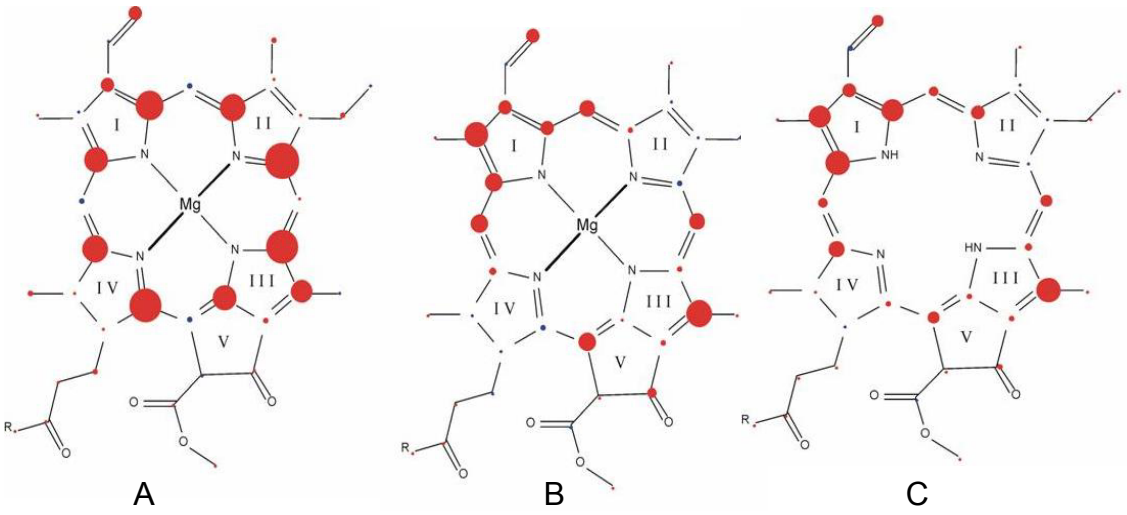

Figure 2.7. Hyperfine anisotropy of ^{13}C nuclei in radical species related to PSI and PSII by DFT computations. (A) Chl *a* radical cation as a model for the donor. (B) Chl *a* radical anion as a model for the acceptor in PSI. (C) Phe radical anion as a model for the acceptor in PSII.

acceptor Chl *a* are similar in the ground state but different in the radical pair state, the intensity pattern provides additional information with respect to the assignment of the carbons to the donor or acceptor.

To utilize this information, computed ^{13}C hyperfine anisotropies of the Chl *a* cation radical as a simple model of the donor are compared with the Chl *a* anion radical as a model of the acceptor (Fig. 2.7). Photo-CIDNP enhancement is strongly correlated to hyperfine anisotropy, but not simply proportional to it, as isotropic hyperfine coupling and the relative orientation of both the *g* and the hyperfine tensor play a minor role (35). Despite the latter complication, it may be concluded from a comparison of Figs. 2.6 and 2.7 that most of the signals very likely originate from the donor. The alternative assignment to the anion radical (Fig. 2.7B) is not convincing. The absence of spin density particularly on C-14, C-16 and C-19 cannot be reconciled. Hence, the assignment of most of the signals to the donor is reasonable. The possible exceptions are the methine carbons C-10 and C-15 and the signal of C-2 which may originate from the acceptor. If these signals are assigned to the acceptor, the common sign would suggest that the TSM mechanism dominates, as the sign for the DD mechanism depends on the sign of the *g*-value difference (35), which is different for the two constituent radicals. The signal at C-8 would not be expected for either the donor or the acceptor, but note that a Chl *a* cation radical may be only a rather crude model for the donor. It also cannot be ruled out that the signal at 144.2 ppm originates from an aromatic amino acid.

There are no significant differences recognised in the chemical shift patterns of P700 and P680 within the limits of the preliminary assignments. The largest difference is observed at the carbon C-14 of 1.9 ppm. This carbon is located on rings III and V, which suggests that the differences between both primary donors are located on this moiety of the Chl cofactor.

Differences on that part of the Chl *a* are expected to be involved into the main changes of the electronic structure causing the shift of the redox potenial in P680 to 1.2 V (31). In PSI, the resonance of the carbonyl C-13[1] appears at about 189 ppm, which suggests that there is no hydrogen-bond or chemical modification on that carbonyl function in PSI (Table 2.1). The signal appears to be relatively broad which may be due to some heterogeneity.

Similar to the photo-CIDNP response for PSII, in PSI only a single resonance has been observed from the methine carbons at 105.4 ppm. In view of its position and relative broadness, it has been assigned to both methine carbons C-10 and C-15. In the photo-CIDNP MAS NMR spectrum of PSII, the signal at 104.6 ppm is clearly the signal with the highest absolute intensity in the spectrum. In PSI, the signal at 105.4 ppm is weaker than several signals of other aromatic carbons. This observation may be linked to a stronger localisation of electron spin density in P680 while it appears broader distributed over P700. Such an interpretation may also explain the differences between the photo-CIDNP pattern and the pattern of ^{13}C hyperfine anisotropies. The DFT computations also suggest that differences in the electronic structure of the acceptors in a similar environment are rather minor (see Table 2.2 and Fig. 2.6 B, C).

2.5 Conclusions

In the photo-CIDNP data of PSI all ^{13}C NMR signals appear to be emissive. A rational picture emerges in the discussion: (i) The TSM, causing emissive signals, dominates over the DD mechanism. Since both mechanisms cause opposite sign of photo-CIDNP, the predominance of the TSM can also be responsible for the remarkable strength of the photo-CIDNP in PSI whereas in the RCs of bacteria and PSII both mechanisms are of comparable intensity. (ii) In PSI the origin of the predominance of the TSM seems to be due the differences in the hyperfine coupling and not decreased Δg-value. A stronger overlap of the SOMOs of donor and acceptor can be related to less symmetry of electron spin density distribution on P700 compared to P680. (iii) The photo-CIDNP signals can be assigned to a single Chl *a* molecule. The predominance of the donor over the acceptor in the ^{13}C photo-CIDNP NMR spectrum is in line with our calculations and analogue to a clear assignment obtained in the bacterial RCs.

References

1. van Gorkom, H.J.; Schelvis, J.P.M., *Photosynth. Res.* **1993**, 38, 297-301.
2. Webber, A.N.; Lubitz, W., *Biochim. Biophys. Acta.* **2001**, 1507, 61-79.
3. Jordan, P.; Fromme, P.; Witt, H.T.; Klukas, O.; Saenger, W.; Krauss, N., *Nature* **2001**, 411, 909-917.
4. Hoff, A.J.; Deisenhofer, J., *Phys. Rep.* **1997**, 287, 2-247.
5. Fromme, P.; Jordan, P.; Krauss, N., *Biochim. Biophys. Acta* **2001**, 1507, 5-31.
6. Breton, J., *Biochim. Biophys. Acta* **2001**, 1507, 180-193.
7. Hastings, G.; Ramesh, V.M.; Wang, R.L.; Sivakumar, V.; Webber, A., *Biochemistry* **2001**, 40, 12943-12949.
8. Breton, J.; Nabedryk, E.; Leibl, W., *Biochemistry* **1999**, 38, 11585-11592.
9. Witt, H.; Schlodder, E.; Teutloff, C.; Niklas, J.; Bordignon, E.; Carbonera, D.; Kohler, S.; Labahn, A.; Lubitz, W., *Biochemistry* **2002**, 41, 8557-8569.
10. Norris, J.R.; Uphaus, R.A.; Crespi, H.L.; Katz, J.J., *Proc. Natl. Acad. Sci. U. S. A.* **1971**, 68, 625-628.
11. Norris, J.R.; Druyan, M.E.; Katz, J.J., *J. Am. Chem. Soc.* **1973**, 95, 1680-1682.
12. Norris, J.R.; Scheer, H.; Druyan, M.E.; Katz, J.J., *Proc. Natl. Acad. Sci. U. S. A.* **1974**, 71, 4897-4900.
13. Hoff, A.J., *Phys. Rep.* **1979**, 54, 75-200.
14. O'Malley, P.J.; Babcock, G.T., *Proc. Natl. Acad. Sci. U. S. A.* **1984**, 81, 1098-1101.
15. Norris, J.R.; Scheer, H.; Katz, J.J., *Ann. New York Acad. Sci.* **1975**, 244, 260-280.
16. Lendzian, F.; Lubitz, W.; Scheer, H.; Hoff, A.J.; Plato, M.; Trankle, E.; Möbius, K., *Chem. Phys. Lett.* **1988**, 148, 377-385.
17. Rigby, S.E.J.; Nugent, J.H.A.; Omalley, P.J., *Biochemistry* **1994**, 33, 10043-10050.
18. Krabben, L.; Schlodder, E.; Jordan, R.; Carbonera, D.; Giacometti, G.; Lee, H.; Webber, A.N.; Lubitz, W., *Biochemistry* **2000**, 39, 13012-13025.
19. Käss, H.; Fromme, P.; Witt, H.T.; Lubitz, W., *J. Phys. Chem. B* **2001**, 105, 1225-1239.
20. Käss, H.; Rautter, J.; Bönigk, B.; Hofer, P.; Lubitz, W., *J. Phys. Chem.* **1995**, 99, 436-448.
21. Käss, H.; Lubitz, W., *Chem. Phys. Lett.* **1996**, 251, 193-203.
22. Käss, H.; Fromme, P.; Lubitz, W., *Chem. Phys. Lett.* **1996**, 257, 197-206.
23. Mac, M.; Tang, X.S.; Diner, B.A.; McCracken, J.; Babcock, G.T., *Biochemistry* **1996**, 35, 13288-13293.
24. Käss, H.; Lubitz, W.; Hartwig, G.; Scheer, H.; Noy, D.; Scherz, A., *Spectrochim. Acta A* **1998**, 54, 1141-1156.
25. Plato, M.; Krauss, N.; Fromme, P.; Lubitz, W., *Chem. Phys.* **2003**, 294, 483-499.
26. Zysmilich, M.G.; McDermott, A., *J. Am. Chem. Soc.* **1994**, 116, 8362-8363.
27. Zysmilich, M.G.; McDermott, A., *J. Am. Chem. Soc.* **1996**, 118, 5867-5873.
28. Zysmilich, M.G.; McDermott, A., *Proc. Natl. Acad. Sci. U. S. A.* **1996**, 93, 6857-6860.
29. Matysik, J.; Alia; Hollander, J.G.; Egorova-Zachernyuk, T.; Gast, P.; de Groot, H.J.M., *Indian J. Biochem. Biophys.* **2000**, 37, 418-423.

30. Matysik, J.; Alia; Gast, P.; Lugtenburg, J.; de Groot, H.J.M. In *Perspectives on solid state NMR in biology*; Kiihne, S., de Groot, H.J.M., Eds.; Kluwer: Dordrecht, 2001; p 215-225.
31. Matysik, J.; Alia; Gast, P.; van Gorkom, H.J.; Hoff, A.J.; de Groot, H.J.M., *Proc. Natl. Acad. Sci. U. S. A.* **2000**, 97, 9865-9870.
32. Schulten, E.A.M.; Matysik, J.; Alia; Kiihne, S.; Raap, J.; Lugtenburg, J.; Gast, P.; Hoff, A.J.; de Groot, H.J.M., *Biochemistry* **2002**, 41, 8708-8717.
33. Prakash, S.; Alia; Gast, P.; Jeschke, G.; de Groot, H.J.M.; Matysik, J., *J. Mol. Struc.* **2003**, 661, 625-633.
34. Jeschke, G., *J. Am. Chem. Soc.* **1998**, 120, 4425-4429.
35. Jeschke, G.; Matysik, J., *Chem. Phys.* **2003**, 294, 239-255.
36. Daviso, E.; Jeschke, G.; Matysik, J. In *Biophysical techniques in photosynthesis*; Aartsma, T.J., Matysik, J., Eds.; Springer: Dordrecht, 2007, p 385-399.
37. Blankenship, R.; McGuire, A.; Sauer, K., *Proc. Natl. Acad. Sci. U. S. A.* **1975**, 72, 4943-4947.
38. van der Est, A., *Biochim. Biophys. Acta* **2001**, 1507, 212-225.
39. Mullet, J.E.; Burke, J.J.; Arntzen, C.J., *Plant Physiol.* **1980**, 65, 814-822.
40. Arntzen, C.J.; Ditto, C.L., *Biochim. Biophys. Acta* **1976**, 449, 259-274.
41. Arnon, D.I., *Plant Physiol.* **1949**, 24, 1-15.
42. Rutherford, A.W.; Mullet, J.E., *Biochim. Biophys. Acta* **1981**, 635, 225-235.
43. Gast, P.; Swarthoff, T.; Ebskamp, F.C.R.; Hoff, A.J., *Biochim. Biophys. Acta* **1983**, 722, 163-175.
44. Bennett, A.E.; Rienstra, C.M.; Auger, M.; Lakshmi, K.V.; Griffin, R.G., *J. Chem. Phys.* **1995**, 103, 6951-6958.
45. Velde, G.T.; Bickelhaupt, F.M.; Baerends, E.J.; Guerra, C.F.; van Gisbergen, S.J.A.; Snijders, J.G.; Ziegler, T., *J. Comput. Chem.* **2001**, 22, 931-967.
46. Chow, H.C.; Serlin, R.; Strouse, C.E., *J. Am. Chem. Soc.* **1975**, 97, 7230-7237.
47. Käss, H.; Bittersmannweidlich, E.; Andreasson, L.E.; Bonigk, B.; Lubitz, W., *Chem. Phys.* **1995**, 194, 419-432.
48. van Lenthe, E.; Snijders, J.G.; Baerends, E.J., *J. Chem. Phys.* **1996**, 105, 6505-6516.
49. van Lenthe, E.; van der Avoird, A.; Wormer, P.E.S., *J. Chem. Phys.* **1998**, 108, 4783-4796.
50. Matysik, J.; Schulten, E.; Alia; Gast, P.; Raap, J.; Lugtenburg, J.; Hoff, A.J.; de Groot, H.J.M., *Biol. Chem.* **2001**, 382, 1271-1276.
51. Alia; Matysik, J.; Soede-Huijbregts, C.; Baldus, M.; Raap, J.; Lugtenburg, J.; Gast, P.; van Gorkom, H.J.; Hoff, A.J.; de Groot, H.J.M., *J. Am. Chem. Soc.* **2001**, 123, 4803-4809.
52. Bonnerjea, J.; Evans, M.C.W., *FEBS Lett.* **1982**, 148, 313-316.
53. MacMillan, F.; Hanley, J.; van der Weerd, L.; Knupling, M.; Un, S.; Rutherford, A.W., *Biochemistry* **1997**, 36, 9297-9303.
54. Rigby, S.E.J.; Muhiuddin, I.P.; Santabarbara, S.; Evans, M.C.W.; Heathcote, P., *Chem. Phys.* **2003**, 294, 319-328.
55. Kamlowski, A.; Zech, S.G.; Fromme, P.; Bittl, R.; Lubitz, W.; Witt, H.T.; Stehlik, D., *J. Phys. Chem. B* **1998**, 102, 8266-8277.
56. Berthold, T.; Bechtold, M.; Heinen, U.; Link, G.; Poluektov, O.; Utschig, L.; Tang, J.; Thurnauer, M.C.; Kothe, G., *J. Phys. Chem. B* **1999**, 103, 10733-10736.
57. Bratt, P.J.; Poluektov, O.G.; Thurnauer, M.C.; Krzystek, J.; Brunel, L.C.; Schrier, J.; Hsiao, Y.W.; Zerner, M.; Angerhofer, A., *J. Phys. Chem. B* **2000**, 104, 6973-6977.

58. Abraham, R.T.; Rowan, A.E. In *Chlorophylls*; Scheer, H., Ed. CRC Press: Boca Raton FL, 1991; p 797-834.

59. Boender, G.J. Ph.D. thesis, University of Leiden, 1996.

60. Dorlet, P.; Xiong, L.; Sayre, R.T.; Un, S., *J. Biol. Chem.* **2001**, 276, 22313-22316.

61. Fischer, M.R.; de Groot, H.J.M.; Raap, J.; Winkel, C.; Hoff, A.J.; Lugtenburg, J., *Biochemistry* **1992**, 31, 11038-11049.

3 Contrasting magnetic field dependence of ^{13}C photo-CIDNP MAS NMR in plant photosystems I and II

Photo-CIDNP is observed in the two photosynthetic reaction centers of plants, PSI and PSII by ^{13}C MAS NMR at three different magnetic fields, 17.6, 9.4 and 4.7 Tesla. There is a significant difference in field dependence detected in the light induced signal pattern of the two photosystems. For PSII the optimal NMR enhancement factor of ~5000 is observed at 4.7 Tesla. On the other hand, the strongest light induced signals of PSI are observed at 9.4 Tesla. Simulations indicate that this contrasting difference between the field dependence of PSI on one hand and purple bacterial RCs and PSII on the other hand is due to differences in the exchange coupling.

3.1 Introduction

Photosynthesis in plants involves the participation of two RCs, PSI and PSII, located in the thylakoid membrane of chloroplasts. The electron transfer chain of both photosystems has two symmetric branches consisting of six chlorin molecules and two quinones. PSI belongs to type-I RCs, characterized by three iron-sulphur clusters as the terminal intrinsic electron acceptors, while PSII belongs to the type-II RCs where a mobile quinone acts as the terminal electron acceptor. The primary donors of both RCs differ in their redox potential by ~700 mV (1). The oxidized electron donor of PSII, is the strongest oxidising agent known in living nature, having a redox potential of 1.2 V (2). In contrast, the electronically excited electron donor of PSI, is probably the most reducing compound in living nature (3). The coupling of these two photosystems facilitates the transfer of electrons across the photosynthetic membrane from water molecules finally into CO_2 in order to build up organic material. Despite their opposite functional roles, structural similarities in the arrangement of transmembrane helices in the cores of the two photosystems have been observed by recent structural data on PSI (4) and PSII (5).

Photo-CIDNP is well known in liquid NMR (6-8) as a method that increases NMR intensities. Strongly enhanced signals of solid samples upon continuous illumination with white light have been observed for the first time by applying ^{15}N MAS NMR to quinone-blocked bacterial RCs of *Rb. sphaeroides* R-26 (9, 10). ^{13}C photo-CIDNP MAS NMR experiments of R-26 (11-14) and WT (15-17) allow for the study of photochemically active

regions in great detail. In addition, photo-CIDNP has also been observed in both plant RCs. The ^{13}C photo-CIDNP MAS NMR signals obtained from the D1D2 complex of PSII provide evidence for a highly asymmetric electron spin density shifted towards the C-15 methine bridge on the donor chlorophyll (18). The ^{13}C photo-CIDNP MAS NMR data of the PSI complex show that all signals are emissive and can be assigned to a single Chl *a* molecule of the donor P700 (Chapter 2). Comparison between the two photosystems reveals that P700 is essentially an undisturbed Chl *a* cofactor, while the electronic structure of the P680 can be interpreted in terms of a monomeric Chl *a* cofactor having strong interaction with the protein matrix (19).

The mechanism of photo-CIDNP has recently been discussed extensively (14, 17, 20). In RCs of *Rb. sphaeroides* WT, photo-CIDNP has been explained as a combination of two mechanisms (17). The TSM mechanism is related to the dipolar and exchange couplings between two electron spins in a correlated radical pair state, leading to enhanced nuclear polarization via the anisotropic hyperfine coupling (21). The DD mechanism also requires anisotropic hyperfine coupling, to transfer the electron spin polarization to nuclear polarisation (22). However, in this case the build up of nuclear polarisation from the spin-correlated radical pair is due to the different lifetimes of the singlet and triplet states. On the other hand, in RCs of *Rb. sphaeroides* R-26, the carotenoid-less mutant, a third mechanism is involved due to the long lifetime of the donor triplet state (14). This DR mechanism is based on relaxation processes involving nuclear polarization on the triplet branch, while the nuclear polarization of the singlet branch survives entirely (23). These interpretations are in line with the magnetic field effects observed, showing NMR enhancement maxima of about 10,000 at 4.7 Tesla in both bacterial RCs (14, 17). Hence, magnetic field dependence of photo-CIDNP signals is a sensitive tool to study photo-CIDNP mechanisms and the linked magnetic parameters. In this chapter the field dependent ^{13}C photo-CIDNP MAS NMR data of plant PSI and PSII are presented.

3.2 Materials and Methods

3.2.1 *Sample Preparation*

PSI RC preparation. The PSI complex containing ~110 Chl/P700 was prepared from spinach (*Spinacia oleracea*) according to the method described in chapter 2. Briefly, the chloroplasts were isolated first, then washed with 10 mM Tricine buffer (pH 7.8) containing 50 mM Sorbitol and 5 mM EDTA, and subsequently re-suspended in buffer containing 10 mM Tricine (pH 7.8) to obtain a final concentration of 0.8 mg Chl/mL. The membranes (0.8 mg/mL) were solubilised with Triton X-100 (final concentration of 0.8% w/v) for 30 minutes at room temperature in the dark with continuous slow stirring. These solubilised membranes were loaded onto a linear sucrose gradient (0.1 - 1.0 M sucrose, 2 M sucrose cushion, 10 mM

Tricine, 0.02% Triton X-100, pH 7.8). PSI-110 particles appeared as a dark green non fluorescent band just above the 2 M sucrose. These particles were then dialysed and concentrated.

PSII RC preparation. PSII (D1D2-cytb559) from spinach (*Spinacia oleracea*) was isolated according to the method described in ref. (18). Briefly, PSII membrane fragments were isolated first and suspended in BTS200 [20 mM [bis(2-hydroxyethyl)amino] tris(hydroxymethyl) methane (Bistris), pH 6.5/20 mM $MgCl_2$/5 mM $CaCl_2$/10 mM $MgSO_4$/0.2 M sucrose/ 0.03% (wt/vol) *n*-dodecyl b-D-maltoside]. These membranes were further purified by removing the light harvesting complex and PSII core antenna proteins to obtain purified PSII RC complex, D1-D2-cytb559 with about 6 attached chlorophylls and 2 pheophytins. The RCs were concentrated for NMR measurements.

3.2.2 *MAS-NMR Measurements*

The NMR experiments were performed in different fields using AV-750, DMX-400 and DMX-200 NMR spectrometers (Bruker GmbH, Karlsruhe, Germany). The samples were loaded into optically transparent 4 mm sapphire rotors. The PSI sample was reduced by the addition of an aqueous solution of 10 mM sodium dithionite and 40 mM glycine buffer (pH 9.5) in an oxygen free atmosphere. Immediately following the reduction, slow freezing of the sample was performed directly in the NMR probe inside the magnet with liquid nitrogen-cooled gas under continuous illumination with white light. The PSII sample was also frozen slowly directly in the NMR probe inside the magnet with liquid nitrogen-cooled gas. The experiments have been performed at a temperature of 223 K, except for experiments at 9.4 Tesla, which were performed at a temperature of 240 K. The illumination set-up was specially designed for the Bruker MAS probe (12). The light and dark spectra were obtained with a Hahn echo pulse sequence and TPPM proton decoupling (24). Experimental line-broadening of 30 (at 4.7 Tesla), 70 (9.4 Tesla) and 120 Hz (17.6 Tesla) was applied. The number of scans was 20 k, unless stated differently.

3.2.3 *Calculations*

Numerical simulations of the field dependence of photo-CIDNP effects for PSI were based on the theory described in ref. (20) as implemented in a home-written Matlab program for density matrix computation using the EasySpin library (25). The program starts from a pure singlet state of the pair and computes time evolution for a Hamiltonian including electron Zeeman, nuclear Zeeman, and hyperfine interaction as well as dipole-dipole and exchange coupling between the two electron spins. Evolution is computed for a total time that exceeds the lifetime of both singlet and triplet pairs by a factor of five, so that radical pairs have completely decayed. The part of the density matrix that decays to the ground state from either singlet or triplet radical pairs is projected out. In this way the nuclear polarization of the

diamagnetic part of the density matrix is determined. This diamagnetic part is further evolved with a Hamiltonian including only the nuclear Zeeman interaction. As an extension to the approach described in ref. (20), this procedure is performed for a full powder average (17), describing all interactions by tensors, except for the nuclear Zeeman interaction since its anisotropy is negligible on a time scale of 100 ns. Powder averaging was performed using the EasySpin spherical grid function sphgrid with 16 knots and C_i symmetry. This yields 481 orientations. Nuclear polarization was normalized to the thermal polarization at the measurement temperature of 223 K and the given field.

Only few of the required spin Hamiltonian parameters for PSI RCs are known from experiments. The principal values for the *g* tensor of the primary donor cation radical, 2.00304, 2.00262, and 2.00220 were taken from ref. (25). To the best of our knowledge, no high-field EPR measurements of the *g* tensor have been reported, neither for the primary acceptor in PSI, which is believed to be a Chl *a* (26), nor for the Chl *a* anion radical. To obtain this missing *g* tensor, the orientations of the principal axes of both *g* tensors, and the ^{13}C hyperfine couplings, DFT computations based on the reported crystal structure of cyanobacterial PS1 have been performed (27). From the PDB structure 1JB0 the chlorophyll molecules CL2 1011 and CL1 1021 as the P700 donor and the chlorophyll molecule CL1 1013 as the putative primary acceptor were extracted. The amino acid residues that coordinate the Mg atoms of the chlorophyll molecules were also extracted, His A680 and His B660 for the P700 donor, and Met A688 for the acceptor. For the DFT computations, histidines were edited to methylimidazole molecules and methionine was edited to ethyl methyl thioether, and the phytyl chains of the chlorophyll molecules were replaced by methyl groups. Hydrogen atoms were added with the program Titan (Wavefunction, Inc., Irvine, CA, USA). In this procedure some sp^3 carbons were wrongly assigned as sp^2 carbons. These were edited by hand to sp^3 in the same program.

DFT computations were performed with the program ADF 2004.1 using the BLYP functional (28). The geometry of the P700 donor cation radical was optimized, using a double-zeta basis set and frozen cores up to 1s for C, N, and O atoms and up to 2p for the Mg atom. The *g* tensor was computed by a spin-restricted spin-orbit relativistic computation within the ZORA approach, using all-electron DZ basis sets for all atoms. Hyperfine couplings were obtained from a spin-unrestricted non-relativistic computation also using all-electron DZ basis sets. In attempts to optimize the geometry of the acceptor anion radical, it was found that the distance between the Mg atom of the chlorophyll and the coordinated S atom of the ethyl methyl thioester, which is 2.6 Å in the crystal structure (27), increased continuously. This may indicate that the unusual sulphur coordination to the magnesium is imposed by the structure of the protein and serves for fine tuning of the electron transfer chain, possibly by influencing the redox potential of the primary acceptor. For DFT

computations of magnetic parameters, the geometry as derived from the crystal structure without further optimization was used. The *g*-tensor of the acceptor anion radical was computed in the same way as for the P700 donor cation radical. While the principal axes directions were directly taken from the computation, the deviations of the principal values from the free electron *g* value were scaled by a factor *F* that gave the best agreement between experimental principal values and rescaled computed values for the BPhe acceptor in bacterial reaction centers. The principal values obtained by this procedure for the PSI acceptor (2.0039, 2.0030, 2.0024) are considered as rough estimates. Hyperfine couplings for the acceptor were obtained from a spin-unrestricted non-relativistic computation using all-electron TZ2P basis sets for all atoms.

The remaining parameters in the spin Hamiltonian, the exchange coupling and dipole-dipole coupling between the two electron spins, and the recombination rates of singlet and triplet radical pairs that influence the radical pair kinetics have not been determined exactly. Since the geometry and general electronic structure of the relevant part of the PSI RC are quite similar to bacterial RCs, it is assumed that the dipole-dipole coupling between the electron spins is rather close to the value determined on bacterial RCs (29). The average lifetime of the $P700^{+\bullet}$-$A_0^{-\bullet}$ radical pair of about 40 ns at zero magnetic field constrains the lifetimes of singlet and triplet pairs (30). These lifetimes, as well as the exchange coupling between the electron spins were varied in our photo-CIDNP simulations as described in the following sections.

3.2.4 *Calculation of the ratio of light induced signal to noise*

In order to compare the photo-CIDNP light induced signal intensity at the three different magnetic fields (17.6 Tesla, 9.4 Tesla and 4.7 Tesla) in PSI and PSII, the ratio of light-induced centerband signals relative to the noise has been determined. This ratio has been standardised to a single scan at different magnetic fields.

3.3 Results and Discussion

3.3.1 *Field effects in the dark and light spectra*

Fig. 3.1 shows the ^{13}C MAS NMR spectra of PSII particles at three different magnetic fields at 17.6 Tesla (750 MHz proton frequency), 9.4 Tesla (400 MHz) and 4.7 Tesla (200 MHz) recorded using a MAS rotational frequency of 8 kHz. All three dark spectra show similar features. Strong signals appear between 110 and 10 ppm, with a weaker response in the aromatic and carbonylic region. The spectra show the characteristic features of ^{13}C MAS NMR spectra of large proteins (31). No spinning sidebands are observed in the three spectra. This is due to the small CSA of aliphatic carbons and the weak signal intensity of the carbonylic and aromatic signals. The spectral quality obtained at 17.6 Tesla is slightly better

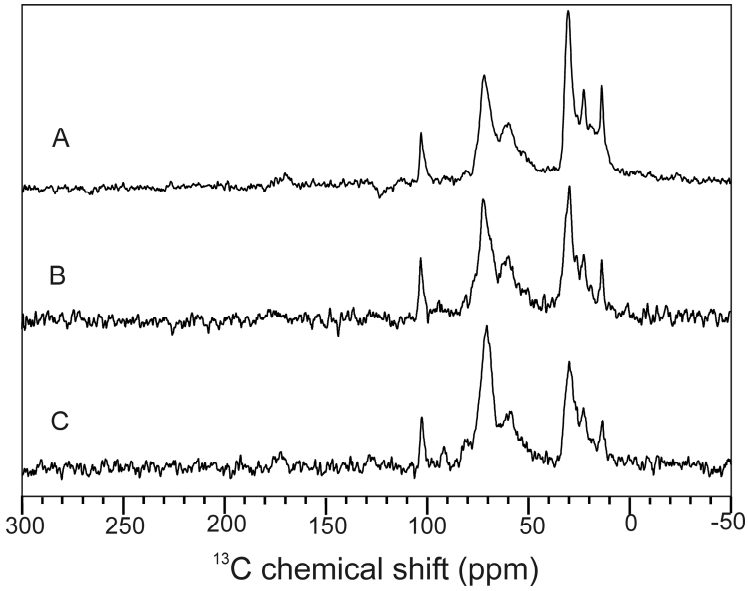

Figure 3.1. ^{13}C MAS NMR spectra of PSII particles obtained in the dark at a MAS frequency of 8 kHz at (A) 17.6, (B) 9.4, and (C) 4.7 Tesla.

than that obtained at 9.4 Tesla. Both Spectra 3.1A and 3.1B are slightly better resolved than Spectrum 3.1C, obtained at 4.7 Tesla. The observed field dependence is due to less Zeeman spitting and chemical shift dispersion at lower fields under Boltzmann conditions.

The ^{13}C MAS NMR spectra of PSI samples at three different magnetic fields at 17.6 Tesla, 9.4 Tesla and 4.7 Tesla recorded using MAS rotational frequency of 8 kHz did not show a significant signal of the protein backbone (data not shown). This is due to the presence of a small amount of protein, which was estimated to be 0.6 mg, present in the rotor, while the amount of protein in the rotor for PSII sample has been determined to be 15.8 mg.

Upon illumination with continuous white light, strong signals emerge in the aromatic region in both, PSI (Fig. 3.2) and for PSII (Fig. 3.3). In PSI, all light induced signals appear to be emissive (negative) between 170 and 80 ppm (19). In the spectrum at 17.6 Tesla (Fig 3.2A), spinning sidebands can be observed, while at lower fields the entire intensity is concentrated in the centerband. The strongest signals are observed at 9.4 Tesla (Fig 3.2B), while the weakest signals are observed at 4.7 Tesla (Fig 3.2C). Table 3.1 expresses the field-dependence of the light-induced centerband signals relative to the noise standardized to a single scan. The table shows a maximum at 9.4 T and about half the intensity at 17.6 Tesla for PSI.

In PSII, strong enhancement is observed at 4.7 and 9.4 Tesla (Fig. 3.3B and C), while at 17.6 Tesla (Fig. 3.3A) the light induced signals are negligible. Comparing Fig 3.3B and C indicates a slightly stronger enhancement compared to the dark signals at 4.7 Tesla. In contrast to the light-induced signals in PSI, both enhanced absorptive and emissive light-

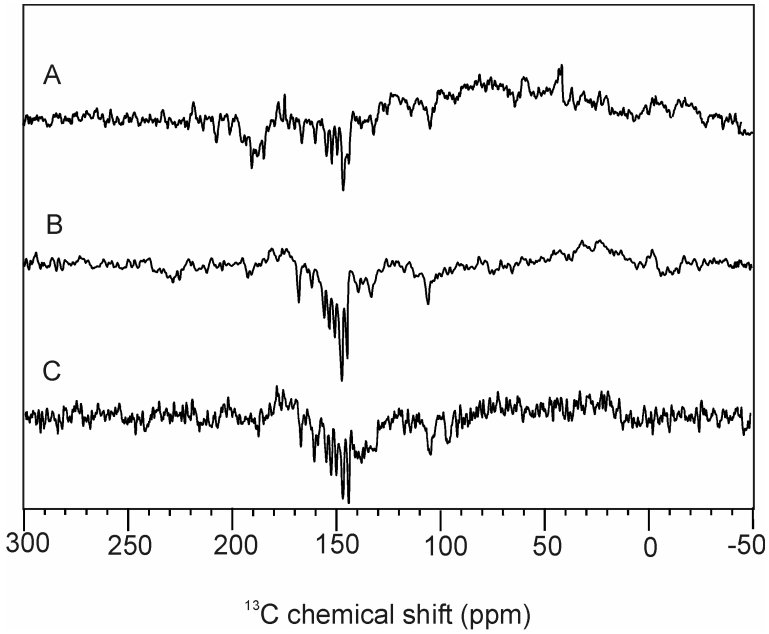

Figure 3.2.^{13}C MAS NMR spectra of PSI particles obtained under continuous illumination with white light at a MAS frequency of 8 kHz at (A) 17.6 Tesla, (B) 9.4 Tesla, and (C) 4.7 Tesla.

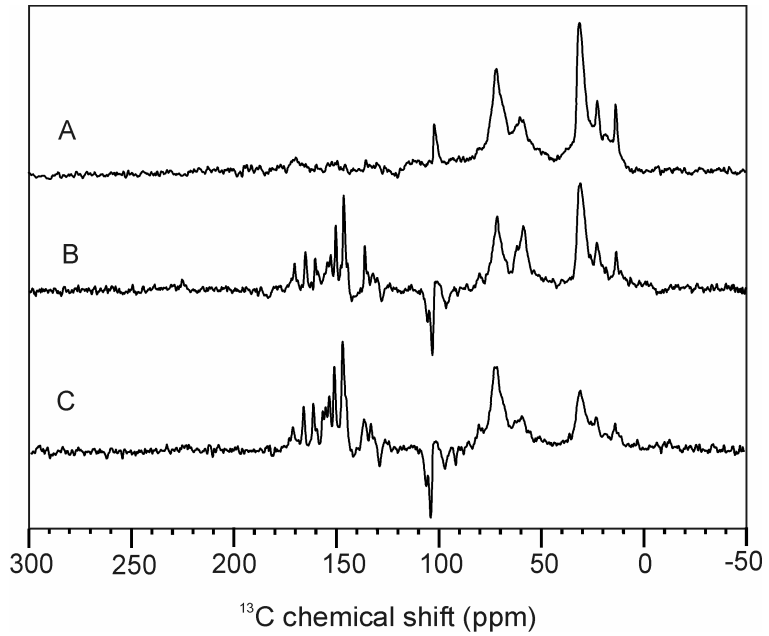

Figure 3.3. ^{13}C MAS NMR spectra of PSII (D1D2) particles obtained under continuous illumination with white light at a MAS frequency of 8 kHz at (A) 17.6 Tesla, (B) 9.4 Tesla, and (C) 4.7 Tesla.

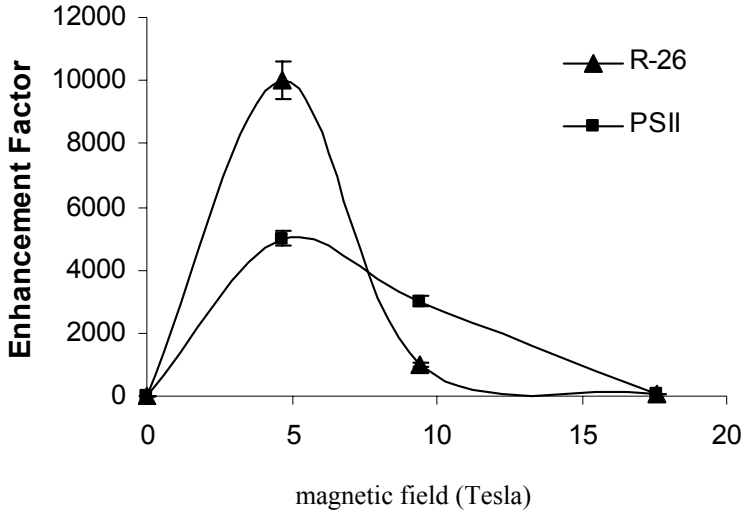

Figure 3.4. Enhancement factors at different magnetic fields calculated for PSII along with R-26. The assumption of an enhancement factor of zero at zero magnetic field is discussed in ref. 20.

induced signals occur.

The emissive signals mainly appear in the region of the methine carbons. In the spectrum at 9.4 T, weak spinning sidebands can be observed. The enhancement factor has been calculated as a ratio of the signal due to a single carbon at 147.3 ppm (positive signal) and 105 ppm (negative signal) to one at 13.7 ppm (in the dark) in the case of PSII. Using the signal from about 900 methyl groups of the entire D1D2 complex at 13.7 ppm as an internal standard, enhancement factors of ≤60 (17.6 Tesla), 3000 (9.4 Tesla) and about 5000 (4.7 Tesla) were calculated for PSII (Fig. 3.4). The enhancement factor for PSI could not be calculated due to absence of reliable dark signals.

The field-dependence of the enhancement factor of PSII is similar to that observed in bacterial RCs of both WT and R-26 (14, 17), showing a maximum at 4.7 Tesla and a strong decay for higher fields. The field-dependence of the ratio between the light induced signal to the standardized noise is shown in Table 3.1, allowing for comparison with PSI suggesting a shift of optimum photo-CIDNP production in PSI to higher fields.

Magnetic field	PSI	PSII
Tesla	S_{Li} / N_{st}	S_{Li} / N_{st}
4.7	2.0	9.4
9.4	10.7	10.0
17.6	4.3	0

Table 3.1. The field-dependence of the ratio of light-induced signal (S_{Li}) to the standardized noise (N_{st}) for PSI and PSII.

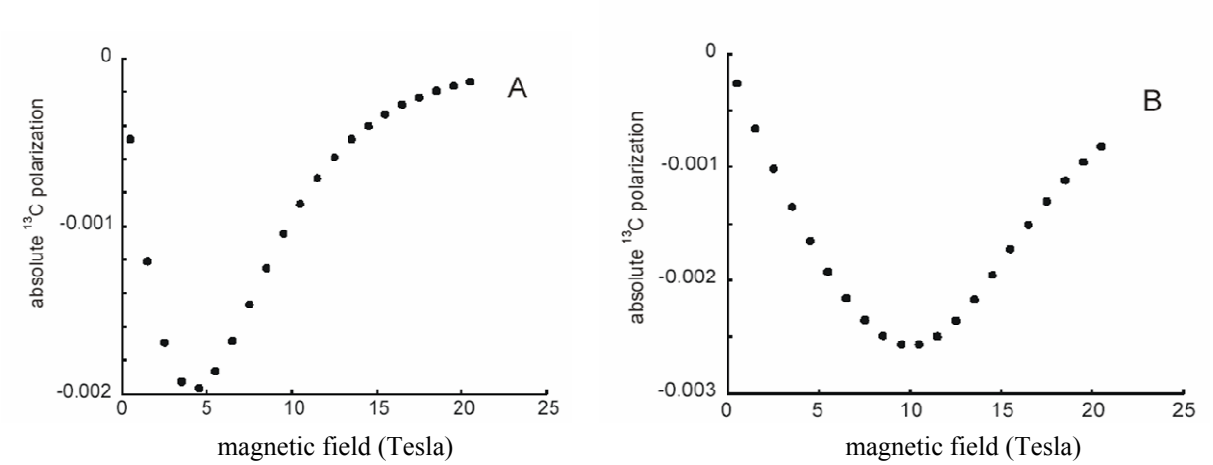

Figure 3.5. Simulated field dependence of the absolute ^{13}C polarization for the methine carbon C-20 of branch B of P700 donor. Similar results are obtained for other carbon atoms in both donor and acceptor. (A) Radical pair lifetimes and exchange coupling as in bacterial RCs. (B) Radical pair lifetime as in bacterial RCs, but exchange coupling increased by a factor of three.

3.3.2 *Simulations of field effects in light spectra of PSI*

The field dependence of the photo-CIDNP effects in PSII is similar to previous observations on bacterial RCs, with maximum polarization at the lowest tested field of 4.7 Tesla (Fig. 3.4). In contrast, PSI exhibits only a relatively weak photo-CIDNP effect at 4.7 Tesla and a significantly stronger polarization at 9.4 Tesla (Fig. 3.2, Table 3.1). As the field dependence of the nuclear polarization is related to the magnetic parameters and lifetimes of the intermediate radical species (17, 20), this difference reflects a difference in the electronic structure between RCs of purple bacteria on the one hand and PSII and PSI RCs on the other hand. To examine what parameter changes can explain the experimental observations simulations were performed of photo-CIDNP in an analogous manner as the simulations of bacterial RCs, which reproduced the experimental field dependence (17). Generally, the field dependence of the nuclear polarization appears similar for all ^{13}C nuclei in both donor and acceptor molecules, as was also found for the bacterial RCs.

The simulation is in line with the experimental observation that the spectral pattern varies only slightly between 4.7 and 17.6 Tesla (Fig. 3.1). In addition, it is found that any reasonable changes in the *g*-tensors (up to ±50% of the deviation from the free electron *g*-value) cause only a scaling of the intensity of the whole spectral pattern by a constant factor, which does not depend significantly on the magnetic field. In other words, uncertainties in the computation of the acceptor *g*-tensor and of the principal axes directions of the *g*-tensors do not lead to significant uncertainties in the computed field dependence of the nuclear polarization. Likewise, any reasonable changes in the dipole-dipole coupling, up to ±30% of the coupling strength, have little effect on the field dependence. This suggests that the pronounced difference between bacterial and PSII RCs on the one hand and PSI RCs on the

other hand can thus be traced back to either a difference in radical pair lifetimes or a difference in the exchange coupling *J*.

Assuming the same *J* and lifetimes as for bacterial RCs, we calculate a very similar field dependence of the nuclear polarization with a maximum close to 5 Tesla. As an example, the dependence for the methine carbon C-20 of the donor for these assumptions is shown in Fig. 3.5A. First it was tested whether the different field dependence observed for PSI RCs can be reproduced by changing the ratio between the lifetime T_S of radical pairs in the singlet state and the lifetime T_T of radical pairs in the triplet state. However, changes in the field dependence of the nuclear polarization are minor when varying the ratio T_S/T_T between 0.5 and 50 (data not shown).

Next, it was tested whether changes in the mean lifetime of radical pairs, defined here as $\sqrt{T_S T_T}$, can reproduce the observations. Indeed the shift of the maximum to a field of approximately 8.5 T can be obtained by decreasing $\sqrt{T_S T_T}$ to 1.6 ns (data not shown). This value cannot directly be compared to the experimental lifetime, as the combination of the lifetimes T_S and T_T to the true mean lifetime depends on the specifics of spin evolution and would have to be computed by including hyperfine coupled protons in the spin Hamiltonian. However, the mean lifetime cannot be larger than the maximum of T_S and T_T, which is 5 ns for simulations that fit the observed field dependence. It seems unlikely that the radical pair lifetime in our samples is by almost a factor of ten shorter than found on cyanobacterial PSI (30). Even if this was to be assumed, still the fact that such a shortening of the lifetime leads to a drastic decrease in the absolute nuclear polarization remains, which does not agree with the similar NMR sensitivity observed in photo-CIDNP experiments on bacterial RCs and plant PSI RCs. Thus a shortening of the radical pair lifetime as the cause for the change in the field dependence is excluded.

Finally, variations of the exchange coupling *J* are considered. An increase of the exchange coupling by a factor of three compared to bacterial RCs to 21G shifts the field where maximum nuclear polarization is attained to about 10 T (Fig. 3.6B). This leads to a slight increase in absolute polarization, which can be reconciled with experimental observations. Such a change in *J* may well be caused by slight rearrangements of the cofactors that lead to an improved overlap between the molecular orbitals of the P700 donor and the accessory Chl *a* or between the molecular orbitals of the accessory chlorophyll and the primary acceptor A_0. The simulations thus indicate that the change in the magnetic field dependence of solid-state photo-CIDNP between bacterial RCs and plant PSI can be traced back to an increase of the exchange coupling between the $P700^{+\bullet}$ and $A_0^{-\bullet}$ radical anions by a factor of approximately three. The underlying cause for this change is the influence of a large exchange coupling on the matching condition (20). In the limit where the exchange coupling is much larger than the hyperfine couplings and the difference of the electron Zeeman frequencies, state mixing is

optimal when the coupling between the electron spins matches the nuclear Zeeman frequency. In the limit of large exchange couplings the optimum magnetic field is thus proportional to the exchange coupling.

References

1. Grotjohann, I.; Jolley, C.; Fromme, P., *Phys. Chem. Chem. Phys.* **2004**, 6, 4743-4753.
2. van Gorkom, H.J.; Schelvis, J.P.M., *Photosynth. Res.* **1993**, 38, 297-301.
3. Webber A.N.; Lubitz W., *Biochim. Biophys. Acta* **2001**, 1507, 61-79.
4. Jordan P.; Fromme P.; Witt H.T.; Klukas O.; Saenger W.; Krauss N., *Nature* **2001**, 411, 909-917.
5. Zouni A.; Witt H.T.; Kern J.; Fromme P.; Krauss N.; Saenger W.; Orth P., *Nature* **2001**, 409, 739-743.
6. Roth, H.D. In *Encyclopaedia of Nuclear Magnetic Resonance*. Wiley: Chichester, U.K., 1996; p 1337-1350.
7. Hore, P.J.; Broadhurst, R.W., *Prog. Nucl. Magn. Reson. Spectrosc.* **1993,** 25, 345-402.
8. Goez, M., A*dv .Photochem.* **1997**, 23, 63-164.
9. Zysmilich M.G.; McDermott A., *J. Am. Chem. Soc.* **1994**, 116, 8362-8363.
10. Zysmilich M.G.; McDermott A., *J. Am. Chem. Soc.* **1996**, 118, 5867-5873.
11. Zysmilich, M.G.; McDermott, A., *Proc. Natl. Acad. Sci. U. S. A.* **1996**, 93, 6857-6860.
12. Matysik, J.; Alia; Hollander, J.G.; Egorova-Zachernyuk, T.; Gast, P.; de Groot, H.J.M., *Indian J. Biochem. Biophys.* **2000**, 37, 418-423.
13. Matysik, J.; Alia; Gast, P.; Lugtenburg, J.; Hoff, A.J.; de Groot, H.J.M. In *Perspectives on solid state NMR in biology*; Kiihne, S., de Groot H.J.M., Eds.; Kluwer: Dordrecht, 2001; p 215-225.
14. Prakash, S.; Alia; Gast, P.; de Groot, H.J.M.; Matysik, J.; Jeschke, G., *J. Am. Chem. Soc.* **2006**, 128, 12794-12799.
15. Schulten, E.A.M.; Matysik, J.; Alia; Kiihne, S.; Raap, J.; Lugtenburg, J.; Gast, P.; Hoff, A.J.; de Groot, H.J.M., *Biochemistry* **2002**, 41, 8708-8717.
16. Prakash, S.; Alia; Gast, P.; Jeschke, G.; de Groot, H.J.M.; Matysik, J., *J. Mol. Struct.* **2003**, 661, 625-633.
17. Prakash, S.; Alia; Gast, P.; de Groot, H.J.M.; Jeschke, G.; Matysik, J., *J. Am. Chem. Soc.* **2005**, 127, 14290-14298.
18. Matysik, J.; Alia; Gast, P.; van Gorkom, H.J.; Hoff, A.J.; de Groot, H.J.M., *Proc. Natl. Acad. Sci. U. S. A.* **2000**, 97, 9865-9870.
19. Diller A.; Alia; Roy E.; Gast P.; van Gorkom H.J.; Zaanen J.; de Groot H.J.M.; Glaubitz C.; Matysik J., *Photosynth. Res.* **2005**, 84, 303-308.
20. Jeschke, G.; Matysik, J., *Chem. Phys*. **2003**, 294, 239-255.
21. Jeschke G., *J. Chem. Phys*. **1997**, 106, 10072-10086.
22. Polenova T.; McDermott A.E., *J. Phys. Chem. B* **1999**, 103, 535-548.
23. McDermott A.; Zysmilich M.G.; Polenova T., *Solid State Nucl. Magn. Reson.* **1998**, 11, 21-47.
24. Bennett A.E.; Rienstra C.M.; Auger M.; Lakshmi K.V.; Griffin R.G., *J. Chem. Phys.* **1995**, 103, 6951-6958.
25. Stoll, S.; Schweiger, A., *J. Magn. Reson*. **2006**, 178, 42-55.
26. Petrenko, A.; Maniero, A.L.; Van Tol, J.; MacMillan, F.; Li, Y.; Brunel, L.-C.; Redding, K., *Biochemistry* **2004**, 43, 1781-1786.
27. Jordan, P.; Fromme, P.; Witt, H.T.; Klukas, O.; Saenger, W.; Krauss, N., *Nature* **2001**, 411, 909-917.

28. Velde, G.T.; Bickelhaupt, F.M.; Baerends, E.J.; Guerra, C.F.; van Gisbergen, S.J.A.; Snijders, J.G.; Ziegler, T., *J. Comput. Chem.* **2001**, 22, 931-967.
29. Hulsebosch, R.J.; Borovykh, I.V.; Paschenko, S.V.; Gast, P.; Hoff, A.J., *J. Phys. Chem. B* **1999**, 103, 6815-6823.
30. Biggins, J.; Mathis, P., *Biochemistry* **1988**, 27, 1494-1500.
31. Castellani, F.; van Rossum, B.; Diehl, A.; Schubert, M.; Rehbein, K.; Oschkinat, H., *Nature* **2002**, 420, 98-102.

4 Photo-CIDNP in the reaction center of the green sulphur bacterium *Chlorobium tepidum* observed by ^{13}C MAS NMR

Photochemically induced dynamic nuclear polarisation has been observed in RCs of the green sulphur bacterium *Chlorobium tepidum* by ^{13}C magic-angle spinning solid-state NMR using continuous illumination with white light. All light-induced ^{13}C NMR signals appear to be emissive, which is similar to the pattern observed in the RCs of plant PSI and purple bacterial RCs of *Rb. sphaeroides* WT. The donor in RCs of green sulphur bacteria clearly differs from the substantially asymmetric special pair of purple bacteria and appears to be similar to the more symmetric donor of PSI.

4.1 Introduction

Photosynthesis is the process in which light energy is transformed into chemical energy and stored by an organism (1). Photosynthetic RCs are classified into two types on the basis of their early electron acceptors (2-4). The RCs containing membrane bound iron-sulphur centers are called 'Fe-S type RC' (Type-I), while those containing (B) Phe and quinones as 'pheophytin-quinone type RC' (Type-II). Type-I RCs are found in green sulphur bacteria, heliobacteria, cyanobacteria as well as in plants. On the other hand, type-II RCs are found in purple bacteria, cyanobacteria and in plants. Oxygenic photosynthetic organisms, such as plants, algae and cyanobacteria, contain both types of photosystems, namely PSI and PSII. The two photosystems have very different redox potential properties. PSII provides a strong positive redox potential, which enables the oxidation of water and production of molecular oxygen, while PSI generates a strong negative redox potential. The question of what are the determining factors of the redox properties has recently been addressed (5-8).

Anoxygenic photosynthetic bacteria contain a single photosystem, either type-I RCs, as found in green sulphur bacteria and heliobacteria, or type-II RCs, in purple and filamentous green bacteria. Green sulphur bacteria have large light-harvesting antenna complexes known as chlorosomes, which contain BChl aggregates (9) and FMO proteins (10).

Interestingly, in green sulphur bacteria and in heliobacteria a single gene of the RC core protein has been identified (11, 12). Structural analysis of the RC core complex of the green sulphur bacteria *C. tepidum* indicated the presence of a homodimer formed by two 82 kDa PscA proteins (13) which is in contrast to a heterodimer formed by PsaA and PsaB in PSI. In

a single PscA protein, eight BChl *a*, two plant Chl *a* derivatives and between two and eleven carotenoids have been reported per RC (14, 15) which is considerably less than the number of chlorophylls found attached to the heterodimeric core of PSI. Until now, no X ray crystal structure of a RC of green sulphur bacteria has been reported.

The primary donor in the RC of green sulphur bacteria is termed P840, due to the absorption maximum at 840 nm. It has been assigned to two BChl *a* molecules (16, 17), probably two C-13^2 epimers (18). The RC of green sulphur bacteria also contains a plant Chl *a*, called Chl 670, presumably acting at the primary electron acceptor (A_0) (19). That Chl *a* cofactor, however, is esterified with Δ2,6-phytadienol, rather than phytol as in plants and cyanobacteria (18). Based on EPR experiments, a menaquinone cofactor has been proposed to be the secondary electron acceptor (A_1) (20, 21). The putative quinone binding site appears to be partially conserved in PSI, green sulphur bacteria and heliobacteria (22). It has been reported that the RCs of green sulphur bacteria and heliobacteria are active without the presence of quinones (23, 24). The terminal electron acceptors are three iron sulphur centers, F_X, F_A and F_B, as detected by EPR studies on the RCs (25). The structural and functional aspects of RCs of green sulphur bacteria have been probed by several spectroscopic methods (26-30).

A rapidly emerging technique in the study of membrane proteins is MAS NMR (31, 32). The chemical shifts allow the exploration of the electronic and protonic structures in the electronic ground state. In RCs upon illumination, photo-CIDNP has been observed by MAS NMR as modification of signal intensity (33, 34, 35). Photo-CIDNP intensities are related to the local electron spin densities. In purple bacterial RCs of *Rb. sphaeroides* WT and carotenoid-less mutant R-26, the strongest enhancement of NMR signals observed is a factor of 10,000 (36, 37). Until now, photo-CIDNP has been observed in four photosynthetic systems: In purple bacterial RCs of *Rb. sphaeroides* WT (36, 38), R-26 (33, 37, 39-41), D1D2 complex of PS II of plants (6, 8) and from PSI complex of plants (Chapter 2).

Recently, it has been shown that three mechanisms can produce photo-CIDNP in solids (34, 35). In the TSM mechanism (42), the extent of the photo-CIDNP effect is maximum when matching of the nuclear Zeeman frequency to coupling between the two electron and hyperfine interaction occurs in the spin-correlated radical pair. The DD mechanism (43) also requires anisotropic hyperfine coupling, but a net photo-CIDNP effect is caused due to the different lifetimes of the two forms of the spin-correlated radical pair, the singlet and triplet states. This mechanism requires a single matching of the nuclear Zeeman frequency to the hyperfine interaction. In addition, a third mechanism appears active in systems having a long-lived triplet state of the donor, leading to the DR process (44).

4.2 Materials and Methods

4.2.1 *Preparation*

C. tepidum strain TLS were grown in a medium described by Wahlund et al. (45). The 3FMO-RC particles of *C. tepidum* were isolated as described in ref. (46). The purity of the FMO-RC particles was analysed by SDS-PAGE. The purified FMO-RC particles were then recovered from the sucrose gradient and dialysed against buffer containing 50 mM Tris/HCl and 10 mM sodium ascorbate (pH 8.3), for 3 h and then ultracentrifuged at 200,000 *g* for 3 h. The pellet containing the particles was dissolved in buffer containing 50 mM glycine and 0.01% Triton X-100 (pH 10.8). For photo-CIDNP studies the sample was reduced by 50 mM sodium dithionite.

4.2.2 *MAS-NMR Measurements*

The NMR experiments were performed by using a DMX-200 NMR spectrometer (Bruker GmbH, Karlsruhe, Germany). The sample was loaded in an optically transparent 4 mm sapphire rotor. The sample was reduced by addition of an aqueous solution of 50 mM sodium dithionite in an oxygen-free atmosphere. Following the reduction, slow freezing of the sample was performed directly in the NMR probe inside the magnet with liquid nitrogen-cooled gas under continuous illumination with white light (47). The illumination setup was specially designed for a Bruker MAS probe (41). Photo-CIDNP ^{13}C MAS NMR spectra were obtained at a temperature of 240 K with a spinning frequency of 8 kHz. The light and dark spectra were measured with a Hahn echo pulse sequence and TPPM proton decoupling (48).

4.3 Results and Discussion

4.3.1 *Dark spectrum*

Fig. 4.1 shows the ^{13}C MAS NMR spectra of natural abundance FMO-RC particles of *C. tepidum* in the dark (A) and under continuous illumination with white light (B) in a magnetic field of 4.7 Tesla. Spectrum 4.1A shows the characteristic features of a ^{13}C-MAS NMR spectrum of a protein, *i.e.*, broad responses between 0 and 50 ppm. The sharp signal at 175.7 ppm arises mainly from glycine which is present in the buffer. Additional weak features of aromatic cofactors and amino acids appear between 190 and 80 ppm.

4.3.2 *Overall spectral pattern*

In spectrum 4.1B, obtained under illumination, several strong emissive (negative) signals appear. A total of ten centrebands has been identified (Table 4.1). These signals appear in the carbonylic region as well as in the aromatic region. The signals observed at lowest frequency arise at about 100 ppm from methine carbons, while no photo-CIDNP is observed in the aliphatic region.

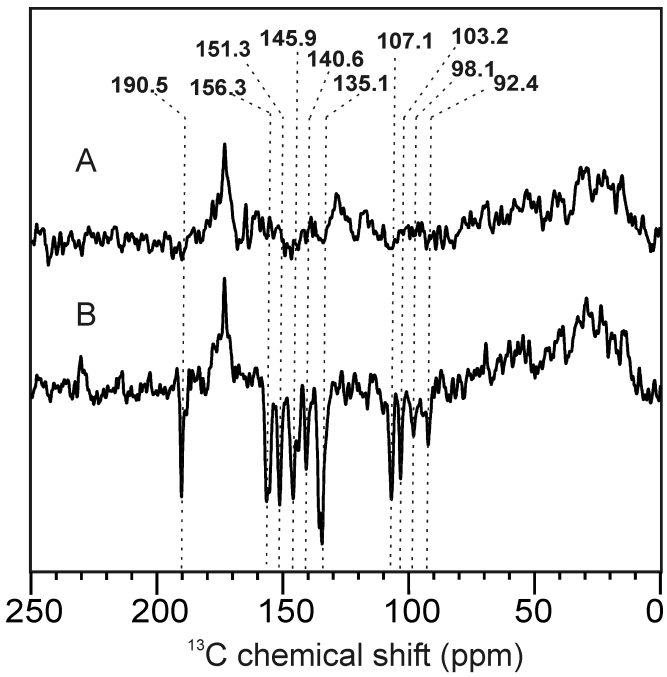

Figure 4.1. ^{13}C MAS NMR spectra of RC complexes of *C. tepidum* at 240 K recorded with a MAS frequency of 8 kHz at 4.7 Tesla. Spectra are obtained: in the dark (A) and under continuous illumination with white light (B). In both experiments, the cycle delay was 12 seconds.

This overall pattern has also been observed in RCs of PSI (Chapter 2) and *Rb. sphaeroides* WT (36) and is in contrast to the pattern of positive aromatic signals combined with negative methine signals as observed in RCs of PSII (6, 8) and *Rb. sphaeroides* R-26 (33, 37, 39-41). In case of the two bacterial RCs of *Rb. sphaeroides*, it has been demonstrated that the difference in the pattern is due to a difference of the lifetime of the donor triplet (37). RCs of *Rb. sphaeroides* WT have a triplet lifetime of 100 ns, while the RCs of the carotene-less mutant R26 have a lifetime of the donor triplet of 100 μs, a time long enough to produce net polarization by the DR effect leading to an inversion of the sign of the donor signals (36, 37). Hence, based on such comparison, we assume that the donor side of the RC of *C. tepidum* contains a carotene which is able to quench efficiently the triplet states of the donor. In fact, similarity observed in the photo-CIDNP pattern in the RCs of *C. tepidum* (49) is also in line with the presence of carotenoids in the RCs.

4.3.3 *Assignments*

Most of the signals can be assigned to a BChl *a* or Chl *a* cofactor (Table 4.1). In the carbonyl region, the strong and sharp signal at 190.5 ppm is detected and can be assigned directly to the carbonyl carbon C-13^1. Such a strong emissive signal of a carbonyl carbon has been observed in the photo-CIDNP spectrum of PSI (Chapter 2), where it has been assigned to the donor, while it is weak in the spectrum of *Rb. sphaeroides* WT (36). The strongest signals are observed in the aromatic region between 120 and 170 ppm. The signal at 156.3 ppm may be doubled and can be assigned to C-9 of a BChl *a* or C-1 and C-6 of a Chl *a*. The

Chl *a*		PSI	Carbon No	BChl *a*		*C.tepidum*
σ_{liq} [a]	σ_{ss} [b]	σ [c]		σ_{liq} [d]	σ_{ss} [e]	σ [f]
189.3	190.6	~190.6.E	**13**[1]	199.3	188.2	190.5 E
172.7	175.3		**17**[3]	173.4	174.0	
171.0	171.2		**13**[3]	171.6	171.4	
167.4	170.0	167.1 E	**19**	167.3	168.9	
161.4	162.0	160.4 E	**14**	160.8	160.7	
154.0	155.9	154.8 E	**1**	151.2	153.5	
155.8	154.4		**6**	168.9	170.2	
151.4	154.0	152.6 E	**16**	152.2	150.1	
148.0	150.7	149.9 E	**4**	150.2	152.2	151.3 E
147.7	147.2	147.2 E	**11**	149.5	147.2	145.9 E
146.1	147.2		**9**	158.5	158.0	156.3 E
144.1	146.2	144.2 E	**8**			
139.0	137.0	138.6 E	**3**	137.7	136.1	135.1 E
135.5	136.1	~136 E	**2**	142.1	140.7	140.6 E
134.2	134.0	~132 E	**12**	123.9	119.9	
134.0	133.4		**7**			
131.5	126.2		**13**	130.5	124.1	
131.5	126.2		**3**[1]	199.3	194.5	
118.9	113.4		**3**[2]			
107.1	108.2	105.4 E	**10**	102.4	100.0	103.2 E
106.2	102.8		**15**	109.7	105.8	107.1 E
100.0	98.1		**5**	99.6	98.8	98.1 E
92.8	93.3		**20**	96.3	93.7	92.4 E

[a]See ref. (52),[b] See ref. (53), [c] (Chapter 2), [d] Ref. (41), [e] Ref. (54), [f] this work.

Table 4.1. ^{13}C chemical shifts of the photo-CIDNP signals observed in *C. tepidum* in comparison to chemical shift data of BChl *a* and Chl *a*.

peak at 151.3 ppm can be assigned to C-4 or C-16 of either a BChl *a* or Chl *a* cofactor. The signal at 145.9 ppm, having a clear shoulder on its low-frequency wing, can arise from a C-11 of a BChl *a* or from C-8 of a Chl *a*. The signal at 140.6 ppm can be assigned to C-2 of a BChl *a*, while an assignment to a Chl *a* is rather unlikely. The signal at 135.1 ppm shows a shoulder and can be assigned to C-3 of BChl *a* or C-2 of Chl *a*. Also in the region of the methine carbons, most signals may be assigned to either the BChl *a* donor molecule(s) or to the Chl *a*

acceptor. The signal at 107.1 ppm can be assigned to the C-15 of a BChl *a* or a C-10 of a Chl *a*, while the response at 103.1 ppm can arise from the C-10 of a BChl *a* or a C-15 of a Chl *a*. The signals at 98.1 and 92.4 ppm originate form the C-5 and C-20, respectively, from either the BChl *a* or the Chl *a*.

Hence, the chemical shift information is not sufficient to assign the photo-CIDNP signals to either the donor or the acceptor, although the strength of the carbonyl signal and the chemical shift of 140.6 ppm indicate that at least some contribution from the donor exists. In analogy to PSI and the RC of *Rb. sphaeroides* WT, in which the downfield signals with shifts ~130 ppm were assigned to the donor based on simulations of donor and acceptor photo-CIDNP intensities, we tend to assign the set of aromatic carbons with shifts greater than 130 ppm to the donor, while there is little evidence for an assignment of the signals of the methine carbons to either the donor or the acceptor.

4.3.4 *Line shape and linewidth*

Some of the signals that are attributed to the donor appear to be doubled or show a shoulder, namely the signals at 156.3, 145.9 and 135.1 ppm. The signal doubling can be interpreted in terms of a slightly asymmetric dimer. If this is the case, small differences between the two halves exist in the electronic ground state, indicated by the chemical shift differences and for the radical cation, indicated by different signal intensities. This interpretation depends on the assignment of these signals to the donor. First, it implies that the two branches of *C. tepidum* RCs differ much less from each other than in RCs of purple bacteria, where a clear asymmetry in the electronic ground state has been demonstrated for the special pair donor (36, 38, 50, 51) and the radical cation state (36). This is hardly surprising, as *C. tepidum* RCs appear to be scaffolded by a protein homodimer, while a heterodimer is found in purple bacteria. The slight asymmetry, however, indicates that the two branches are not fully equivalent, which in turn implies that the symmetry of the homodimer is broken. Data on RCs of *C. limicola* ENDOR and Special TRIPLE spectroscopies show that $P840^{+\bullet}$ has a symmetrical distribution over the two halves of the pair, having approximately a 1:1 distribution of electron spin density (27). This conclusion on the radical-pair state matches with our observation of similar photo-CIDNP intensities of both parts of split signals, making an interpretation of an asymmetric dimer $P840^{+\bullet}$ unlikely (30). On the other hand, circular dichroism data on RCs of *C. tepidum* were interpreted in terms of a difference in asymmetry of the P840 donor relative to the special pair in purple bacteria (29). Our chemical shift data do not allow for an interpretation of a strong asymmetry within the P840 donor dimer in the ground state. This contrasts with the photo-CIDNP data for the special pair of RCs of purple bacteria, were the symmetry is already broken in the electronic ground state (36, 38, 50, 51). Hence, the difference observed by CD spectroscopy may have a different origin than

electronic ground-state asymmetry. FTIR data on the primary donor have shown that at least one of the two BChl *a* forming the primary donor is free from hydrogen bonding (30).

The five signals at 190.5, 151.3, 140.6, 103.2 and 106.6 ppm do not indicate any doubling and appear to be remarkably narrow, as indicated by full width at half-height of 54.1, 68.9, 64.0, 56.6 and 73.8 Hz, respectively. These linewidths are similar to those found in PSI (Chapter 2) and reveal a rigid, ordered as well as structurally and electrostatically stable donor side, keeping the reorganization energies of the electron transfer low. Hence, the donor of the RC of *C. tepidum* is probably similar in electronic structure and rigidity to that of PSI, despite the difference in the chemical structure of the cofactors.

4.4 Conclusions

Photo-CIDNP has been observed in RCs of the green sulphur bacterium *C. tepidum.* It appears that photo-CIDNP is an inherent property of all types of natural RCs. In the ^{13}C photo-CIDNP MAS NMR spectrum of the RC of *C. tepidum*, all signals are emissive (negative). The overall photo-CIDNP pattern is similar to that observed in PSI. The carbonylic and aromatic signals can be assigned to the two BChl *a* molecules of the donor side. Doubling of several signals suggests an only slightly asymmetric dimer in both the electronic ground state and radical cation state of the donor side. Hence, the donor in RCs of green sulfur bacteria clearly differs from the substantially asymmetric special pair of purple bacteria and appears to be similar to the more symmetric donor of PSI.

References

1. Mayer, J.M., *Ann. Chem. Pharm.* **1842**, 42, 233-240.
2. Blankenship, R.E., *Photosynth. Res.* **1992**, 33, 91-111.
3. Golbeck, J.H., *Proc. Natl. Acad. Sci. U. S. A.* **1993**, 90, 1642-1646.
4. Barber, J.; Andersson, B., *Nature* **1994**, 370, 31-34 (1994) 31-34.
5. Mulkidjanian, A.Y., *Biochim. Biophys. Acta* **1999**, 1410, 1-6.
6. Matysik, J.; Alia; Gast, P.; van Gorkom, H.J.; Hoff, A.J.; de Groot, H.J.M., *Proc. Natl. Acad. Sci. U. S. A.* **2000**, 97, 9865-9870.
7. Witt, H.T., *Photosynth. Res.* **2004**, 80, 86-107.
8. Diller, A.; Alia; Roy, E.; Gast, P.; van Gorkom, H.J.; Zaanen, J.; de Groot, H.J.M.; Glaubitz, C.; Matysik, J., *Photosynth. Res.* **2005**, 84, 303-308.
9. de Boer, I.; Matysik, J.; Erkelens, K.; Sasaki, S.; Miyatake, T.; Yagai, S.; Tamiaki, H.; Holzwarth, A.R.; de Groot, H.J.M.; *J. Phys. Chem. B* **2004**, 108, 16556-16566.
10. Matthews, B.W.; Fenna, R.E.; Bolognesi, M.C.; Schmid, M.F.; Olson, J.M., *J. Mol. Biol.* **1979**, 131, 259-285.
11. Buttner, M.; Xie, D.L.; Nelson, H.; Pinther, W.; Hauska, G.; Nelson, N., *Proc. Natl. Acad. Sci. U. S. A.* **1992**, 89, 8135-8139.
12. Buttner, M.; Xie, D.L.; Nelson, H.; Pinther, W.; Hauska, G.; Nelson, N., *Biochim. Biophys. Acta* **1992**, 1101, 154-156.
13. Tsiotis, G.; Hager-Braun, C.; Wolpensinger, B.; Engel, A.; Hauska, G., *Biochim. Biophys. Acta* **1997**, 1322, 163-172.
14. Permentier, H.P.; Schmidt, K.A.; Kobayashi, M.; Akiyama, M.; Hager-Braun, C.; Neerken, S.; Miller, M.; Amesz, J., *Photosynth. Res.* **2000**, 64, 27-39.
15. Takaichi, S.; Oh-Oka, H.; *Plant Cell Physiol.* **1999**, 40, 691-694.
16. Sybesma, C.; Vredenberg, W.J., *Biochim. Biophys. Acta* **1963**, 75, (3), 439-441.
17. Feiler, U.; Hauska, G. In *Anoxygenic Photosynthetic Bacteria*; Blankenship, R. E., Madigan, M.T., Bauer, C.E., Eds. Kluwer: Dordrecth, 1995; p 665-685.
18. Kobayashi, M.; Oh-Oka, H.; Akutsu, S.; Akiyama, M.; Tominaga, K.; Kise, H.; Nishida, F.; Watanabe, T.; Amesz, J.; Koizumi, M.; Ishida, N.; Kano, H., *Photosynth. Res* **2000**, 63, 269-280.
19. Nuijs, A.M.; Vasmel, H.; Joppe, H.L.P.; Duysens, L.N.M.; Amesz, J., *Biochim. Biophys. Acta* **1985**, 807, 24-34.
20. Nitschke, W.; Feiler, U.; Lockau, W.; Hauska, G., *FEBS Lett.* **1987**, 218, 283-286.
21. Kjaer, B.; Frigaard, N.U.; Yang, F.; Zybailov, B.; Miller, M.; Golbeck, J.H.; Scheller, H.V., *Biochemistry* **1998**, 37, 3237-3242.
22. Schubert, W.D.; Klukas, O.; Krauss, N.; Saenger, W.; Fromme, P.; Witt, H.T., *J. Mol. Biol.* **1997**, 272, 741-769.
23. Kleinherenbrink, F.A.M.; Ikegami, I.; Hiraishi, A.; Otte, S.C.M.; Amesz, J., *Biochim. Biophys. Acta* **1993**, 1142, 69-73.
24. Frankenberg, N.; Hager-Braun, C.; Feiler, U.; Fuhrmann, M.; Rogl, H.; Schneebauer, N.; Nelson, N.; Hauska, G., *Photochem. Photobiol.* **1996**, 64, 14-19.

25. Vassiliev, I.R.; Antonkine, M.L.; Golbeck, J.H., *Biochim. Biophys. Acta* **2001**, 1507, 139-160.
26. Nitschke, W.; Feiler, U.; Rutherford, A.W., *Biochemistry* **1990**, 29, 3834-3842.
27. Rigby, S.E.J.; Thapar, R.; Evans, M.C.W.; Heathcote, P., *FEBS Lett.* **1994**, 350, 24-28.
28. Noguchi, T.; Kusumoto, N.; Inoue, Y.; Sakurai, H., *Biochemistry* **1996**, 35, 15428-15435.
29. Olson, J.M.; Miller, M.; Dolieslager, J., *Biochemistry* **1995**, 34, 15230-15234.
30. Mezzetti, A.; Seo, D.; Leibl, W.; Sakurai, H.; Breton, J., *Photosynth. Res.* **2003**, 75, 161-169.
31. de Groot, H.J.M., *Curr. Opin. Struc. Biol.* **2000**, 10, 593-600.
32. Laws, D.D.; Bitter, H.M.L.; Jerschow, A., *Angew. Chem. Int. Ed.* **2002**, 41, 3096-3129.
33. Zysmilich, M.G.; McDermott, A., *J. Am. Chem. Soc.* **1994**, 116, 8362-8363.
34. Jeschke, G.; Matysik, J., *Chem. Phys.* **2003**, 294, 239-255.
35. Daviso, E.; Jeschke, G.; Matysik, J. In *Biophysical techniques in photosynthesis*; Aartsma, T.J., Matysik, J., Eds. Springer: Dordrecht, 2007, p 385-399.
36. Prakash, S.; Alia; Gast, P.; de Groot, H.J.M.; Jeschke, G.; Matysik, J., *J. Am. Chem. Soc* **2005**, 127, 14290-14298.
37. Prakash, S.; Alia, Gast, P.; de Groot H.J.M.; Matysik, J.; Jeschke, G., *J. Am. Chem. Soc.* **2006**, 128, 12794-12799.
38. Schulten, E.A.M.; Matysik, J.; Alia; Kiihne, S.; Raap, J.; Lugtenburg, J.; Gast, P.; Hoff, A.J.; de Groot, H.J.M., *Biochemistry* **2002**, 41, 8708-8717.
39. Zysmilich, M.G.; McDermott, A., *J. Am. Chem. Soc.* **1996**, 118, 5867-5873.
40. Zysmilich, M.G.; McDermott, A., *Proc. Natl. Acad. Sci. U. S. A.* **1996**, 93, 6857-6860.
41. Matysik, J.; Alia; Hollander, J.G.; Egorova-Zachernyuk, T.; Gast, P.; de Groot, H.J.M., *Indian J. Biochem. Biophys.* **2000**, 37, 418-423.
42. Jeschke, G., *J. Am. Chem. Soc.* **1998**, 120, 4425-4429.
43. Polenova, T.; McDermott, A.E., *J. Phys. Chem. B* **1999**, 103, 535-548.
44. McDermott, A.; Zysmilich, M.G.; Polenova, T., *Solid State Nucl. Magn. Reson.* **1998**, 11, 21-47.
45. Wahlund, T.M.; Woese, C.R.; Castenholz, R.W.; Madigan, M.T., *Arch. Microbiol.* **1991**, 156, 81-90.
46. Francke, C.; Permentier, H.P.; Franken, E.M.; Neerken, S.; Amesz, J., *Biochemistry* **1997**, 36, 14167-14172.
47. Fischer, M.R.; de Groot, H.J.M.; Raap, J.; Winkel, C.; Hoff, A.J.; Lugtenburg, J.; *Biochemistry* **1992**, 31, 11038-11049.
48. Bennett, A.E.; Rienstra, C.M.; Auger, M.; Lakshmi, K.V.; Griffin, R.G., *J. Chem. Phys.* **1995**, 103, 6951-6958.
49. Bialek-Bylka, G.E.; Fujii, R.; Chen, C.H.; Oh-Oka, H.; Kamiesu, A.; Satoh, K.; Koike, H.; Koyama, Y., *Photosynth. Res.* **1998**, 58, 135-142.
50. Prakash, S.; Tong, S.H.; Alia, Gast, P.; de Groot, H.J.M.; Jeschke, G.; Matysik, J. In *Photosynthesis: Fundamental Aspects to Global Perspectives*; van der Est, A., Bruce, D. Eds.; Allen Press: Montreal, 2004; p 236-238.
51. Prakash, S. Ph.D. thesis, University of Leiden, 2006. (http://hdl.handle.net/1887/4555)
52. Abraham, R.T.; Rowan, A.E. In *Chlorophyll.* CRC Press: Boca Raton FL, 1991; p 797-834.

53. Boender, G.J. Ph.D. thesis, University of Leiden, 1996.

54. Matysik, J.; Alia; Gast, P.; Lugtenburg, J.; de Groot, H.J.M. In *Perspectives on Solid State NMR in Biology*; Kiihne, S., de Groot, H.J.M., Eds.; Kluwer: Dordrecht, 2001; p 215-225.

5 Photo-CIDNP observed by ^{13}C MAS NMR in isolated membrane fragments of *Heliobacillus mobilis*

Photo-CIDNP has been observed in entire membrane fragments of heliobacteria *Heliobacillus mobilis* by ^{13}C MAS solid-state NMR at magnetic fields of 4.7, 9.4 and 17.6 Tesla. At the highest magnetic field all signals are emissive, while at the lower fields part of the signal is absorptive and two sets of tetrapyrrole cofactors appear. One set, showing the enhanced absorptive signals, is assigned to the BChl *g* donor, while the set of emissive signals is assigned to the acceptor, 8^1-hydroxy Chl *a*. Both donor and acceptor appear to be monomeric. (4-^{13}C) ALA labelling reveals an isotope effect on the photo-CIDNP intensities.

5.1 Introduction

Heliobacteria are found to be closely related to cyanobacteria and are characterized by the presence of a unique BChl *g* cofactor (Fig. 5.1A) (1-4). The RCs of heliobacteria are less complex in their architecture compared to photosystems of cyanobacteria and purple bacteria, with the antenna pigments and RC bound to a single pigment protein complex which is embedded in the cytoplasmic membrane (5-7). The RCs lack light harvesting antenna complexes like chlorosomes found in green sulphur bacteria and light harvesting complexes LH I, LH II found in purple bacteria, thus having a reduced amount of antenna chlorophylls associated with the RC (8). They are grouped with the type I RCs, along with RCs of green sulphur bacteria, PSI of cyanobacteria and plants. From two members of this category, structural data are now available, namely from PSI of cyanobacteria (9) and of higher plants (10, 11).

The primary electron donor in the RC of heliobacteria is termed either as P798 (12) or P800 (5) and has been reported to be a dimer comprising of two BChl *g* (13) or the 13^2-epimers BChl *g* and BChl *g*′ (14). On the basis of experimental data the primary electron acceptor is proposed to be a Chl *a* like pigment absorbing at 670 nm (15, 16). Chemical analysis established the structure to be 8^1-hydroxy Chl *a* esterified with a farnesol sidechain (17) (Fig. 5.1B). The pigment composition per RC is about 35-40 molecules of BChl *g* (6), two molecules of BChl *g*′ (14) and two molecules of 8^1-hydroxy Chl *a* (17, 18) and about two to three carotenoid molecules (19, 20). Membranes of heliobacteria contain menaquinone, but

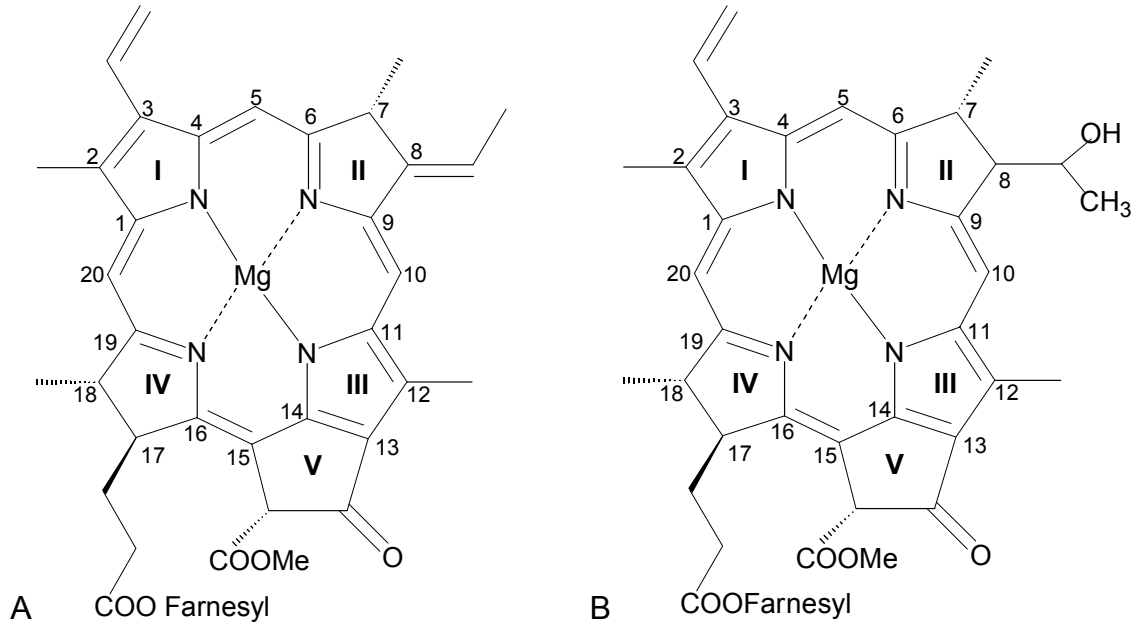

Figure 5.1. The structure of (A) BChl *g* and (B) 8^1-hydroxy Chl *a*, using IUPAC numbering.

there is no clear evidence establishing its role as an intermediate in the forward electron transfer (21-24). EPR and optical spectroscopic data indicate the presence of an iron-sulphur centre similar to F_x (13, 25-28) in PSI where it acts as electron acceptor and recently the presence of F_A and F_B clusters in the RCs have been reported (21).

Photo-CIDNP is an effect well known in liquid NMR and is used for example to explore protein surfaces (30, 31). In solids, photo-CIDNP has been observed for the first time in 1994 by MAS solid-state NMR, in quinone-blocked frozen samples of RCs of *Rb. sphaeroides* R-26 under illumination (32-35). Since then this technique has been employed in investigating RCs ranging from purple bacterial RCs from *Rb. sphaeroides* WT (36), plant PSI (Chapter 2), PSII (37, 38) and RCs from green sulphur bacterium *C. tepidum* (Chapter 4). NMR signals were detected in entire membrane bound photosynthetic units and even whole cells of *Rb. sphaeroides* (35, 39). Until now, the observation of the solid-state photo-CIDNP effect is limited to natural photosynthetic RCs.

In this chapter isolated membrane fragments of *Hba. mobilis* are investigated using photo-CIDNP. Photo-CIDNP MAS NMR provides information of the electronic ground-state structures of the electron donor and acceptor forming a correlated radical pair. In addition, photo-CIDNP MAS NMR intensities are related to the local electron spin densities in the electron donor and the electron acceptor forming the correlated radical pair state (40, 41). Selective ^{13}C isotope labelling at various cofactor positions in bacterial RCs provided insight into the ground-state electronic structure of the special pair (42, 43). The origin of the photo-CIDNP observed in the solid-state in photosynthetic RCs has been explained by the occurrence of three mechanisms, called the TSM, DD, and DR (35, 44-46).

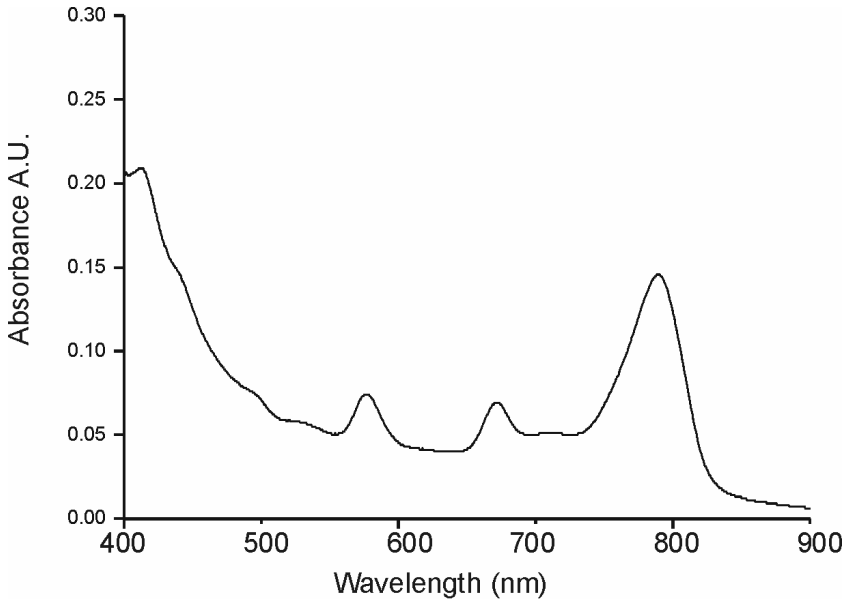

Figure 5.2. Absorption spectrum of *Hba. mobilis* membrane fragments.

5.2 Materials and Methods

5.2.1 *Sample preparation*

Hba. mobilis cells were grown in medium no. 1552 as described by van de Meent *et al*. (6). The cells were harvested after a period of seven days by centrifugation and re-suspended in a buffer containing 20 mM Tris-HCl and 10 mM sodium ascorbate (pH 8.0). All buffers used were thoroughly degassed. All the preparation was performed in the dark and care was taken to minimise the exposure of the samples to oxygen. The membrane fragments were prepared by sonication for 35 min followed by a 15 min centrifugation step at 40,000 *g* to remove unbroken cells and large fragments. The resulting supernatant was ultra centrifuged for 2 h at 200,000 *g* at a temperature of 4ºC. The pellet containing the membrane fragments was re-suspended in buffer containing 50 mM glycine and 0.02% SB-12 (pH 10.8). The absorbance spectrum of the isolated membrane fragments is shown in Fig. 5.2. The spectrum shows a BChl *g* peak at 790 nm and a peak at 690 nm from Chl *a* like pigments (5). For photo-CIDNP experiments the sample was reduced by 50 mM sodium dithionite under nitrogen air flow.

5.2.2 *Preparation of selectively ^{13}C labelled membrane fragments*

Selective isotope enrichment of (B)Chl in *Hba. mobilis* was done by growing the bacterial cultures (80 mL) anaerobically in the presence of 1.0 mM [4-^{13}C]- δ-aminolevulinic acid (Fig. 5.3A) ([4-^{13}C]-$COOHCH_2CH_2{}^{13}COCH_2NH_2$·HCl, 99% ^{13}C-enriched) purchased from Cambridge Isotope Laboratories (Andover, USA). ALA is a precursor of naturally occuring tetrapyrroles, including (B)Chl (47). The incorporation of [4-^{13}C]-ALA produces (B)Chl labelled at the C-1, C-3, C-6, C-8, C-11, C-13, C-17 and C-19 (Fig. 5.3). The preparation of isolated membranes was done as described above.

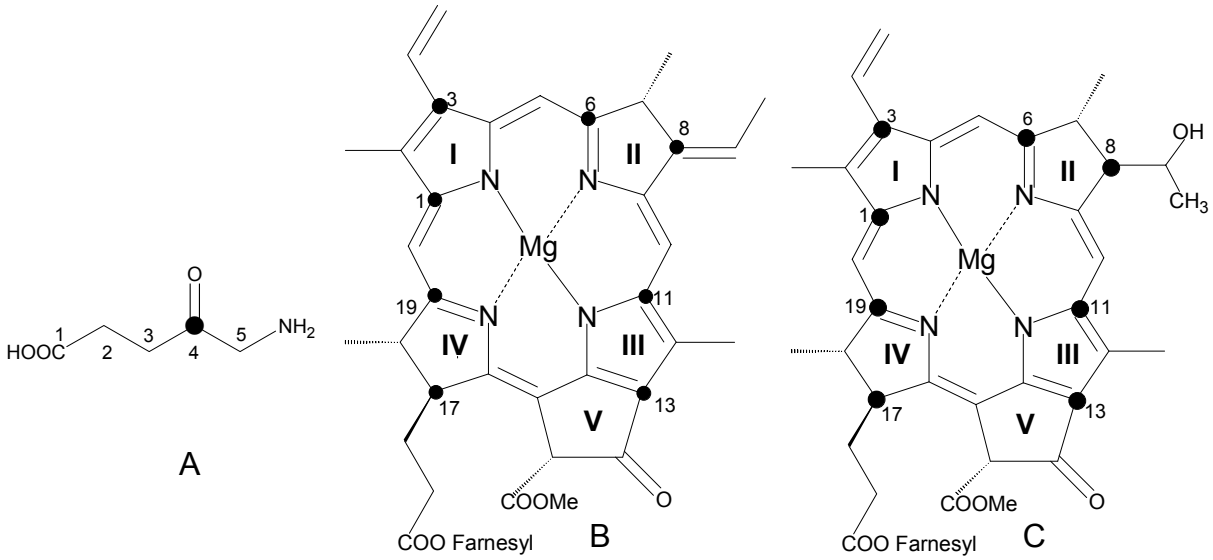

Figure 5.3. (A) (4- ^{13}C) δ-Aminolevulinic acid. (B) BChl *g* and (C) 8^{1}-hydroxy Chl *a*, ^{13}C labelled at eight positions indicated by filled circles (•).

5.2.3 *Determination of isotope incorporation*

BChl *g* is highly sensitive to light and oxygen, while its product of pheophytinization, BPhe *g*, is considerably more stable (4). Since the formation of BPhe is by the loss of Mg from BChl it can be assumed that the isotopic incorporations of the tetrapyrolle moiety of BChl *g* and BPhe *g* are identical, and the isotope enrichment was determined from the pheophytin form (48).

The frozen cells (1mL) from unlabelled and 4-ALA labelled samples were first centrifuged at 5,000 *g* for 30 min and the supernatant was removed. The cell pellets were re-suspended in acetone/methanol (7/2 v/v) and shaken thoroughly. The mixture was kept for 20 min followed by centrifugation at 5,000 *g* for 25 min. The supernatant was transferred into a dark bottle. This procedure was repeated until the pellet was grey/white. The solvents were evaporated using nitrogen airflow. All the preparation steps were conducted in the dark. The absorption spectrum of the extract showed the characteristic peaks of BChl *g* and a small amount of a Chl *a*-like compound that is a degradation product of BChl *g* (5). In order to obtain BPhe *g* the crude pigment extract was dissolved in diethyl ether solution and bubbled with a stream of N_2 containing gaseous HCl as described in Watanabe *et al*. (49). After washing with water, the solvent was removed and the residue was purified by chromatography on Silica gel 60 (Fluka Chemie, Switzerland) using hexane/acetone (80/20, v/v) as the eluting agent. The dark green fraction containing BPhe *g* was characterized by absorption spectroscopy (data not shown).

The mass spectrometry measurements were performed by diluting a small fraction of the purified pigment in methanol containing 1% ammonium acetate. The mass spectrum was acquired in positive ion mode by direct infusion (5 μL/min) using a LTQ FT hybrid mass spectrometer (ThermoFischer, Bremen, Germany) equipped with an electrospray ionization

source. The capillary was typically held at 3.5 kV, the transfer capillary was maintained at 280 °C and the tube lens was set to 240 V. For each experiment, 15 scans were accumulated.

5.2.4 *MAS-NMR measurements*

The NMR experiments were performed by using AV-750, DMX-400 and DMX-200 NMR spectrometers (Bruker-Biospin GmbH, Karlsruhe, Germany). The samples were loaded into optically transparent 4 mm sapphire rotors. The illumination setup has been specially designed for a Bruker MAS probe (41, 50). The light and dark spectra were obtained with a Hahn echo pulse sequence and TPPM proton decoupling (51).

5.3 Results and Discussion

5.3.1 *Field-dependence of the strength of the photo-CIDNP*

All ^{13}C MAS NMR spectra obtained from natural abundance sample of *Hba. mobilis* membrane fragments in the dark (Fig. 5.4) show similar features. Strong signals are observed between 0 and 50 ppm and are characteristic for a ^{13}C-MAS NMR spectrum of a large protein (52). Weak resonances from aromatic cofactors and amino acids appear between 120 and 140 ppm. The signal at 174.5 ppm arises mainly from the buffer. Dark spectra were obtained at different magnetic fields, (A) 17.6 Tesla, (B) 9.4 Tesla and (C) 4.7 Tesla. The signals obtained with the highest field (Fig. 5.4A) appear slightly better in terms of signal to noise, while several signals are not resolved at 4.7 Tesla (Fig. 5.4C). The ^{13}C photo-CIDNP MAS NMR spectrum obtained with continuous illumination (Fig. 5.5) shows both strong emissive (negative) and enhanced absorptive (positive) signals between 80 and 200 ppm. These spectra are obtained at three different magnetic fields, at (A) 17.6 Tesla, (B) 9.4 Tesla and (C) 4.7 Tesla. The strongest photo-CIDNP effect is observed at 4.7 Tesla (Fig. 5.5C), while at higher fields the effect decreases. Using the broad dark signal at about 30 ppm as an internal standard, the photo-CIDNP signal intensity at 9.4 Tesla is found to be by a factor of 3 higher than at 17.6 Tesla while at 4.7 Tesla the relative photo-CIDNP intensity increases further to a factor of 10 relative to the effect at 17.6 Tesla. The same pattern has been observed in bacterial RCs of *Rb. sphaeroides* WT and R-26 (35, 36) and PSII (Chapter 3). In contrast, the field dependence of the photo-CIDNP effect in PSI shows a maximum strength at 9.4 Tesla (Chapter 3). In addition the enhancement observed in the light induced signals from *Hba. mobilis* sample appears very strong, considering that the spectra are obtained from unlabelled RCs in membrane fragments.

5.3.2 *Field dependence on the sign of photo-CIDNP effect*

At high fields, the photo-CIDNP effect in the sample of *Hba. mobilis* is entirely emissive (Fig. 5.5A) as also observed for RCs of *Rb. sphaeroides* WT (36) and for PSI (Chapter 3). In contrast, at 9.4 Tesla, a mixed pattern of absorptive and emissive signals is observed (Fig. 5.5

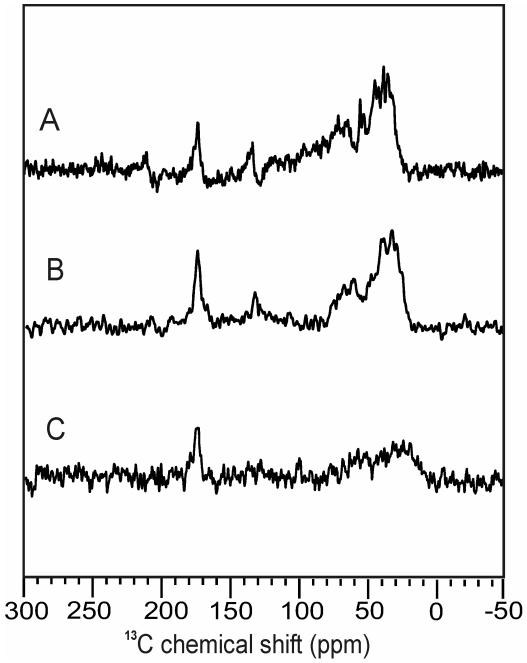

Figure 5.4. ^{13}C MAS NMR spectra of membrane fragments of *Hba. mobilis* obtained in the dark at different magnetic fields, (A) 17.6 Tesla, (B) 9.4 Tesla and (C) 4.7 Tesla, at a temperature of 240 K with a MAS frequency of 8 kHz.

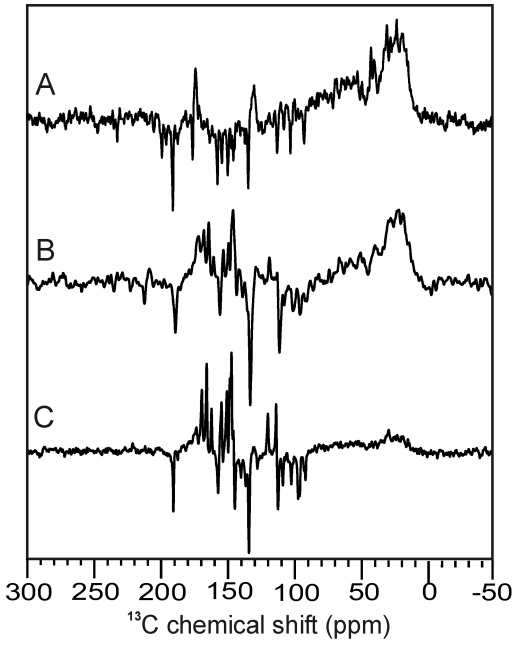

Figure 5.5. ^{13}C MAS NMR spectra of membrane fragments of *Hba. mobilis* obtained using continuous illumination with white light in different magnetic fields, (A) 17.6 Tesla, (B) 9.4 Tesla and (C) 4.7 Tesla at a temperature of 240 K with a MAS frequency of 8 kHz.

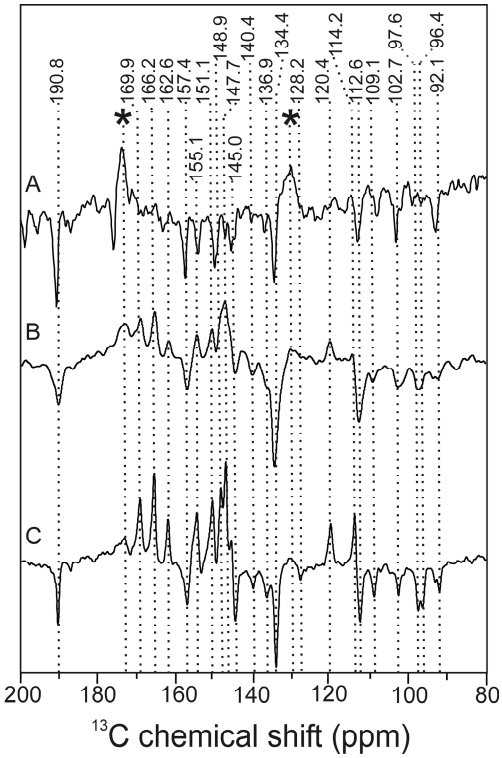

Figure 5.6. Detailed view of the region showing photo-CIDNP at different magnetic fields, (A) 17.6 Tesla, (B) 9.4 Tesla, and (C) 4.7 Tesla. The centerbands are shown in dashed lines and the dark signals are marked by asterisks.

B). A pattern of absorptive and emissive signals are also observed in RCs of *Rb. sphaeroides* R-26 and PSII at all three fields (ref. 35, Chapter 3). At 4.7 Tesla a similar mixed pattern appears (Fig. 5.5C). Hence, there must be an inversion point of the sign of the sub-set of signals between 9.4 and 17.6 Tesla. Such a field-dependent sign change of a sub-set of signals has not yet been observed in any other system. Details can be seen in Fig. 5.6, showing the olefinic and carbonylic regions on an expanded scale. The signals labelled with a star (*) originate from the protein and are not light-induced. All other signals are due to the photo-CIDNP effect. The best spectral resolution is obtained at 4.7 Tesla (Fig. 5.6C), despite the reduced Zeeman splitting and correspondingly less spectral dispersion.

5.3.3 *Effect of selective isotope labelling*

Selectively [4-^{13}C]-ALA isotope labelling of *Hba. mobilis* results in label patterns of the tetrapyrrole macrocyles as shown in Fig. 5.3B and C. Since eight molecules of labelled ALA can be used to synthesize one molecule of BChl *g*, a maximum of eight ^{13}C labels can be incorporated in BChl *g* and in BPhe *g* (42). The mass spectra of the unlabelled and labelled BPhe *g* are shown in Fig. 5.7 A and B, respectively. The mass spectrum of the unlabelled BPhe *g* exhibits a molecular peak at *m/z* = 797.5, which corresponds to BPhe *g* ($[M+H]^+$, *i.e.* $C_{50}H_{60}N_4O_5$) as well as three peaks resulting from the ^{13}C, ^{15}N and ^{18}O in natural abundance.

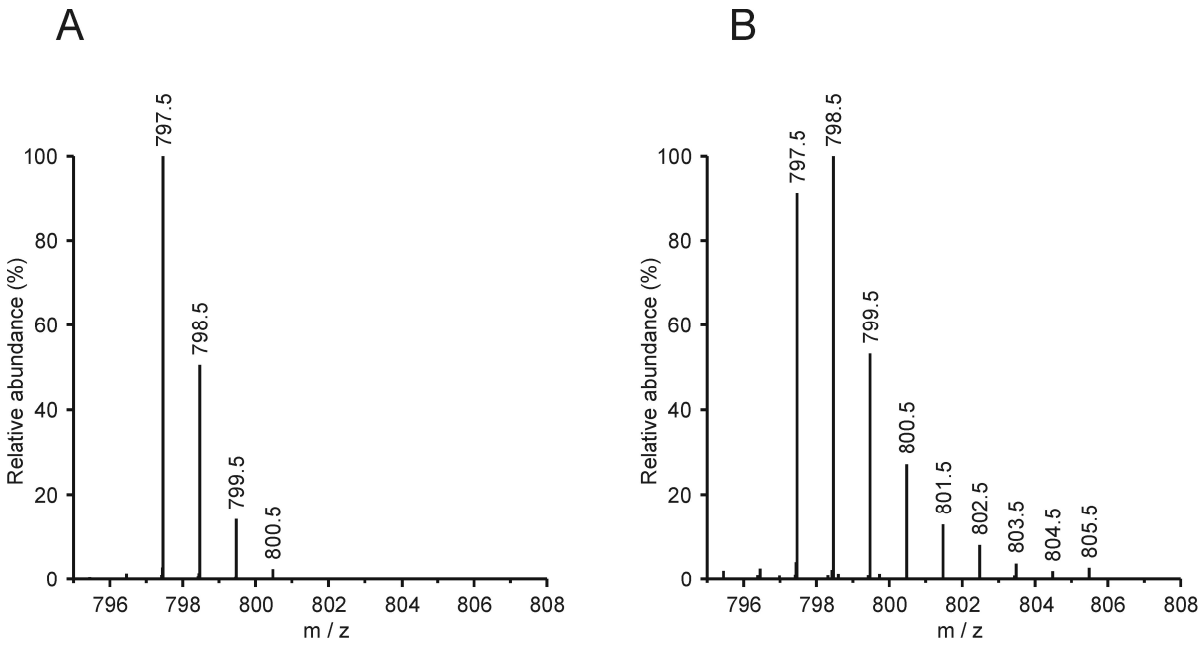

Figure 5.7. Mass spectra of (A) natural abundance BPhe g and (B) 4-Ala labelled $^{13}C_8$ BPhe g.

The mass spectrum of the labelled sample shows the peak due to unlabelled BPhe *g* as well as peaks resulting from the incorporation of ^{13}C isotopes (M+1 to M+8). The isotopic pattern of the unlabelled sample was used to calculate the intensities of the labelled BPhe *g* (53). The total incorporation of the ^{13}C was calculated to be 12%. The statistical analysis suggests that 50% of the BChl *g* cofactors in the *Hba. mobilis* sample were not labelled. The ^{15}N and ^{18}O contributions were not taken into account for the calculations of the isotope enrichment.

5.3.4 *Effect of isotope labelling*

The BChl *g* molecule (Fig. 5.3B) contains eight ^{13}C labelled positions from which one is aliphatic (C-17). In the 8^1-hydroxy Chl *a* cofactor (Fig. 5.3C), also eight positions are labelled, however two carbons are aliphatic. ^{13}C photo-CIDNP spectra were measured at 4.7 Tesla (Fig. 5.8A) and 9.4 Tesla (Fig. 5.8B). Both spectra show a pattern of absorptive and emissive photo-CIDNP signals, similar to the unlabelled sample. At 4.7 Tesla, five strongly absorptive signals dominate the spectrum, while the emissive signals are much weaker. Comparing the averaged intensity ratios of positive and negative signals, the relative intensity of the positive signals (Spectrum 5.7A) is a factor of 5 stronger than for the unlabelled samples (Spectrum 5C). Assuming that the TSM causes emissive signals, while the DD generates positive signals, as found in bacterial RCs (36), it appears that the isotope labelling affects the outcome of the two mechanisms to a different extent. Hence, it may be that the TSM is weakened or that the DD is enhanced. Magnetic isotope effects have been shown to affect the intersystem crossing frequency (54), and it appears reasonable that this generates positive signals at the expense of the negative TSM by isotope labelling, with little effect on

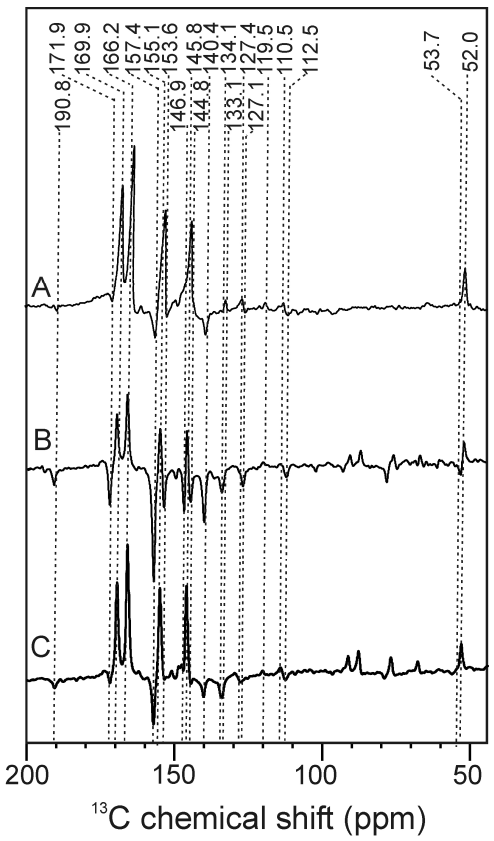

Figure 5.8. ^{13}C Photo-CIDNP MAS NMR spectra obtained in the dark and with continuous illumination with white light at (A) 4.7 Tesla using a cycle delay of 4sec (B) 9.4 Tesla using a cycle delay of 4sec and (C) 9.4 Tesla using a cycle delay of 0.4sec. A spinning frequency of 8 kHz and a temperature at 240 K were used for the experiments.

the DD. Since mass spectrometry data analysis shows an isotope label concentration of 12%, compared to the natural abundance concentration of 1%, a signal enhancement by a factor of 12 due to isotope labelling would be expected. Comparing signal intensities of labelled and unlabelled signals (discussed in following paragraphs), an enhancement factor of about 6 has been found upon labelling for both emissive and enhanced absorptive signals. The loss of signal may be due to spin diffusion, or due to an effect of the isotope labelling on the spin-chemical machinery producing photo-CIDNP.

In the unlabelled sample, no photo-CIDNP is observed in the aliphatic region, while in the 4-ALA labelled sample, a signal appears at 52.0 ppm (Figs. 5.5 and 5.8). Hence an assumption can be made that this aliphatic signal is build-up by spin diffusion. Similar intensity equilibration of photo-CIDNP signals under the steady-state conditions of continuous illumination experiment has been observed previously in RCs of *Rb. sphaeroides* WT (39). This would imply that also the intensities of the aromatic photo-CIDNP signals have been equilibrated by spin diffusion and the small difference in intensity reflects different local relaxation properties.

5.3.5 *Effect of fast scanning*

Relaxation MAS NMR studies on the RC of *Rb. sphaeroides* WT demonstrate that the T_1 relaxation times of carbon atoms of the more rigid parts of the donor cofactor are around 17 seconds (41). All spectra presented until now have been measured at long cycle delays allowing for sufficient relaxation. Unlabelled samples were measured at 12 seconds, and for labelled samples 4 seconds cycle delay has been applied. As shown for various RCs, this difference in cycle delay has very little effect on the spectral pattern (55). However, the use of very fast cycle delays may prevent complete relaxation, and signals of cofactors having a long T_1 may be quenched. The spectrum in Fig. 5.8C is obtained using a high cycle frequency of 0.4 seconds favouring signals of carbons having a short T_1 relaxation rate. Evidently the set of emissive signals decays dramatically compared to the spectrum measured at the same field with longer cycle delay (Fig. 5.8B). Recently it has been shown that the active role of the triplet involves fast enhanced recovery of the donor signals by relaxation mechanisms (55). If relaxation channels open up when the triplet is present the assignment of the positive signals to the donor would be more reasonable and may indicate the possibility of cross relaxation. Alternatively, when only TSM and DD are present, it is reasonable to assume that the emissive signals arise from the donor side, which is generally known to be very rigid (ref. 56 and Chapter 2).

5.3.6 *Signal assignment*

The single aliphatic photo-CIDNP signal appears at 52.0 ppm in the 4-ALA labelled sample (Fig. 5.8A) and can be unambiguously assigned to the C-17, the only aliphatic ^{13}C labelled carbon in BChl *g* (Table 5.1). Such an assignment would imply that the positive signals originate from the donor and are caused by the DR mechanism. If the aliphatic response would originate from the acceptor, two signals would be expected, from the hydroxyl moiety at the 8^1 position and the C-17, however, there is no indication for a second signal in the spectrum (Fig. 5.8A). Hence this corroborates the assignment of the enhanced absorptive signals to the donor side, associating the positive signals to the BChl *g* (Fig. 5.1A). This would imply that the emissive signals originate from the acceptor cofactor, which means that the negative signals would be related to the modified plant Chl *a* (Fig. 5.1B).

Upon 4-ALA labelling, four strong signals at 169.9, 166.2, 155.1 and 145.8 appear in the aromatic region (Fig. 5.8A). Additionally, four small signals are observed at 133.1, 127.4, 119.5 and 110.5 ppm. Together with the aliphatic signal at 52.0 ppm, which is assigned to the C-17, nine positive signals can be identified which arise presumably from the donor. The ^{13}C BChl *g* chemical shifts have not yet been reported. However, except for the pyrrole ring II and the esterifying alcohol, the chemical composition of the tetrapyrrole ring of BChl *g* is identical to the well studied plant Chl *a*. The chemical shift of the C-6 may be quite close to the C-6 in BChl *a*, which is expected at 168.9 ppm (Table 5.1).

Chl *a*		Carbon No.	BChl *a*		*Hba. mobilis*	
σ_{liq} [a]	σ_{ss} [b]		σ_{liq} [c]	σ_{ss} [d]	Positive signals	Negative signals
189.3	190.6	**13**[1]	199.3	188.2		190.8
172.7	175.3	**17**[3]	173.4	174.0		
171.0	171.2	**13**[3]	171.6	171.4		
167.4	170.0	**19**	167.3	168.9	166.2	171.9
161.4	162.0	**14**	160.8	160.7	162.6	
154.0	155.9	**1**	151.2	153.5	155.1	157.4
155.8	154.4	**6**	168.9	170.2	169.9	153.6
151.4	154.0	**16**	152.2	150.1	151.1	
148.0	150.7	**4**	150.2	152.2	148.9	
147.7	147.2	**11**	149.5	147.2	145.8	145.0
146.1	147.2	**9**	158.5	158.0	147.7	
144.1	146.2	**8**	55.6			
139.0	137.0	**3**	137.7	136.1		140.4
135.5	136.1	**2**	142.1	140.7		
134.2	134.0	**12**	123.9	119.9		
134.0	133.4	**7**				
131.5	126.2	**13**	130.5	124.1	133.1	134.4
131.5	126.2	**3**[1]	199.3	194.5	127.4	
118.9	113.4	**3**[2]			119.5	
107.1	108.2	**10**	102.4	100.0	110.5	109.1
106.2	102.8	**15**	109.7	105.8		102.7
100.0	98.1	**5**	99.6	98.8		97.6, 96.4
92.8	93.3	**20**	96.3	93.7		92.1
51.6	51.4	**17**	50.4		52.0	53.7

Table 5.1. Tentative ^{13}C chemical shifts assignment of the observed negative and positive photo-CIDNP signals in *Hba. mobilis* membrane fragments when compared to published chemical shift data for Chl *a* and BChl *a*. (a) Ref. 57, the liquid NMR data (b) Ref. 58, the solid-state NMR data, which have been obtained from aggregates. (c) Ref. 59 (d) Ref. 59.

The two strong signals appearing at 169.9 and 166.2 ppm can be assigned convincingly to C-6 and C-19, respectively. Since for a Chl *a*, only a single carbon signal is expected downfield, the assignment of the positive signals to the BChl *g* donor is plausible. The signals at 155.1 and 145.8 ppm match well with C-1 and C-11 respectively. The labelled carbon C-13 may be assigned to the weak signal at 133.1 ppm. The other three small positive signals arise from positions that were not labelled. The signals at 127.4, 119.5 and 110.5 may be assigned to the C-3^1, C-3^2 and C-10 carbons or could originate from histidine, which has a response in this region (60). There is no evidence for a positive signal from C-3 and C-8, which are labeled, while the nearby C-1 and C-6 yield strong signals. In the unlabelled sample, nine enhanced absorptive signals are observed at 169.9, 166.2, 162.6, 155.1, 151.1, 148.9, 147.7, 120.4, 114.2 ppm (Fig. 5.6C). The signal at 162.6 ppm can be assigned to the C-14, and the signal at

151.1 ppm to the C-16. The signals at 148.9 and 147.7 ppm match the NMR signals from carbons C-4 and C-9 for Chl *a* in the solid-state and in solution. The weak signals at 120.4 and 114.2 ppm are in the range of the histidine resonances and occur with similar intensity as for the labelled sample.

In the 4-ALA labelled sample, the negative signals are most pronounced at 9.4 Tesla (Fig. 5.8B). Signals appear at 190.8, 171.9, 157.4, 153.6, 146.9, 144.8, 140.4, 134.1, 127.1, 112.5 and 53.7 ppm. Assuming that the emissive signals originate from the acceptor, which is 8^1-hydroxy Chl *a*, an assignment of the signal at 190.8 ppm to the 13^1 carbonyl is reasonable. A 13^1 carbonyl signal has also been observed from PSI (Chapter 2) and the RC of *C. tepidum* (Chapter 4). However, it is remarkable that an unlabelled carbon shows such a strong, signal intensity. The signal at 171.9 ppm could be assigned to the C-19, which is labelled. The strongest emissive signal for the labelled sample appears at 157.4 ppm, which matches quite well to the response of the C-1 position for Chl *a* in the solid-state and in solution. The signal at 153.6 ppm in the labelled sample overlaps with the strong positive signal at 155.0 ppm, and can be attributed to the C-6 carbon. The two emissive minima at 146.9 and 144.8 for the labelled sample cannot be separated because of overlap with the positive signal at 145.9 ppm. Both may originate from a single emissive signal of the C-11. The shifts of the signals at 140.4 and 134.1 ppm match the shifts expected for the labelled C-3 and C-13, respectively. The two signals at 127.1 and 112.5 ppm again may be assigned to histidines (60). In the aliphatic region, an emissive signal appears at 53.7 ppm and can be assigned to C-8 or C-17. Due to overlap with a positive signal, the exact shift is difficult to determine.

For the unlabelled sample, the negative signals are best resolved at 4.7 Tesla (Fig. 5.6C). Five strong signals appear at 190.8, 157.4, 145.0, 134.4 and 112.6 ppm. The signal at 190.8 ppm, which originates from the C-13^1 carbonyl, is also clearly observed in the labelled sample. The resonance at 157.4 ppm is the strongest for the labelled sample and has been assigned to the C-1. This signal can be detected without spectral overlap and has similar intensity to the carbonyl signal. The sharp negative features at 146.9 and 144.8 ppm in the spectrum of the labelled compound may originate from C-11 which gives a response at 145.0 ppm in the unlabelled sample. The signal at 134.4 ppm may be assigned to the C-13. The signal at 112.6 ppm, which does not change its intensity upon 4-ALA labelling, can be from histidine. In addition, five weak signals appear in the methine region at 109.1, 102.7, 97.6, 96.4 and 92.1 ppm. Assuming that both signals at 97.6 and 96.4 ppm originate from a C-5, the other signals can be assigned to the methine carbons C-10, C-15, C-5 and C-20. The origin of the small splitting of the C-5 signal is not clear. The intensities of the signals of the four methine carbons are roughly similar, suggesting a homogeneous distribution of the electron spin density over the acceptor. This suggests that both donor and primary acceptor are monomeric.

5.4 Conclusions

Strong photo-CIDNP signals have been observed by ^{13}C MAS NMR in isolated membrane fragments of *Hba. mobilis*. A single complete set of positive signals, assigned to the BChl *g* donor, is detected, demonstrating a monomeric character. The emissive signals are assigned to the monomeric acceptor. The shifts suggest that histidines may be carrying electron spin density, probably at both the donor and the acceptor site. The ratio of positive to negative signals is strongly magnetic field dependent. At high fields, the donor signals turn to be emissive. In addition, isotope labeling affects the ratio of positive to negative signals suggesting an involvement of magnetic isotopes into the spin-chemical photo-CIDNP process in the solid-state.

References

1. Xiong, J.; Fischer, W.M.; Inoue, K.; Nakahara, M.; Bauer, C.E., *Science* **2000**, 289, 1724-1730.
2. Amesz, J., *J. Photochem. Photobiol. B* **1995**, 30, 89-96.
3. Brockmann, H.; Lipinski, A., *Arch.Microbiol.* **1983**, 136, 17-19.
4. Michalski, T.J.; Hunt, J.E.; Bowman, M.K.; Smith, U.; Bardeen, K.; Gest, H.; Norris, J.R.; Katz, J.J., *Proc. Natl. Acad. Sci. U. S. A.* **1987**, 84, 2570-2574.
5. Trost, J.T.; Blankenship, R.E., *Biochemistry* **1989**, 28, 9898-9904.
6. van de Meent, E.J.; Kleinherenbrink, F.A.M.; Amesz, J., *Biochim. Biophys. Acta* **1990**, 1015, 223-230.
7. Liebl, U.; Mockensturm-Wilson, M.; Trost, J.T.; Brune, D.C.; Blankenship, R.E.; Vermaas, W., *Proc. Natl. Acad. Sci. U. S. A.* **1993**, 90, 7124-7128.
8. Oh-Oka, H., *Photochem. Photobiol.* **2007**, 83, 177-186.
9. Jordan, P.; Fromme, P.; Witt, H.T.; Klukas, O.; Saenger, W.; Krauss, N., *Nature* **2001**, 411, 909-917.
10. Ben-Shem, A.; Frolow, F.; Nelson, N., *Nature* **2003**, 426, 630-635.
11. Amunts, A.; Drory, O.; Nelson, N., *Nature* **2007**, 447, 58-63.
12. Liebl, U.; Nitschke, W.; Mattioli, T.A., *Photochem. Photobiol.* **1996**, 64, 38-45.
13. Brok, M.; Vasmel, H.; Horikx, J.T.G.; Hoff, A.J., *FEBS Lett.* **1986**, 194, 322-326.
14. Kobayashi, M.; van de Meent, E.J.; Erkelens, C.; Amesz, J.; Ikegami, I.; Watanabe, T., *Biochim. Biophys. Acta* **1991**, 1057, 89-96.
15. Nuijs, A.M.; Vandorssen, R.J.; Duysens, L.N.M.; Amesz, J., *Proc. Natl. Acad. Sci. U. S. A.* **1985**, 82, 6865-6868.
16. van Kan, P.J.M.; Aartsma, T.J.; Amesz, J., *Photosynt. Res.* **1989**, 22, 61-68.
17. van de Meent, E.J.; Kobayashi, M.; Erkelens, C.; van Veelen, P.A.; Amesz, J.; Watanabe, T., *Biochim. Biophys. Acta* **1991**, 1058, 356-362.
18. van de Meent, E.J.; Kobayashi, M.; Erkelens, C.; van Veelen, P.A.; Otte, S.C.M.; Inoue, K.; Watanabe, T.; Amesz, J., *Biochim. Biophys. Acta* **1992**, 1102, 371-378.
19. Takaichi, S.; Inoue, K.; Akaike, M.; Kobayashi, M.; Oh-oka, H.; Madigan, M.T., *Arch. Microbiol.* **1997**, 168, 277-281.
20. Neerken, S.; Amesz, J., *Biochim. Biophys. Acta* **2001**, 1507, 278-290.
21. Heinnickel, M.; Gaozhong, S.; Golbeck, J.H., *Biochemistry* **2007**, 46, 2530-2536.
22. Hiraishi, A., *Arch. Microbiol.* **1989**, 151, 378-379.
23. Kleinherenbrink, F.A.M.; Amesz, J., *Biochim. Biophys. Acta* **1993**, 1143, 77-83.
24. Brettel, K.; Leibl, W.; Liebl, U., *Biochim. Biophys. Acta* **1998**, 1363, 175-181.
25. Muhiuddin, I.P.; Rigby, S.E.J.; Evans, M.C.W.; Amesz, J.; Heathcote, P., *Biochemistry* **1999**, 38, 7159-7167.
26. Prince, R.C.; Gest, H.; Blankenship, R.E., *Biochim. Biophys. Acta* **1985**, 810, 377-384.
27. Kleinherenbrink, F.A.M.; Chiou, H.C.; Lobrutto, R.; Blankenship, R.E., *Photosynth. Res.* **1994**, 41, 115-123.

28. Fischer, M.R., *Biochim. Biophys. Acta* **1990**, 1015, 471-481.
29. Heinnickel, M.; Agalarov, R.; Svensen, N.; Krebs, C.; Golbeck, J.H., *Biochemistry* **2006**, 45, 6756-6764.
30. Hore, P.J.; Broadhurst, R.W., *Prog. Nucl. Magn. Reson. Spectrosc.* **1993**, 25, 345-402.
31. Goez, M., *Adv. Photochem.* **1997**, 63-163.
32. Zysmilich, M.G.; McDermott, A., *J. Am. Chem. Soc.* **1994**, 116, 8362-8363.
33. Zysmilich, M.G.; McDermott, A., *Proc. Natl. Acad. Sci. U. S. A.* **1996**, 93, 6857-6860.
34. Zysmilich, M.G.; McDermott, A., *J. Am. Chem. Soc.* **1996**, 118, 5867-5873.
35. Prakash, S.; Alia; Gast, P.; de Groot, H.J.M.; Matysik, J.; Jeschke, G., *J. Am. Chem. Soc.* **2006**, 128, 12794-12799.
36. Prakash, S.; Alia; Gast, P.; de Groot, H.J.M.; Jeschke, G.; Matysik, J., *J. Am. Chem. Soc.* **2005**, 127, 14290-14298.
37. Matysik, J.; Alia; Gast, P.; van Gorkom, H.J.; Hoff, A.J.; de Groot, H.J.M., *Proc. Natl. Acad. Sci. U. S. A.* **2000**, 97, 9865-9870.
38. Diller, A.; Alia; Roy, E.; Gast, P.; van Gorkom, H.J.; Zaanen, J.; de Groot, H.J.M.; Glaubitz, C.; Matysik, J., *Photosynth. Res.* **2005**, 84, 303-308.
39. Prakash, S.; Alia; Gast, P.; Jeschke, G.; de Groot, H.J.M.; Matysik, J., *J. Mol. Struc.* **2003**, 661, 625-633.
40. Jeschke, G.; Matysik, J., *Chem. Phys.* **2003**, 294, 239-255.
41. Daviso, E.; Jeschke, G.; Matysik, J. In *Biophysical techniques in photosynthesis*; Aartsma, T.J., Matysik, J., Eds.; Springer: Dordrecht, 2007, p 385-399.
42. Schulten, E.A.M.; Matysik, J.; Alia; Kiihne, S.; Raap, J.; Lugtenburg, J.; Gast, P.; Hoff, A.J.; de Groot, H.J.M., *Biochemistry* **2002**, 41, 8708-8717.
43. Prakash, S. Ph.D. thesis, Leiden University, 2006. (http://hdl.handle.net/1887/4555)
44. Jeschke, G., *J. Am. Chem. Soc.* **1998**, 120, 4425-4429.
45. Polenova, T.; McDermott, A.E., *J. Phys. Chem. B* **1999**, 103, 535-548.
46. McDermott, A.; Zysmilich, M.G.; Polenova, T., *Solid State Nucl. Magn. Reson.* **1998**, 11, 21-47.
47. Jordan, P.M. In *Biosynthesis of tetrapyrroles*, Jordan, P.M., Ed. Elsevier: Amsterdam, 1991; p 1-66.
48. Beale, S.I.; Weinstein, J.D. In *Biosynthesis of tetrapyrroles*, Jordan, P.M., Ed. Elsevier: Amsterdam, 1991; p 155-235.
49. Watanabe, T.; Nakazato, M.; Konno, M.; Saitoh, S.; Honda, K., *Chem. Lett.* **1984**, 1411-1414.
50. Matysik, J.; Alia; Hollander, J.G.; Egorova-Zachernyuk, T.; Gast, P.; de Groot, H.J.M., *Indian J. Biochem. Biophys.* **2000**, 37, 418-423.
51. Bennett, A.E.; Rienstra, C.M.; Auger, M.; Lakshmi, K.V.; Griffin, R.G., *J. Chem. Phys.* **1995**, 103, 6951-6958.
52. Castellani, F.; van Rossum, B.; Diehl, A.; Schubert, M.; Rehbein, K.; Oschkinat, H., *Nature* **2002,** 420, 98-102.
53. Biemann, S. In *Mass spectrometry: organic chemical applications*. McGraw-Hill book company: New York, 1962.
54. Buchachenko, A.L., *Chem. Rev.* **1995,** 95, 2507-2528.

55. Diller, A.; Prakash, S.; Alia; Gast, P.; Jeschke, G.; Matysik, J., *J. Phys. Chem. B* **2007**, 111, online.

56. Fischer, M.R.; de Groot, H.J.M.; Raap, J.; Winkel, C.; Hoff, A.J.; Lugtenburg, J., *Biochemistry* **1992**, 31, 11038-11049.

57. Abraham, R.T.; Rowan, A.E. In *Chlorophylls*, Scheer, H., Ed. CRC Press: Boca Raton FL, 1991; p 797-834.

58. Boender, G.J. Ph.D. thesis, University of Leiden, 1996.

59. Matysik, J.; Alia; Gast, P.; Lugtenburg, J.; de Groot, H.J.M. In *Perspectives on solid state NMR in biology*; Kiihne, S., de Groot, H.J.M., Eds.; Kluwer: Dordrecht, 2001; p 215-225.

60. Alia; Matysik, J.; Soede-Huijbregts, C.; Baldus, M.; Raap, J.; Lugtenburg, J.; Gast, P.; van Gorkom, H.J.; Hoff, A.J.; de Groot, H.J.M., *J. Am. Chem. Soc.* **2001**, 123, 4803-4809.

6 Future Outlook

6.1 Introduction

The observation of the photo-CIDNP effect on photosynthetic RCs by solid-state NMR opened a new area for the application of this technique in the study of photosynthetic RCs. However, these studies were mainly from the purple bacteria *Rb. sphaeroides* WT and R-26 followed by PSII from plants which belong to the group of type II RCs as described earlier in chapter 1. The observation of photo-CIDNP signals from plant PSI (Chapter 2), RCs from green sulphur bacteria (Chapter 4) and heliobacteria (Chapter 5) covers the major representative groups of organisms having type I RCs. Green filamentous bacterial RCs are the only group which has not yet been studied. This thesis shows that photo-CIDNP is not restricted to only RCs from purple bacteria and plants but extends to six systems from diverse photosynthetic organisms which have different evolutionary origin. Regarding the evolution of photosynthesis there are various competing concepts at the level of photosynthetic organisms and the various components associated with photosynthesis, for example RC proteins, in the literature. The various unlabelled RCs studied till now show two major photo-CIDNP spectral patterns, with (a) all signals are negative or (b) a mixed pattern of both positive and negative signals. On the basis of this spectral pattern one cannot categorise the RCs, albeit that type II RCs in general show a mixed pattern of both positive and negative signals, with the exception of *Rb. sphaeroides* WT, while type I RCs show only an emissive pattern with the exception of heliobacteria. The RCs of heliobacteria though structurally and functionally related to RCs of green sulphur bacteria and PSI (1) show a photo-CIDNP pattern of positive and negative signals similar to that observed in type II RCs.

6.2 Functional relevance of photo-CIDNP for light-induced electron transfer

Due to the small Zeeman splitting and resulting unfavourable Boltzmann distribution, all magnetic resonance methods have intrinsically low sensitivity. Photo-CIDNP MAS NMR has been shown to be a method to overcome this limitation by production of non-Boltzmann nuclear spin distributions by photochemical reactions in solids and to allow for detailed studies of the photochemical machineries of RCs. Enhancement factors of about 10,000 have been observed in several RCs. The underlying spin-chemical processes producing such high polarization are now better understood (2, 3) and full control over the ruling parameters may allow for enhancement of a factor of more than 100,000 (4).

The window of occurrence of this effect has been shown to be very limited by kinetic and magnetic parameters (4, 5), however, it appears that evolution remained confined on this small area of the infinite parameter landscape. Hence, it appears that the conditions required for the solid-state photo-CIDNP effect in photosynthetic RCs is highly conserved.

6.3 Future experiments

Evolution happens at conditions of the earth magnetic field (50 μTesla). However, current theory on the solid-state photo-CIDNP effect would predict a maximum solid-state photo-CIDNP effect at medium fields and decay of the effect at low fields (4, 5). On the other hand, the current theory has been developed for conditions of medium and high fields and does not include cross-relaxation effects and new possibilities occurring at low fields. At low fields (*i.e.*, below 7 mTesla = 0.3 MHz proton frequency = 0.07 MHz ^{13}C frequency), the three triplet states T_+, T_- and T_0 are degenerate and offer additional options for singlet-triplet mixing which may provide new channels for photo-CIDNP. In liquid-state photo-CIDNP, for example, S-T_- mixing is well known to occur at low fields (6). The entire theory on the solid-state photo-CIDNP effect developed until now is based on high-field conditions which are characterized by a complete separation of the three triplet states simplifying the theory since solely T_0 is allowed to mix with the singlet states. In addition, current experiments have been limited to primary radical pairs, while under natural conditions secondary radical pairs may play a much more important role. Their natural lifetime is sufficiently long to allow the build-up of nuclear polarization via hyperfine interaction, and the lower electron-electron coupling parameters may fulfill the matching conditions required at lower fields.

Despite extensive efforts in artificial RC systems, having low quantum yield <~20%, photo-CIDNP has not yet been observed. Therefore, there may be a link between the occurrence of photo-CIDNP in RCs and the conditions of the unsurpassed efficient initial light-induced electron transfer in RCs. There may be some until now unknown fundamental principles ruling the spin-chemistry of photosynthetic charge separation and stabilization. Understanding of the interaction of all four electron-spin states at low magnetic fields may provide the key to these fundamental principles of efficient electron transfer. Knowledge of these principles may help in the synthesis of efficient artificial RCs. The current photo-CIDNP mechanisms may appear just to be the special case of these fundamental principles for high-field conditions. Hence, for future photo-CIDNP solid-state NMR studies a fruitful spin-chemical *terra incognita* may open at low magnetic fields.

References

1. van de Meent, E.J. Ph.D. thesis, University of Leiden, 1992.
2. Prakash, S.; Alia; Gast, P.; de Groot, H.J.M.; Jeschke, G.; Matysik, J., *J. Am. Chem. Soc.* **2005**, 127, 14290-14298.
3. Prakash, S.; Alia; Gast, P.; de Groot, H.J.M.; Matysik, J.; Jeschke, G., *J. Am. Chem. Soc.* **2006**, 128, 12794-12799.
4. Jeschke, G.; Matysik, J., *Chem. Phys.* **2003,** 294, 239-255.
5. Daviso, E.; Jeschke, G.; Matysik, J. *Biophysical methods in photosynthesis*. In Aartsma, T.J., Matysik, J., Eds. Springer: Dordrecht, 2007, p 385-399.
6. Hayashi, H. In *Introduction to dynamic spin chemistry*, World Scientific: New Jersey, 2004.

Summary

Photosynthesis is an important biological process that converts light energy into chemical energy which is storable and usable. This process takes place in photosynthetic organisms which have pigment protein complexes located in their membranes. First, light is captured by pigment protein complexes constituting the antenna system and is then transferred to a protein complex termed as reaction center (RC). The RC contains a special pigment molecule called the primary electron donor and a chain of cofactors that form the electron transfer chain and serve as electron carriers. Photosynthetic electron transport consists of a series of individual electron transfer steps. Upon photon absorption, charge separation occurs in the primary electron donor resulting in the release of an electron to the next electron carrier, called primary electron acceptor which is then passed to a final electron acceptor. The initial charge separation is a highly optimized step having a quantum yield close to unit (**Chapter 1**). Photosynthesis is performed in plants algae, cyanobacteria, purple bacteria, green sulphur bacteria, heliobacteria and green filamentous bacteria.

Chemically induced dynamic nuclear polarization (CIDNP) is produced in thermal or photochemical reactions and can be detected by NMR spectroscopy as enhanced positive or negative signals. Since the first observation of photo-CIDNP by MAS NMR in frozen bacterial RCs of *Rhodobacter* (*Rb.*) *sphaeroides* R-26 in 1994, it has developed as a technique used to study the light-induced electron transfer in photosynthetic membrane proteins at the atomic level. The photo-CIDNP effect in solids is explained by three mechanisms, (a) three spin mixing mechanism (TSM), (b) differential decay mechanism (DD) and (c) differential relaxation mechanism (DR). This thesis investigates photo-CIDNP effect in photosynthetic RCs from diverse photosynthetic organisms, ranging from plants, heliobacteria and green sulphur bacteria (**Chapter 1**).

Photo-CIDNP observed in photosystem I (PSI) of spinach by ^{13}C MAS solid-state NMR under continuous illumination with white light is presented in **chapter 2**. The photo-CIDNP data gives the first tentative set of chemical shifts of the aromatic ring carbons of a single Chl *a* molecule. All light-induced ^{13}C NMR signals appear negative and this is proposed by a predominance of the TSM mechanism over the DD mechanism.

The magnetic field effect observed in PSI and PSII from spinach is significantly different as shown in **chapter 3**. There are contrasting field dependence observed in the light-induced signal pattern of the two photosystems at three different magnetic fields, 17.6, 9.4 and 4.7 Tesla. For PSII the optimal NMR enhancement factor of ~5000 is observed at 4.7 Tesla, while the strongest light-induced signals of PSI are observed at 9.4 T. Since field dependence of

nuclear polarization is related to the magnetic parameters and lifetimes of the intermediate radical species, simulations were performed to examine what parameter changes can explain the experimental observations. The simulations indicate that an increase of the exchange coupling leads to a slight increase in absolute polarization, which can be reconciled with experimental observations. Such a change in the exchange coupling may well be caused by slight rearrangements of the cofactors that lead to an improved overlap between the molecular orbitals of the donor and the accessory chlorophyll (Chl) *a* or between the molecular orbitals of the accessory chlorophyll and the primary acceptor. Hence, this change in the magnetic field dependence of solid-state photo-CIDNP between bacterial RCs and plant PSI can be traced back to an increase of the exchange coupling between the donor and acceptor radical anions.

In **chapter 4** isolated RCs of green sulphur bacteria *Chlorobium tepidum* have been investigated. The light-induced ^{13}C MAS NMR spectra appear negative and can be tentatively assigned to the two bacterio chlorophyll (BChl) *a* molecules of the donor side. The observed doubling of several signals suggests only a slightly asymmetric dimer in both the electronic ground-state and radical-cation state of the donor side. Comparing with other RCs the dimer appears to be similar to the more symmetric donor of PSI rather than the substantially asymmetric special pair of purple bacteria.

Membrane fragments containing RCs of heliobacterium, *Heliobacillus mobilis* are analysed in **chapter 5**. The photo-CIDNP spectral pattern at lower magnetic fields (4.7 Tesla), appear to be both positive and negative, which is similar to the pattern observed in the RCs of plant PSII and purple bacterial reaction centers of *Rb. sphaeroides* R-26. However, unlike the other RCs studied by photo-CIDNP, this system is unique, at high fields of 17.6 Tesla, the positive signals undergo a sign change and the spectra appear negative.

The future outlook of the study of natural RCs by photo-CIDNP is addressed in **chapter 6**. The observation of this effect in all natural photosynthetic RCs from diverse photosynthetic organisms leads to the conclusion that the principles leading to this effect are an inherent property conserved in natural RCs from biologically diverse photosynthetic organisms. This suggests that photo-CIDNP is a good technique which can be used for evaluating the efficiency of artificial photosynthetic systems.

Samenvatting

Fotosynthese is een belangrijk biologisch proces dat licht omzet in chemische energie welke opgeslagen en gebruikt kan worden. Dit proces vindt plaats in fotosynthetische organismen met pigment proteïne complexen in hun membranen. Allereerst wordt het licht opgevangen door pigment-eiwit complexen die onderdeel uitmaken van het antenne systeem, vervolgens wordt het doorgegeven aan een ander eiwit complex, het reactie centrum (RC). Het RC bevat een speciaal pigment molecuul, de primaire elektron donor, en een reeks co-factoren die samen de elektron overdrachtsketen vormen, en als elektronen dragers dienen. Fotosynthetisch elektronen transport bestaat uit een aantal individuele stappen van elektronen overdracht. Bij absorptie van een foton wordt een lading afgescheiden uit de primaire elektron donor, wat resulteert in vrijgeven van een elektron aan de volgende elektronen drager, de primaire elektronen acceptor, welke het doorgeeft aan een uiteindelijke elektronen acceptor. De eerste stap uit deze reeks is een bijzonder geoptimaliseerde stap, met een hoge quantum opbrengst bijna 100% (**Hoofdstuk 1**). Fotosynthese vindt plaats in planten, algen, blauwalgen, paarse bacteriën, groene zwavel bacteriën, heliobacteriën en groene filamentbacteriën.

Chemically induced dynamic nuclear polarization (CIDNP) genereert een niet-evenwichts verdeling van kern spin toestanden, die met behulp van kern spin resonantie (NMR) gedetecteerd kan worden als versterkte positieve of negatieve signalen. Sinds de eerste waarneming van foto-CIDNP door middel van magische hoek rotatie (MAS) NMR in bacteriële RCs van *Rhodobacter* (*Rb.*) *sphaeroides* R-26 in 1994, heeft het zich ontwikkeld als een techniek om de lichtgeïnduceerde elektronen overdracht in fotosynthetische membraaneiwitten op atoomniveau te bestuderen. Het foto-CIDNP effect in vaste stoffen kan worden uitgelegd met behulp van drie mechanismen, a) het three spin mixing (TSM) mechanisme, b) het differential decay (DD)mechanisme en c) het differential relaxation (DR) mechanisme. Dit proefschrift bestudeert het foto-CIDNP effect in de fotosynthetische RCs van diverse fotosynthetische organismen, variërend van planten tot heliobacteriën en groene zwavel bacteriën (**Hoofdstuk 1**).

Hoofdstuk 2 behandelt het ongekend sterke foto-CIDNP effect in fotosysteem I (PSI) van spinazie onder continue belichting met wit licht, waargenomen met ^{13}C MAS vaste stof NMR. De foto-CIDNP data geeft voorlopige toekenning van de chemische verschuiving van de aromatische koolstoffen in een enkel chlorofyl (Chl) *a* molecuul. Alle lichtgeïnduceerde ^{13}C NMR signalen onder continue belichting lijken gerelateerd aan emissie processen, wat

verklaard zou kunnen worden door een sterk TSM effect, in vergelijking met het DD mechanisme.

De magnetische veld effecten waargenomen in PSI en PSII van spinazie verschillen significant, zoals aangetoond in **hoofdstuk 3**. Voor PSII wordt een optimale versterkings factor van ~5000 waargenomen bij 4.7 T, terwijl de sterkste lichtgeïnduceerde signalen van PSI waargenomen worden bij 9.4 T. Aangeziende veld afhankelijkheid van kernspin polarisatie afhangt van de magnetische parameters en levensduren van de radikaal intermediairen in het fotosynthese proces, zijn simulaties uitgevoerd om te bestuderen welke waarden van de parameters een verklaring bieden voor de experimentele waarnemingen. De simulaties geven aan dat een toename in de exchange coupling kan leiden tot een lichte toename in absolute polarisatie, wat overeenkomt met hetgeen experimenteel is waargenomen. Een dergelijke verandering in exchange coupling wordt mogelijk veroorzaakt door een specifieke positionering van de co-factoren in het eiwit complex, wat kan leiden tot een sterke overlap van de molekuul orbitalen van het chlorofyl donor complex en een nabije chlorofyl (Chl) *a*, of van de molekuul orbitalen van de nabij chlorofyl en de primaire acceptor chlorofyl.

In **hoofdstuk 4** zijn geïsoleerde RCs van groene zwavel bacteriën *Chlorobium tepidium* bestudeerd. De lichtgeïnduceerde ^{13}C MAS NMR spectra vertonen emissie (zijn negatief) en kunnen toegeschreven worden aan de twee BChl *a* moleculen aan de donor zijde. De waargenomen verdubbeling van signalen suggereert dat er slechts één licht asymmetrische dimeer aanwezig is in zowel de elektronische grondtoestand als de geoxideerde toestand aan de donor zijde van het eiwit. Deze licht asymmetrische dimeer is vergelijkbaar met de donor van PSI, in tegenstelling tot de aanzienlijke asymmetrie waargenomen voor de dimeer donor van paarse bacteriën.

Membraan fragmenten met RCs van de heliobacterie, *Heliobacillus mobilis*, worden geanalyseerd in **hoofdstuk 5**. Bij een lagere veldsterkte van 4.7 Tesla lijkt het foto-CIDNP spectrale patroon zowel absorptie als emissie te vertonen. Dit is vergelijkbaar met het waargenomen patroon in de PSII RCs van planten en paarse bacteriële reactie centra van *Rb. sphaeroides* R-26. Echter, in tegenstelling tot andere RCs bestudeerd met foto-CIDNP, is dit systeem uniek. Bij hoge veldsterkte (17.6 Tesla) veranderen de absorptie signalen van teken, waardoor de spectra alleen emissie vertonen van een onverwachte signaalsterkte.

De toekomst perspectieven van de analyse van de biodiversiteit van het foto-CIDNP effect in natuurlijke RCs worden besproken in **hoofdstuk 6**. Het waarnemen van dit effect in alle natuurlijke fotosynthetische RCs van diverse fotosynthetische organismen leidt tot de conclusie dat de principes verantwoordelijk voor dit effect inherent verbonden zijn met het moleculaire mechanisme van de fotosynthese. Dit suggereert dat foto-CIDNP een goed techniek is voor analse en validatie van efficiënte artificiel fotosynthese systemen.

List of Publications

‘Photochemically induced dynamic nuclear polarization in photosystem I of plants observed by ^{13}C magic-angle spinning NMR’
Alia, E. Roy, P. Gast, H.J. van Gorkom, H.J.M. de Groot, G. Jeschke, J. Matysik.
J. Am. Chem. Soc. (2004) 126, 12819-12826.

‘Photo-CIDNP solid-state NMR on photosystems I and II: What makes P680 special?’
A. Diller, Alia, E. Roy, P. Gast, H.J. van Gorkom, J. Zaanen, H.J.M. de Groot, C. Glaubitz, J. Matysik.
Photosynth. Res. (2005) 84, 303-308.

‘Magnetic field dependence of ^{13}C photo-CIDNP MAS NMR in plant photosystems I and II’
E. Roy, A. Diller, Alia, P. Gast, H.J. van Gorkom, H.J.M. de Groot, G. Jeschke, J. Matysik.
Appl. Mag. Res. (2007) 31, 193-204.

‘Photochemically induced dynamic nuclear polarisation in the reaction center of the green sulphur bacterium *Chlorobium tepidum* observed by ^{13}C MAS NMR’
E. Roy, Alia, P. Gast, H.J. van Gorkom, H.J.M. de Groot, G. Jeschke, J. Matysik.
Biochim. Biophys. Acta (2007) 1767, 610-615.

‘^{15}N-photo-CIDNP MAS NMR analysis of the electron donor of photosystem II’
A. Diller, E. Roy, P. Gast, H.J. van Gorkom, H.J.M. de Groot, C. Glaubitz, G. Jeschke, J. Matysik, A. Alia.
Proc. Natl. Acad. Sci. U. S. A. (2007) 104, 12843-12848.

‘^{13}C photo-CIDNP MAS NMR on the reaction center of the green sulphur bacterium at two different magnetic fields’
E. Roy, A. Alia, P. Gast, H.J. van Gorkom, G. Jeschke, J. Matysik.
Proceedings of the 14th International Congress on Photosynthesis, (J.F. Allen, E. Gantt, J.H. Golbeck and B. Osmond Eds.), Springer Dordrecht, submitted.

‘Photo-CIDNP in isolated membrane fragments of *Heliobacillus mobilis* observed by ^{13}C MAS NMR’
E. Roy, A. Alia, T. Rohmer, P. Gast G. Jeschke, J. Matysik.

Curriculum Vitae

In 1994, after completing high school education, I started my studies in the department of Bioscience in Jamia Millia Islamia University in New Delhi. I obtained my bachelor's degree in Biosciences in 1999 and proceeded with my masters, with subject's biochemistry, animal physiology, plant physiology, microbiology and environmental biology. In the summer of 2000 I started with my masters dissertation, entitled "*Refining the protocol for regeneration of Sorghum bicolor (L) Moench from scutellum*", in the Plant Physiology and Biotechnology Laboratory under the supervision of Prof. P. Saradhi. I did an internship for a month in molecular biology techniques at the National Environmental Engineering Research Institute in Nagpur. I received my master's degree in June 2001. In October 2001 I was employed at the Central Institute of Cotton Research, in the Department of Biotechnology at Nagpur in a research project aimed for developing transgenic cotton for insect resistance.

In June 2003 I started my PhD in the solid-state NMR group of Prof H.J.M. de Groot, under the supervision of Dr. J. Matysik. During my PhD I attended the 35th Spring school "Physics meets Biology" organised by the Institute of Solid State Research in 2004 at Jülich and had the opportunity to present my work in the form of posters at the *13th International Congress of Photosynthesis* (2004) at Montreal, Canada, *26th Annual meeting on Magnetic Resonance* (2004) at Aachen, *EUROMAR* (2005) at Veldhoven, Netherlands, *Spin-Chemistry meeting* (2005) at Oxford, *Photosynthesis in the post genomic era* (2006) at Pushchino, Russia, the *14th International Congress of Photosynthesis* (2007) in Glasgow and *XXIIIrd International Conference of Photochemistry* (2007) in Köln.

Nawoord

The years in Leiden have been memorable. I spent considrable time in the Biophysics group for sample preparation. A congenial atmosphere in the lab was provided by Wouter, Tatiana, Mohamad, Yan and Lu-Ning. I worked with Drè, whose expertise in handling bacterial cultures and his aid in emergency situations was beneficial. The stimulating discussions with Peter were helpful. Alia shared her experience and knowledge in sample preparation since my first year. Johan Hollander, Fons Lefeber and Kees Erkelens were always helpful with the solid-state NMR setup. The complex theory behind photo-CIDNP was made simple to understand by Prof. Gunnar Jeschke of the University of Konstanz who gave his precious time to answer any queries.

The time spent with Adriaan, Alexey, Arjan van Wijk, Ania, Anjali, Eugenio, Francesco, Frans, Geerten, Ido, Ineke, Jan, Kathick, Louise, Piotr, Prasad, Prativa, Richard, Rob de Jong, Samira, Sylvia, Suzanne and Thierry, was enjoyable. Liesbeth has always extended a warm hearted welcome and helped with administrative forms. The conversations with Rob van der Steen, Reinier and Arjan Siebum always provided the welcome relief from mundane days and melancholy. I am grateful to Niels for having taken the time for the Dutch translation of my thesis summary. I will always remember Anna, Prashant, Shipra and Swapna for being great friends.

The Banerji family has always welcomed me and I am grateful for their help during my convalescence. Mishal, your positive attitude provided the much needed motivation in the past years. I am indebted to my parents who have always been encouraging, jovial and patient listeners especially during the trying times.